	Ag	As	Sb	Hg
Au	0.72	0.74	0.68	0.54
Ag		0.69	0.72	0.61
As			0.80	0.60
Sb				0.68

3-7 Considerations

The mineralization in this area is most significant at the Dakuniba Prospect. It is characterized by narrow quartz veins extending for more than 1 km in length, although in many places discontinuous in surface outcrop. Au values higher than 1g/t Au are identified only in the Nagagani Creek area. Around the Dakuniba area alteration is less well developed and the structural control on the mineralization is difficult to specify. However, the E-W trending fault is suspected to be a conduit for the hydrothermal fluid convection. This assumption is based on the direction of the E-W trending basalt dykes and N-S trending fold axes indicating tensional fractures may havebeen generated in an E-W direction under an E-W compressional stress field. The center of the upflow of hydrothermal fluid is suspected to have been near the Nagagani Creek.

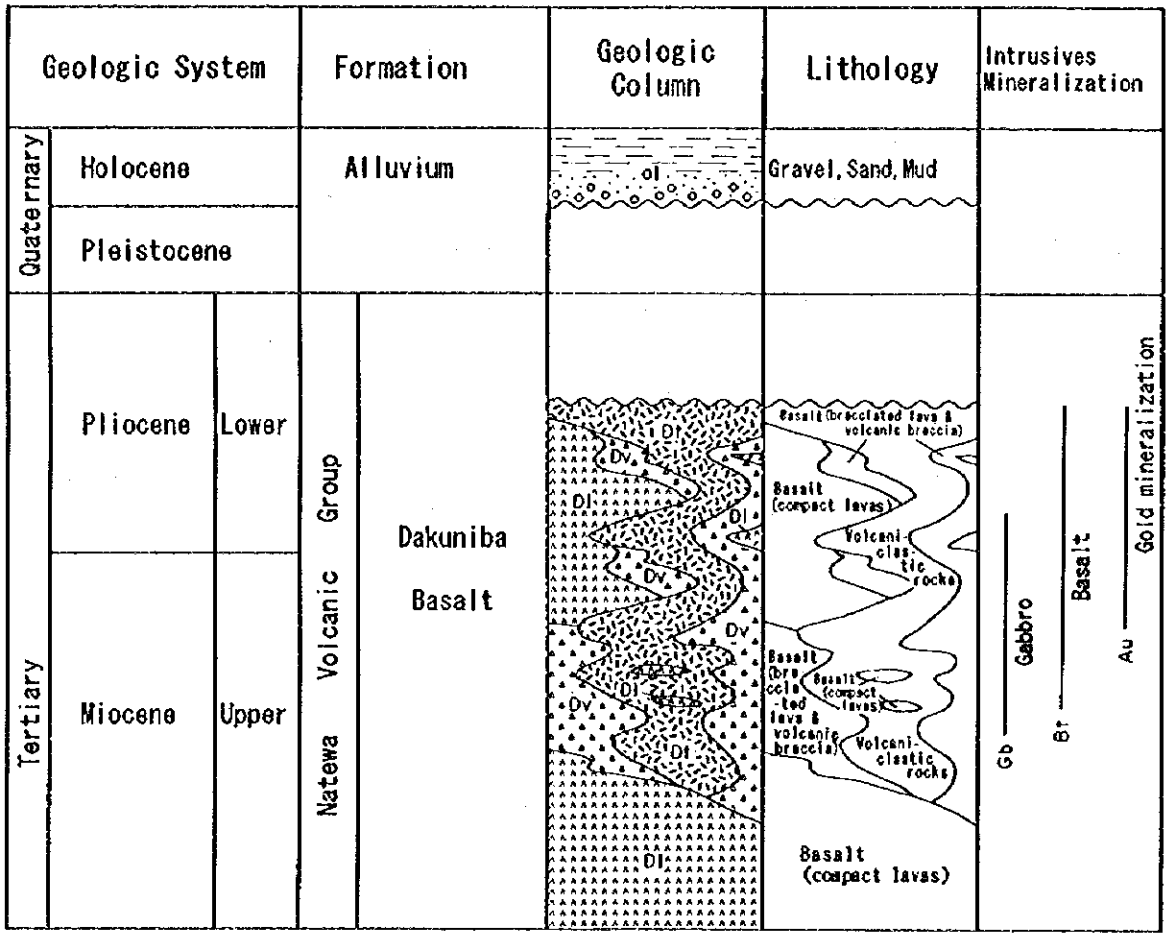

Fig. 2-3-1 Schematic Stratigraphic Columns of the Dakuniba Area

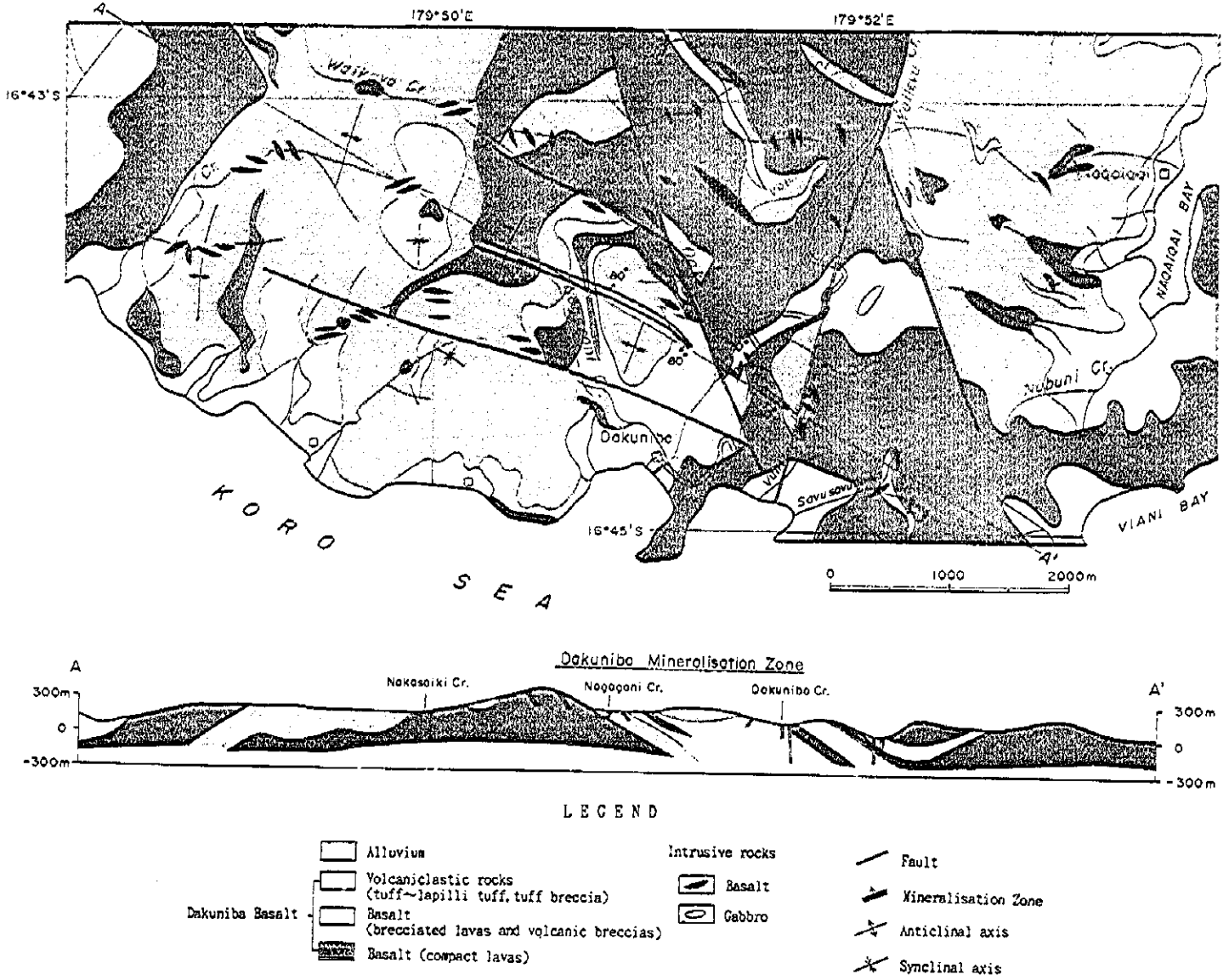

Fig. 2-3-2 Geologic Map of the Dakuniba Area

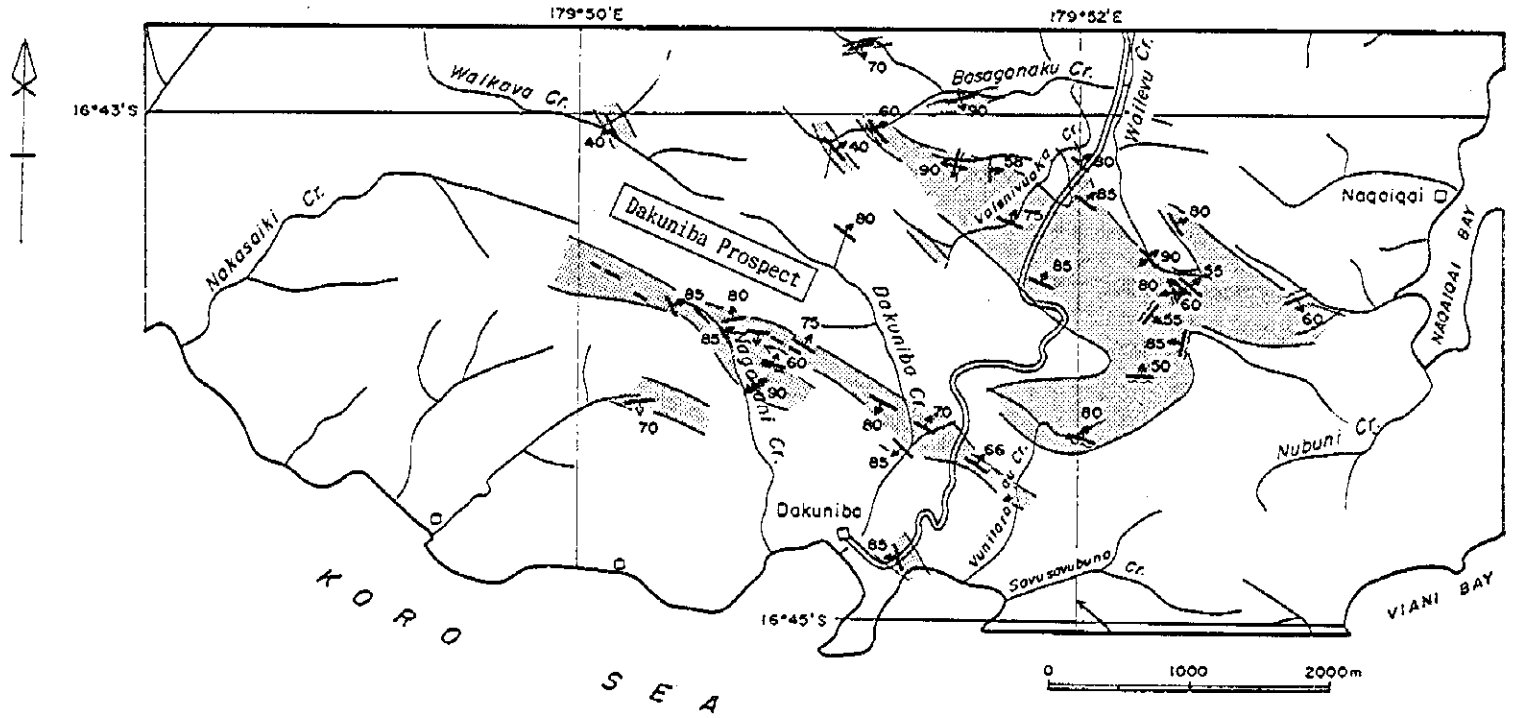

LEGEND

Quartz vein

Clay vein

Alteration zone
(pyrite dissemination)

Fig. 2-3-3 Distribution Map of Prospects and Alteration Zones in the Dakuniba Area

No.	Sample No.	Au g/t	Ag g/t
1	DB 107	5.72	9.8
2	DB 108	5.11	6.5
3	DB 109	4	16.6
4	DB 110	4.55	47
5	DB 111	2.89	6.4
6	DB 113	0.38	11.1
7	DB 114	0.1	<0.4
8	DB 115	0.318	0.5
9	DB 116	0.13	1.2
10	DB 117	4.45	12.3
11	DB 118	6.7	8.5
12	DB 119	6.56	10.4
14	DB 137	0.02	2.8
15	DB 139	0.12	1.2
16	DB 140	0.2	<0.4
17	DB 141	0.03	<0.4
18	DB 142	1.77	1.2
19	DB 143	<0.01	<0.4
20	DB 144	0.11	0.4
21	DB 145	<0.01	<0.4
22	DB 146	0.69	36.7
23	DB 147	0.71	47
24	DB 148	12.4	46
25	DB 149	2.18	5.6
26	DB 150	0.045	2.4
27	DB 151	1.33	4.6
28	DB 152	0.54	7.2
29	DB 153	2.28	11.3
30	DB 154	4.61	8.3
31	DB 155	16.1	78
32	DB 156	<0.01	<0.4
33	DM 118	<0.01	<0.4
34	DM 119	0.825	2.2
35	DM 120	<0.01	<0.4
36	DM 121	<0.01	<0.4
37	DM 122	<0.01	<0.4
38	DM 123	<0.01	<0.4
39	DM 124	<0.01	<0.4
40	DM 125	0.063	2.2
41	DM 126	0.085	2.5
42	DM 127	0.06	<0.4
43	DM 128	0.288	0.9
44	DM 129	0.028	0.5
45	DM 130	0.557	0.4
46	DM 131	2.85	0.7
47	DM 132	0.072	1
48	DM 133	<0.01	<0.4
49	DM 134	0.137	<0.4
50	DM 135	0.327	0.9
51	DM 136	0.11	0.8
52	DM 137	0.027	0.4
53	DM 138	2.11	2.2
54	DM 139	0.112	0.5
55	DM 140	4.05	78
56	DM 141	0.5	0.7
57	DM 142	3.2	4.1
58	DM 143	0.75	0.5
59	DM 144	<0.01	<0.4
60	DM 145	0.05	1.4
61	DM 146	0.08	0.4
62	DM 147	0.77	1.1
63	DM 148	0.86	1.3
64	DM 149	0.135	0.6
65	DM 150	0.23	0.4
66	DM 151	0.01	<0.4
67	DM 152	<0.01	<0.4
68	DM 153	<0.01	<0.4
69	DM 154	0.05	0.5
70	DM 155	0.03	0.6
71	DM 156	0.23	<0.4
72	DM 157	<0.01	1.3
73	DM 158	0.01	<0.4
74	DM 159	0.015	<0.4
75	DM 160	0.01	0.4
76	DM 161	0.02	0.6
77	DM 162	0.12	0.5
78	DM 163	0.18	0.9
79	DM 164	0.05	1.0
80	DM 165	<0.01	0.7
81	DM 166	<0.01	<0.4
82	DM 167	0.13	3.4
83	DM 168	0.31	4.0
84	DM 169	0.454	151.0
85	DM 170	0.1	5.3
86	DM 171	0.053	2.2
87	DM 172	0.039	0.5
88	DM 173	0.027	1.8
89	DM 174	0.033	2.6
90	DM 175	0.034	2.5
91	DM 176	0.03	3.9
92	DM 078	<0.01	<0.4
93	DM 131	<0.01	<0.4
94	DM 132	<0.01	<0.4
95	DM 079	<0.01	<0.4
96	DM 133	0.02	0.8
97	DM 134	0.07	2.4
98	DM 136	0.136	5.5
99	DM 080	<0.01	0.6
100	DM 081	0.07	2.8
101	DM 185	<0.01	0.5
102	DM 187	<0.01	<0.4
103	DK 101	0.12	<0.4
104	DK 102	2.55	0.6
105	DK 103	0.07	0.4
106	DK 104	0.015	<0.4
107	DK 105	0.19	2.2
108	DK 106	0.14	1.0
109	DK 107	0.56	0.4
110	DK 108	0.05	<0.4
111	DK 109	0.052	<0.4
112	DK 110	0.049	<0.4
113	DK 111	0.173	<0.4
114	DK 112	0.049	<0.4
115	DK 113	0.435	12.2
116	DK 114	0.04	<0.4
117	DK 115	0.162	1.7
118	DK 116	0.12	0.4
119	DK 117	0.204	16.1
120	DK 118	0.01	<0.4
121	DK 119	0.012	<0.4
122	DK 120	<0.01	<0.4
123	DK 121	<0.01	0.4
124	DK 122	0.012	<0.4
125	DK 123	<0.01	0.6
126	DK 126	<0.01	<0.4
127	DK 127	<0.01	1.2
128	DK 128	0.01	0.4
129	DK 129	0.01	<0.4
130	DK 130	0.01	<0.4
131	DS 076	0.688	3.4
132	DS 079	0.157	<0.4
133	DS 080	0.282	1.1
134	DS 081	0.015	<0.4
135	DS 082	0.04	0.4
136	DS 083	<0.01	<0.4
137	DS 084	0.468	6.1
138	DS 085	<0.01	<0.4

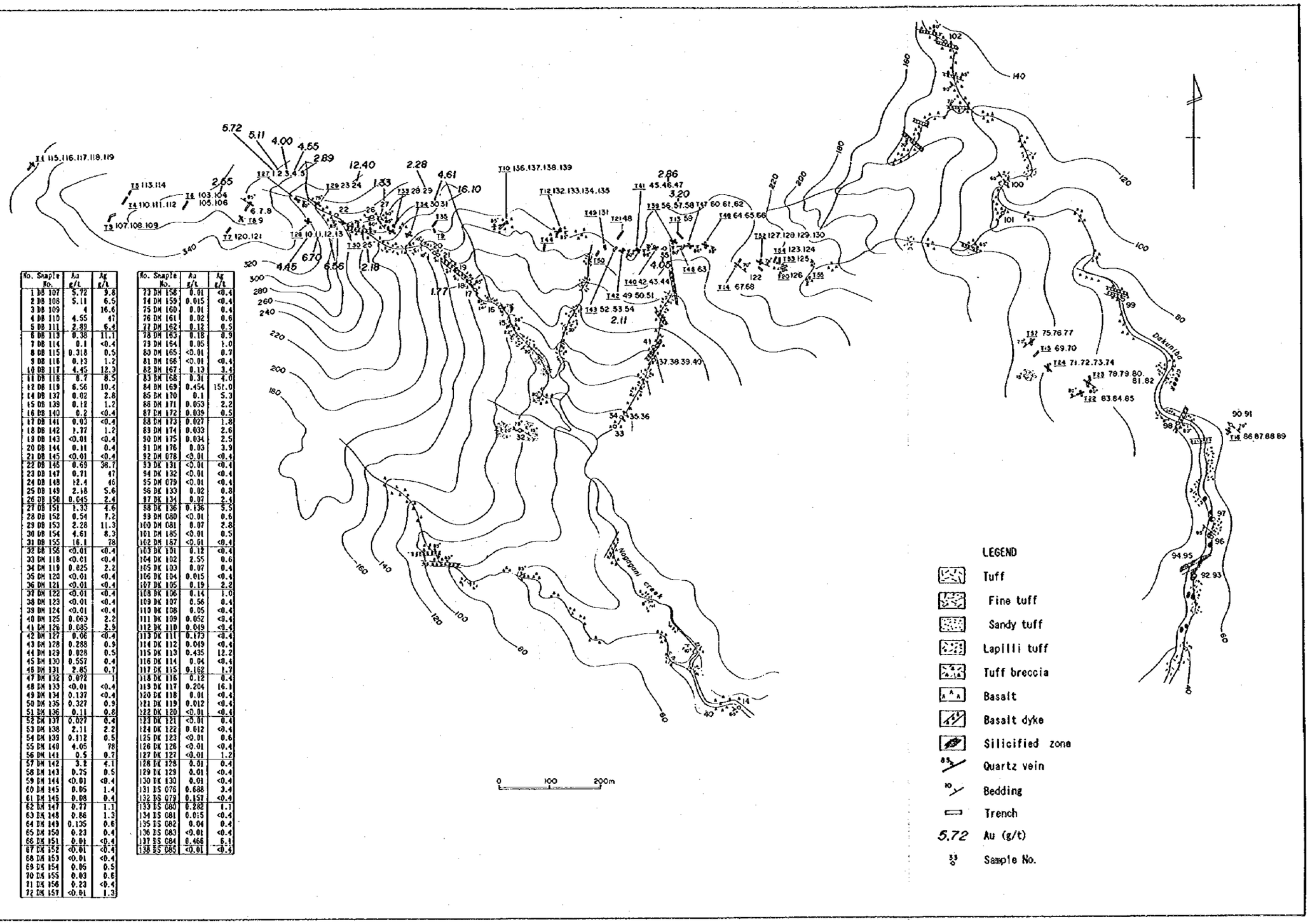

Fig. 2-3-4 Detailed Survey Results of the Dakuniba Prospect

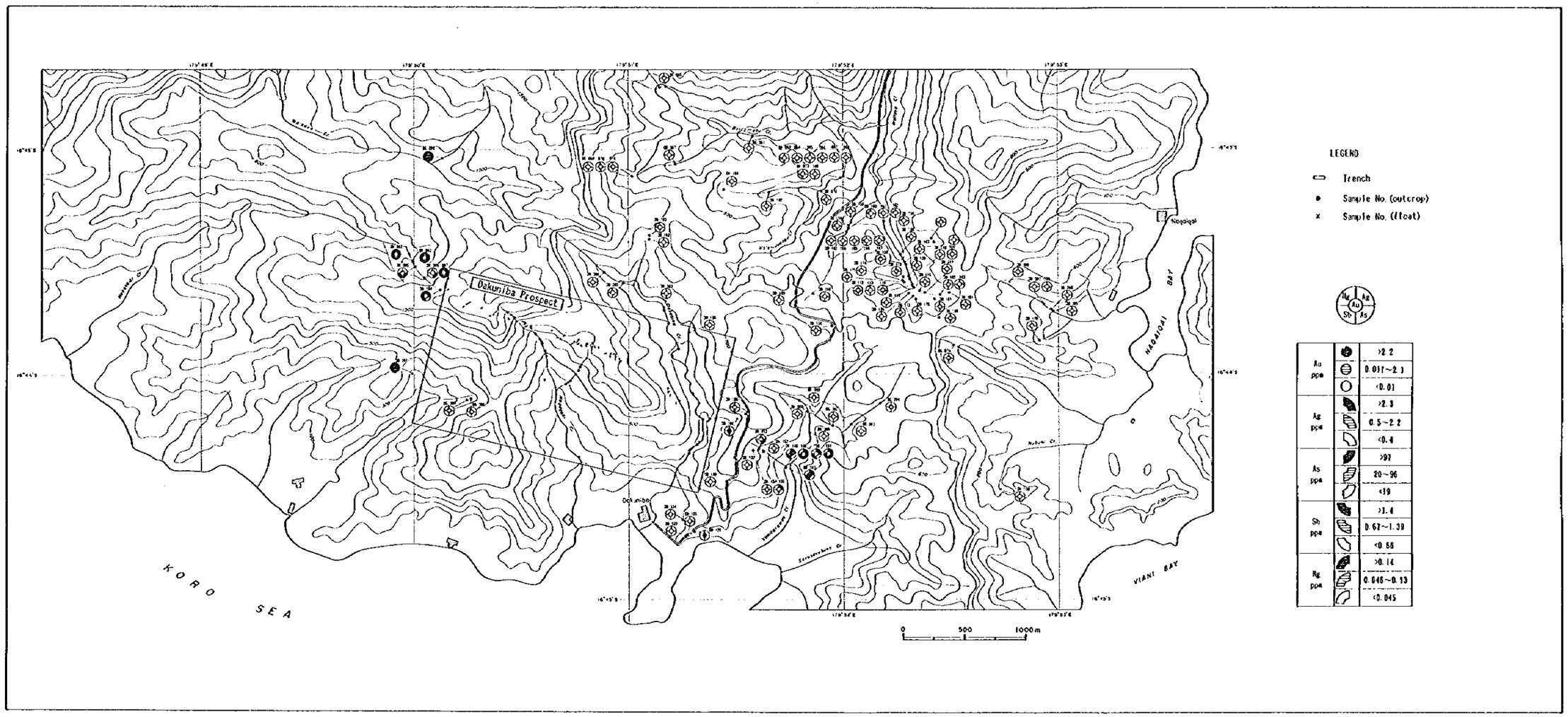

Fig. 2-3-5 Geochemical Survey Results of the Dakuniba Area

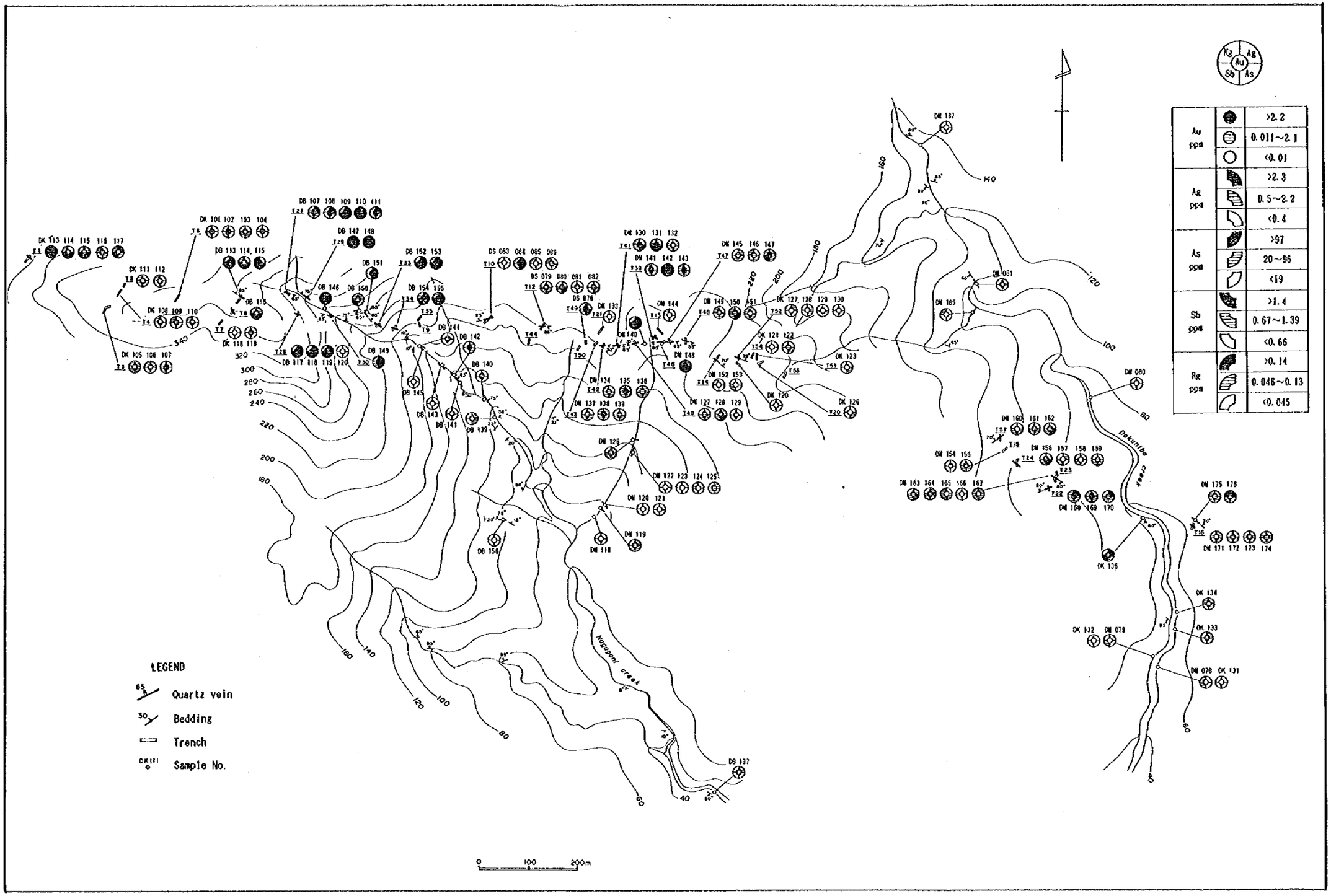

Fig. 2-3-6 Geochemical Survey Results of the Dakuniba Trenches Area

Dakuniba Prospect

Trench No.28

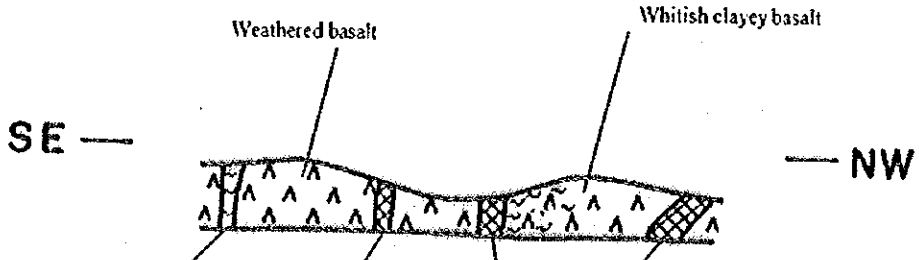

Sample	width(cm)	Au (g/t)	Ag (g/t)
DB117	10	4.45	1.23
DM118	40	6.70	8.5
DB119	5	6.56	10.4

Trench No.34

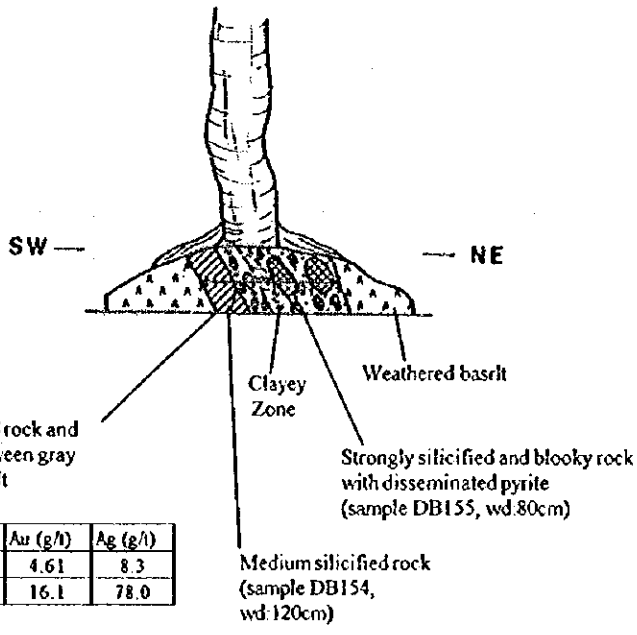

Sample	width(m)	Au (g/t)	Ag (g/t)
DB154	1.2	4.61	8.3
DB155	0.8	16.1	78.0

Fig. 2-3-7 Sketch of Trenches at the Dakuniba Prospect

Chapter 4 Geology of the Waimotu Area

4-1 Outline of Geology

Host rocks to the ore deposits and mineralization in this area are andesite and basalt lavas and volcaniclastic rocks of the same composition.

The mineralized zones around the three prospects are limited to areas previously worked. Beyond these areas, alteration and mineralization are weak and there is no significant geochemical anomaly.

On the other hand, the altered volcaniclastic rocks that are distributed widely to the north of the area are characterized by disseminated pyrite and the presence of smectite.

The eastern part of the fault that runs from the north through the center of the survey area to the south is underlain by basalt and andesite lavas which are not altered, except at the Nuku Prospect. On the other hand, the western part of the fault is underlain by weak but extensive alteration where basalt shows green in color.

Samples of chalcedony and quartz vein from the outcrop of the Main and East Lodes of Waimotu Lodes returned 24 g/t Au over 1 m. At Bill's Hill a silicified and argillic (kaolin) zone are developed that is cut by quartz stockwork that strikes N-S and dips steeply. The Au values are less than 1 g/t Au. At Nuku, a chalcedony and quartz stockwork zone has been confirmed about 8 m in width. This zone strikes N-S and is assumed to dip westward. The maximum assay results grade 4.3 g/t Au.

4-2 Stratigraphy

The area is underlain by the Koroutari Andesites and Korotini Breccias of the Natewa Volcanic Group. The Koroutari Andesites consist of basaltic to andesitic lavas. The Korotini Breccias consist of tuff breccia, lapilli tuff and tuff. The two formations are divided into four units. The basalt lavas are mainly distributed in the central and western part of the area. They are generally compact, dark green in color and have undergone regional alteration. Basalt-andesite lavas are distributed to the north of the Nuku Prospect, and separated only by unaltered andesite that is dark in color, although it has undergone alteration near the Nuku Prospect. Andesite lavas are distributed in the southwestern part and they are compact, hard and dark green in color.

Volcaniclastic rocks are intercalated with the previously mentioned three lava units. The unit in the north is composed mainly of tuff breccia that grades into lapilli tuff and tuff.

The unit is generally not bedded and is green to pale green in color. Lithic fragments are andesitic. Andesitic lithic fragments are composed of phenocrysts of pyroxene and plagioclase in a groundmass of plagioclase, pyroxene and glass. The tuff breccia unit in the northern part contains presumably essential quartz grains, that may indicate dacitic volcaniclastic rocks are intercalated.

Basalt is porphyritic and composed of phenocrysts of olivine, orthopyroxene in a plagioclase and groundmass of clinopyroxene, plagioclase and glass. Olivine is replaced by smectite, and plagioclase by carbonates.

Basalt-andesite lavas unit is porphyritic and composed of phenocrysts of olivine, clinopyroxene, orthopyroxene and plagioclase, in a groundmass of clinopyroxene and plagioclase and glass. The olivine phenocrysts have been decomposed and replaced by smectite.

Andesite is porphyritic and composed of phenocrysts of clinopyroxene and plagioclase, in a groundmass of orthopyroxene and plagioclase and glass. The clinopyroxene phenocrysts are replaced by chlorite and glass are partly altered to carbonates.

The total thickness of the Koroutari Andesites and Korotini Breccias is estimated to be more than 1800 m.

4-3 Intrusive Rocks

In this area intrusive rocks of basalt, andesite, quartz diorite porphyry and gabbro crop out. The basaltic intrusive rocks occur at many locations. In the northern part of the area, dykes dominantly trend in a N-S~NNE-SSW direction, while in the central part a N-S~NW-SE, and in the southern part, a N-S and NE-SW direction is dominant. The basaltic dykes are composed of phenocrysts of plagioclase in a groundmass of olivine, clinopyroxene, plagioclase and glass.

The trend of the outcropping andesite dyke is N-S in the central part of the area. It is composed of phenocrysts of plagioclase and a groundmass of plagioclase, K-feldspar and glass. Glass is altered into smectite.

The quartz diorite porphyry crops out in narrow areas but float is more widely distributed. It is composed of phenocrysts of clinopyroxene and orthopyroxene and plagioclase, in a groundmass comprising the same minerals and glass. Glass has altered to smectite.

Gabbro crops out in the southern part of the area. This rock is porphyritic with a doleritic texture composed of phenocrysts of olivine, clinopyroxene, orthopyroxene and plagioclase.

4-4 Geological Structure

The geological structure is different in the northern part and southern part of the area. The northern part is characterized by small scale NE-SW trending folds, while in the south folds are characterized by homoclinal structures a N-S strike and E-dip.

4-5 Mineralization and Alteration

The mineralized zones around the three prospects are limited to areas coinciding with the previous workings. Beyond these, alteration and mineralization are weak and there is no significant geochemical anomaly.

On the other hand, the volcaniclastic rocks that are distributed widely to the north of the area are characterized by disseminated pyrite and presence of smectite.

The eastern part of the fault that runs from the north through the center of the survey area to the south is underlain by basalt and andesite lavas which are not altered, except at the Nuku Prospect. On the other hand, the western part of the fault is underlain by weak but extensive alteration where the basalt is green in color.

The Main Lode of the Waimotu Lodes can be traced over 70m with a width of 0.8 m~1.2 m, the best assay grading 24 g/t Au over 1 m of chalcedony and quartz vein. The East Lode crops out at one trench and returned a grade of 12.5 g/t Au over 0.8m. The West Lode does not crop out and the sample taken in front of a collapsed adit returned 0.92 g/t Au.

At Bill's Hill, a silicified and argillic (kaolin) zone in lapilli tuff and tuff breccia has developed on the eastern slope . The zone is cut by quartz stockwork that strikes N-S and dips steeply. The Au values are less than 1 g/t Au.

At Nuku, a chalcedony and quartz stockwork zone about 8 m width has been confirmed (Fig.2-4-6). The zone strikes N-S and is assumed to dip westward. The maximum grade returned 4.3 g/t Au.

4-6 Geochemical Survey Results

(1) Whole Waimotu Area

A total of 77 samples were taken for chemical analysis. A statistical analysis has been carried out including all samples. Threshold values have been calculated for the whole area (Fig. 2-A-7~9).

Au: 0.01 g/t (detection limit) and 2.2 g/t (average+σ) are selected for the threshold values.

Ag: 0.4 g/t (detection limit) and 2.3 g/t (average+2 $\times$ σ) are selected for the threshold values.

As: 19 ppm (average) and 97 ppm (average+σ) are selected for threshold values.

Sb: 0.66 ppm (average) and 1.4 ppm (average+σ) are selected for the threshold values.
Hg: 0.045 ppm (average+σ) and 0.14 ppm (average+2 × σ) are selected for threshold values.

(2) Waimotu Lodes

Au: The highest value of 42.5 g/t was from the West Lode, while a sample 1 m south returned a grade of 2.4 g/t. The Main Lode graded 7.2 g/t for an average of 4 samples over 70 m. A sample from the West Lode is 0.92g/t.

Ag: Silver values are not high compared to the Au values, resulting in the ratios of Ag and Au are mostly less than 1.

Hg, As and Sb are anomalous and absolute values appears low compared to other epithermal deposits. The Waimotu Lodes consist of quartz and adularia veins and is not accompanied by significant amount of sulfides. Minor amounts of goethite has replaced some sulfides.

(3) Bill's Hill Prospect

The highest grade from the quartz veins returned 0.21 g/t Au. Ag values are low. Weak Hg, Sb and As anomalies over the hill. In general, samples from the quartz veinlets do not contain sulfide while small amount of goethite occurs. A float sample, however, contains trace amount of chalcopyrite. Core from previous drill holes exhibits intense pyrite dissemination in the silicified zone.

(4) Nuku Prospect

The average gold value of line samples within 150m along strike is 1.3 g/t over 7 m, with the highest value being 4.3g/t. Ag is of the same order of magnitude as gold (315 g/t). As and Hg are anomalous with the highest values being 2.4 ppm and 0.092 ppm, respectively. One sample consisted of mainly quartz and opal with minor amounts of pyrite. The other specimen contains acanthite and Ag is as low as 0.5 g/t.

Element(unit)	Au(ppm)	Ag(ppm)	As(ppm)	Sb(ppm)	Hg(ppm)
Detection Limit	0.01	0.4	1.0	0.5	0.005
Average	0.16	0.4	19	0.66	0.014
Minimum	<0.008	<0.4	<1.0	<0.5	<0.005
Maximum	42.5	7	460	2.4	0.26
Average+σ	2.2	0.93	97	1.4	0.045
Average+2 x σ	30.4	2.3	509	2.8	0.14

(5) Correlations

Over the whole area, Au exhibits a normal correlation with Ag, while As, Sb and Hg do not show any clear correlation. The samples from Bill's Hill and the Waimotu Lodes exhibits a strong correlation between Au and Ag, while samples from the Nuku Prospect exhibits weak correlation. Au exhibits a weak normal correlation with Hg at Bill's Hill, while the correlation is not clear at the Waimotu Lodes and the Nuku Prospect. The correlation between As and Sb is strong over the whole area.

Correlation coefficients for whole Waimotu Area

	Ag	As	Sb	Hg
Au	0.70	0.52	0.60	0.28
Ag		0.22	0.30	0.12
As			0.91	0.34
Sb				0.35

Correlation coefficients for each Prospect
(Au and other elements)

Prospect	Ag	As	Sb	Hg
Bill's Hill(11)	0.92	-0.08	0.31	0.58
Waimotu Lode(12)	0.97	-0.26	-0.27	-0.21
Nuku(26)	0.46	-0.02	0.20	-0.11

4-7 Considerations

(1) Waimotu Lodes

The Main Lode was drifted by two adits that are separated by 15 m. The length of the upper and the lower adits are about 50m and 60m, respectively. Two of the three drill holes that aimed about 50m below the lower adit did not intercept the main lode because the lengths were too short. Three of the seven holes intercepted the East Lode with one intercept grading 6.9 g/t Au over 1 m and the other two returning grades below 1.5 g/t Au. Core recoveries for these holes were poor.

At the Waimotu Lodes, the previous exploration to test for down dip extension did not test was not successful.

(2) Bill's Hill

Primary sulfides in outcrop at Bill's Hill Prospect has oxidized to form iron oxide. Previous drill holes are have shown that oxidation extends to a depth of 15~20 m below which quartz stockwork, veinlets, pyrite dissemination and silicification have developed.

Existing data shows the surface of this area is characterized by a silicified cap and a chalcedony and quartz stockwork zone with secondary enrichment of gold(the chalcedony quartz stockwork grades 0.17 g/t~0.77 g/t over the 5.6m~21.8m interval). Past exploration was conducted aiming at discovering bulk mineable low grade deposits, however the identified mineralized zone turned out to be too small. One hole (BH 87-8) drilled to a depth of approximately 200m intercepting more than 5 quartz-chalcedony veinlets similar to the Waimotu veins being scarce in sulfides.

In view of the above, at Bill's Hill two modes of mineralization: silcification and pyrite dissemination which replaced porous tuff breccia, and quartz-chalcedony veining with minor amounts of sulfide occur.

(3) Nuku Prospect

It was revealed that the mineralization zone at the Nuku Prospect dips toward the west, however it appears to dip eastward on the surface. It may be important to reveal the reason for this difference, for example by displacement of the zone by a low angle fault or a sudden change in the direction of the dip.

The assay results show that the highest values are 4.3 g/t Au over the stockwork zone of a width of 7 m.

The mineral potential for the area surrounding the Nuku Prospect seems to be low because the north and south extension of the stockwork zone cannot be traced. Only a weakly altered zone without a Au anomaly continues to the north, while the area to the south is underlain by unaltered basalt lava and alluvium. The sudden disruption of the stockwork zone to the south may imply that a fault has dislocated the zone or that the unaltered basalt lava is younger than mineralization because basalt lavas in the area have been undergone alteration widely and the basalt at the south of the Nuku prospect is unaltered.

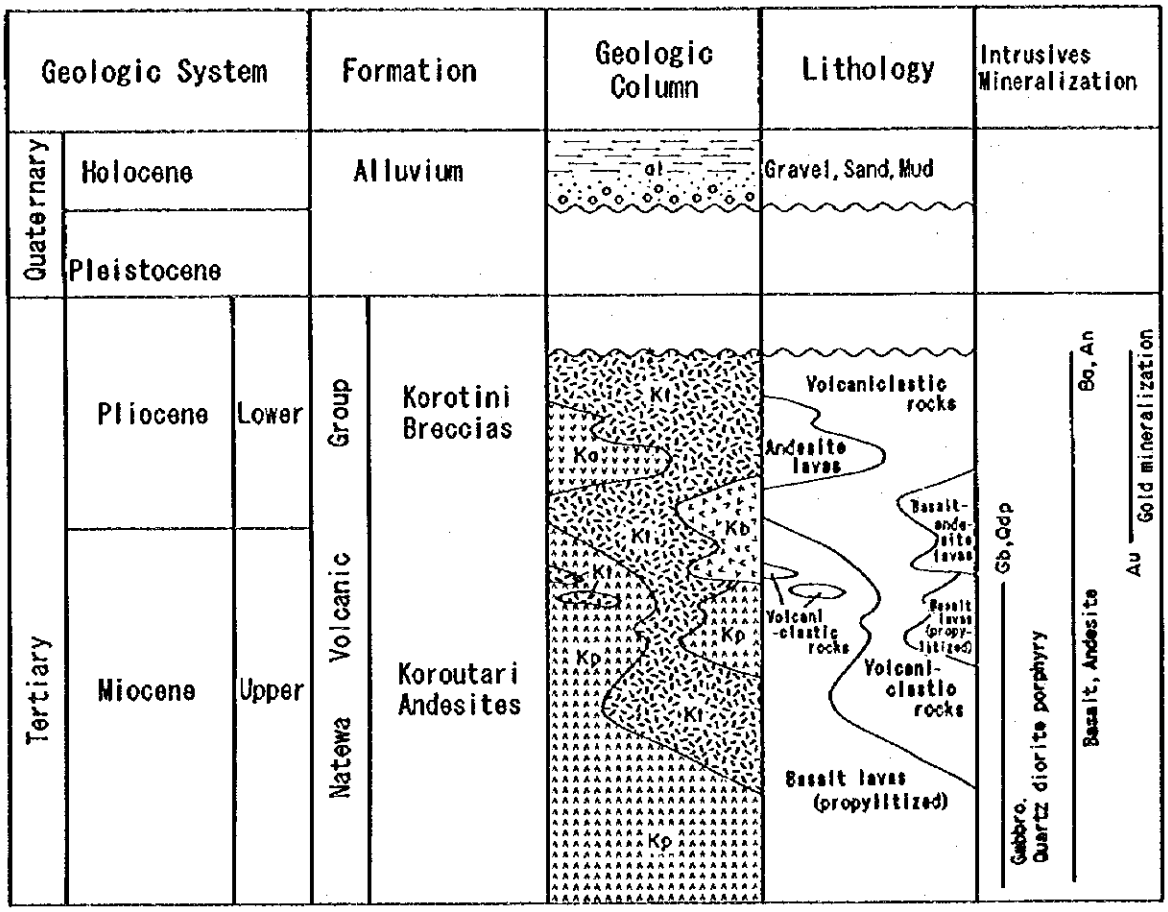

Fig. 2-4-1 Schematic Stratigraphic Columns of the Waimotu Area

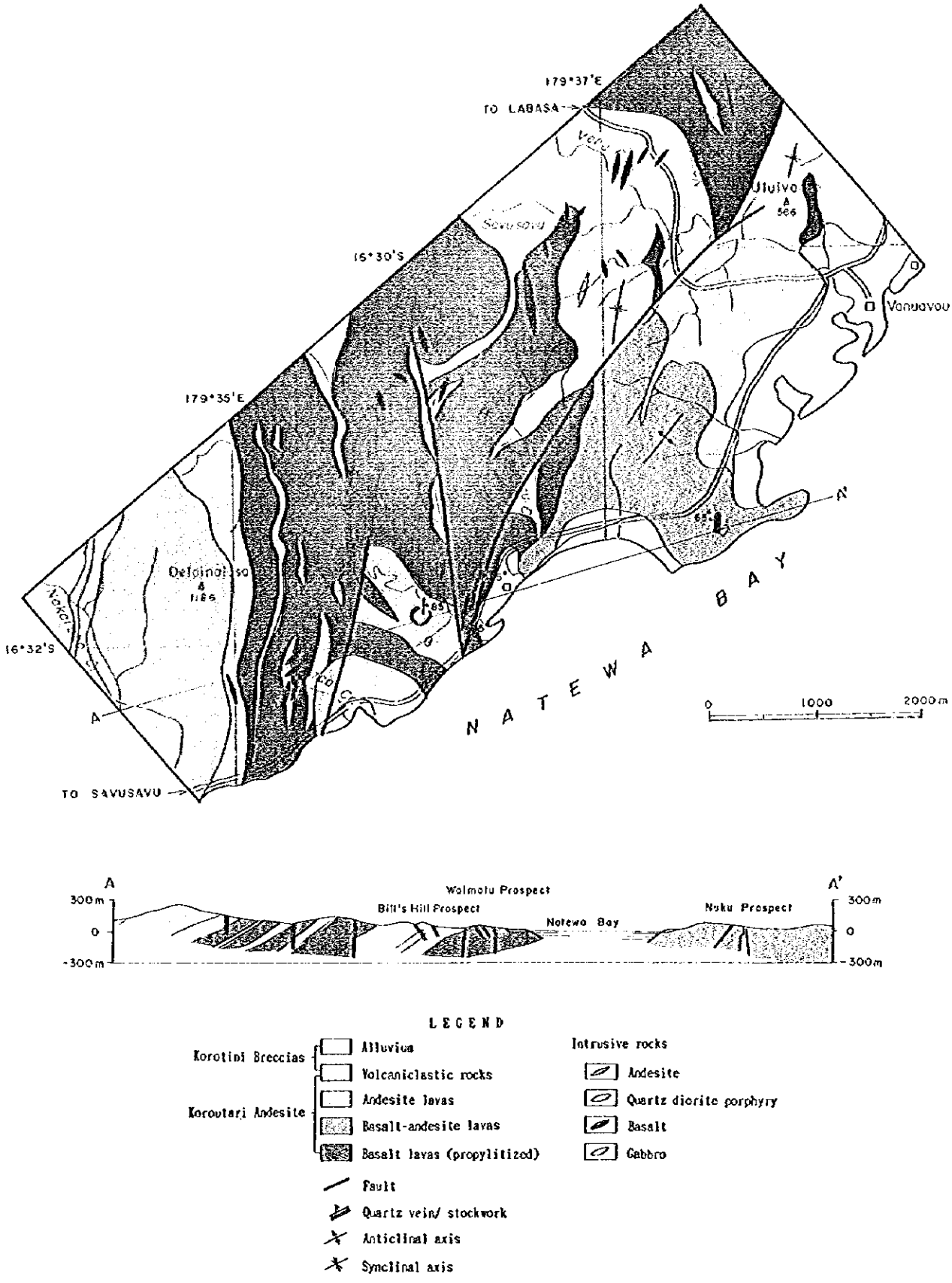

Fig. 2-4-2 Geologic Map of the Waimotu Area

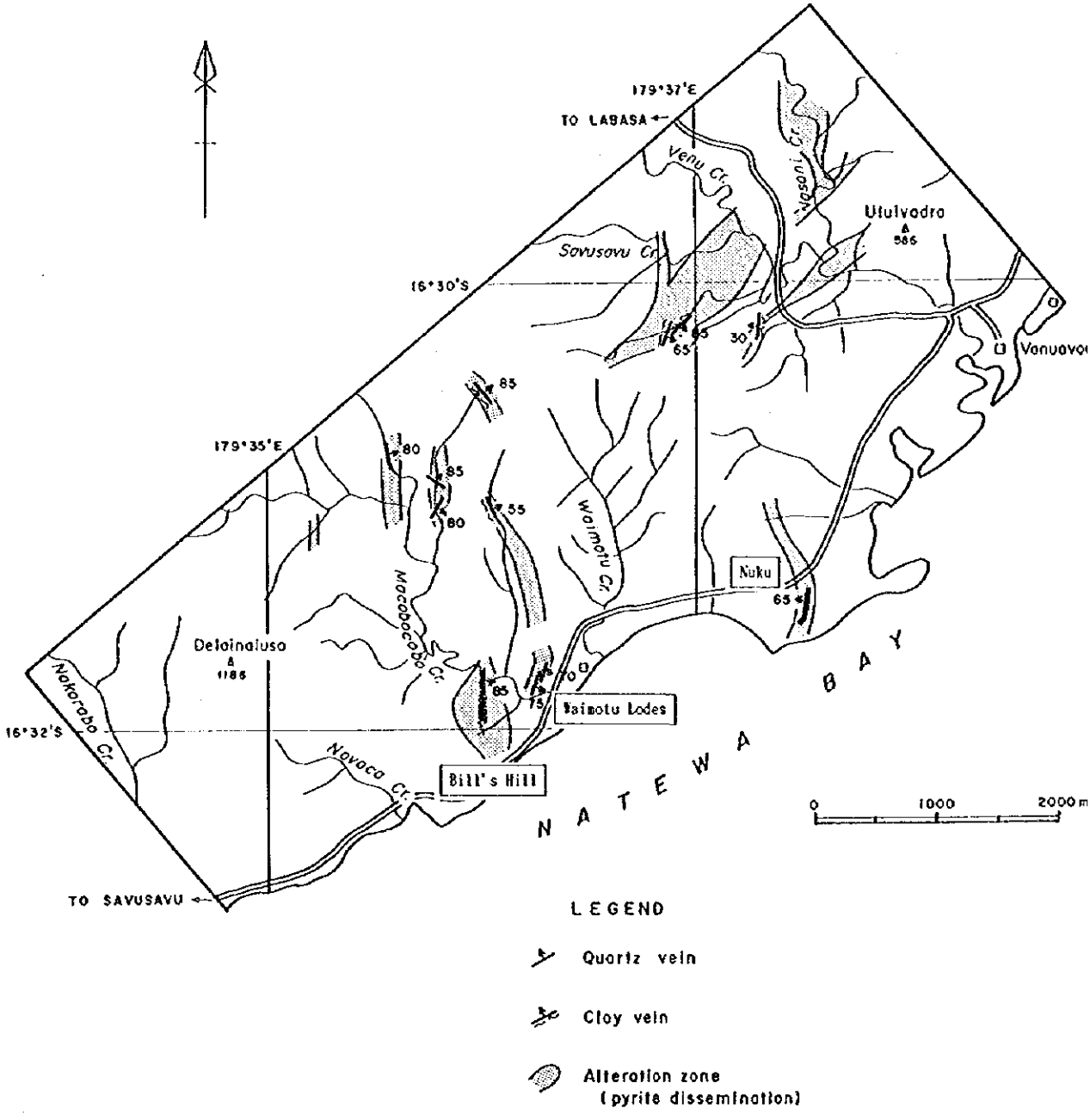

Fig. 2-4-3 Distribution Map of Prospects and Alteration Zones in the Waimotu Area

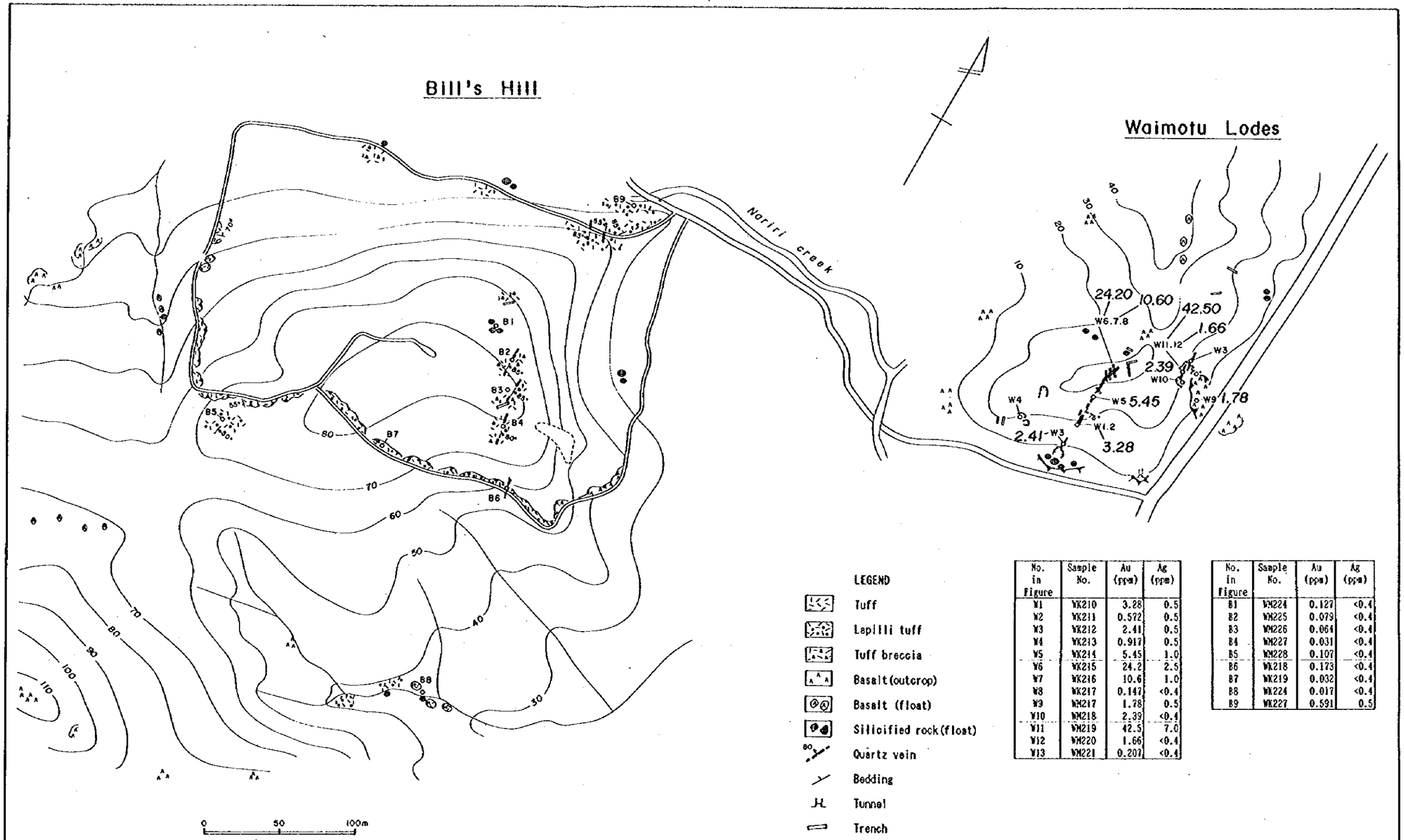

LEGEND

- Tuff
- Lapilli tuff
- Tuff breccia
- Basalt (outcrop)
- Basalt (float)
- Silicified rock (float)
- Quartz vein
- Bedding
- Tunnel
- Trench
- 5.45 Au (g/t)
- Sample No.

No. in Figure	Sample No.	Au (ppm)	Ag (ppm)
W1	WK210	3.28	0.5
W2	WK211	0.572	0.5
W3	WK212	2.41	0.5
W4	WK213	0.917	0.5
W5	WK214	5.45	1.0
W6	WK215	24.2	2.5
W7	WK216	10.6	1.0
W8	WK217	0.147	<0.4
W9	WM217	1.78	0.5
W10	WM218	2.39	<0.4
W11	WM219	42.5	7.0
W12	WM220	1.66	<0.4
W13	WM221	0.207	<0.4

No. in Figure	Sample No.	Au (ppm)	Ag (ppm)
B1	WM224	0.127	<0.4
B2	WM225	0.079	<0.4
B3	WM226	0.064	<0.4
B4	WM227	0.031	<0.4
B5	WM228	0.107	<0.4
B6	WK218	0.173	<0.4
B7	WK219	0.032	<0.4
B8	WK224	0.017	<0.4
B9	WK227	0.591	0.5

Fig. 2-4-4 Detailed Survey Results of the Waimotu Lodes and Bill's Hill Prospect

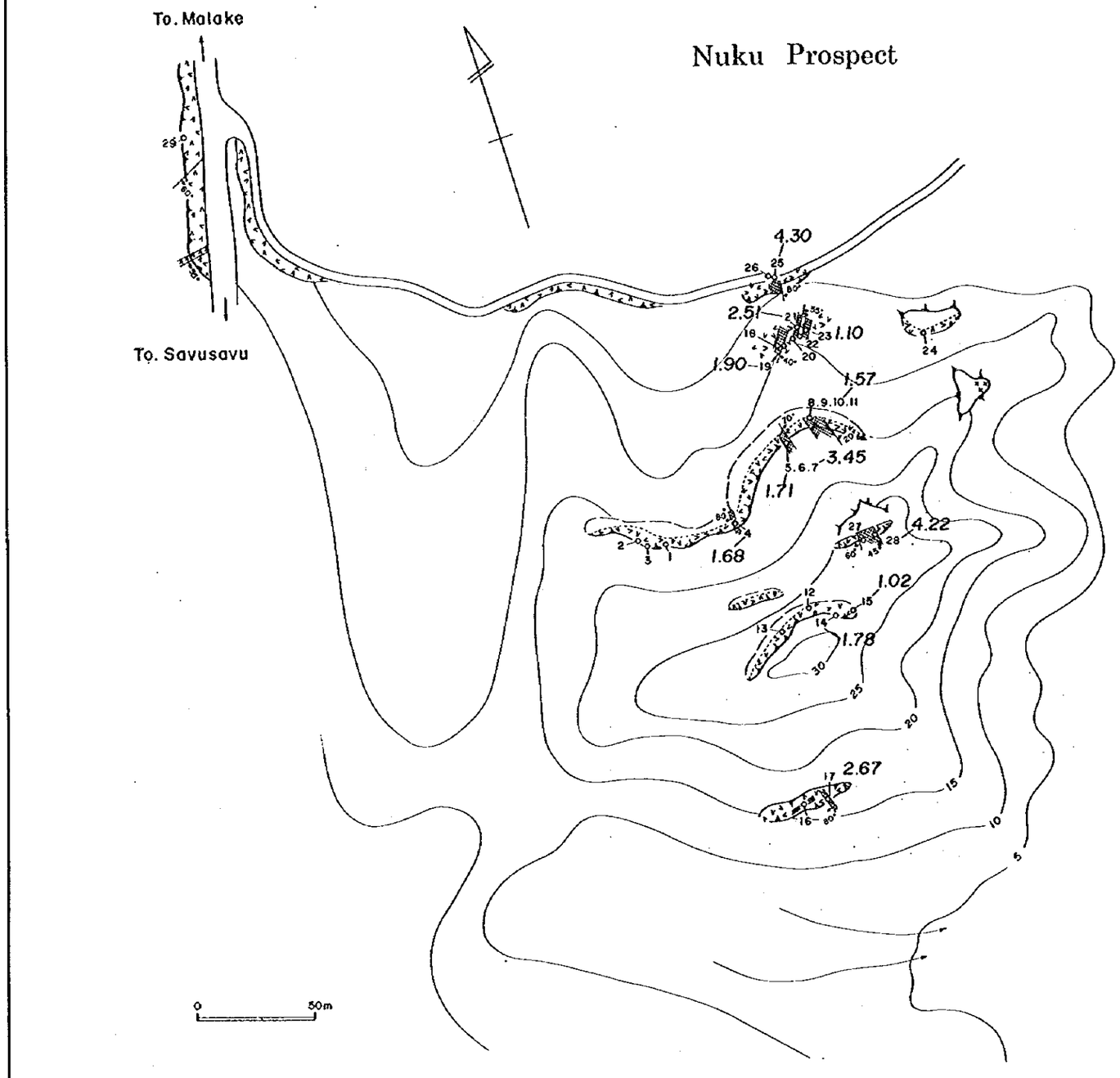

LEGEND

- Andesite~basalt
- Basalt dyke
- Quartz diorite porphyry
- Silica vein
- 2.44 Au (g/t)
- 12 Sample No.

No. in Figure	Sample No.	Au (ppm)	Ag (ppm)
1	WB204	0.02	<0.4
2	WB205	<0.008	<0.4
3	WB206	0.063	<0.4
4	WB207	1.68	<0.4
5	WB208	1.71	1.0
6	WB209	0.641	<0.4
7	WB210	3.45	1.5
8	WB211	0.921	3.0
9	WB212	0.274	<0.4
10	WB213	1.57	1.0
11	WB214	0.637	1.5
12	WB215	0.212	<0.4
13	WB216	<0.008	<0.4
14	WB217	1.78	0.5
15	WB218	1.02	0.5
16	WB219	0.297	<0.4
17	WB220	2.67	0.5
18	WB221	0.598	0.5
19	WB222	1.9	0.5
20	WB223	0.921	1.5
21	WB224	2.51	3.5
22	WB225	0.517	<0.4
23	WB226	1.1	0.5
24	WB228	0.711	1.5
25	WB230	4.3	2.0
26	WB231	0.314	1.5
27	WB234	0.915	<0.4
28	WB235	4.22	1.0
29	WS115	<0.008	<0.4

Fig. 2-4-5 Detailed Survey Results of the Nuku Prospect

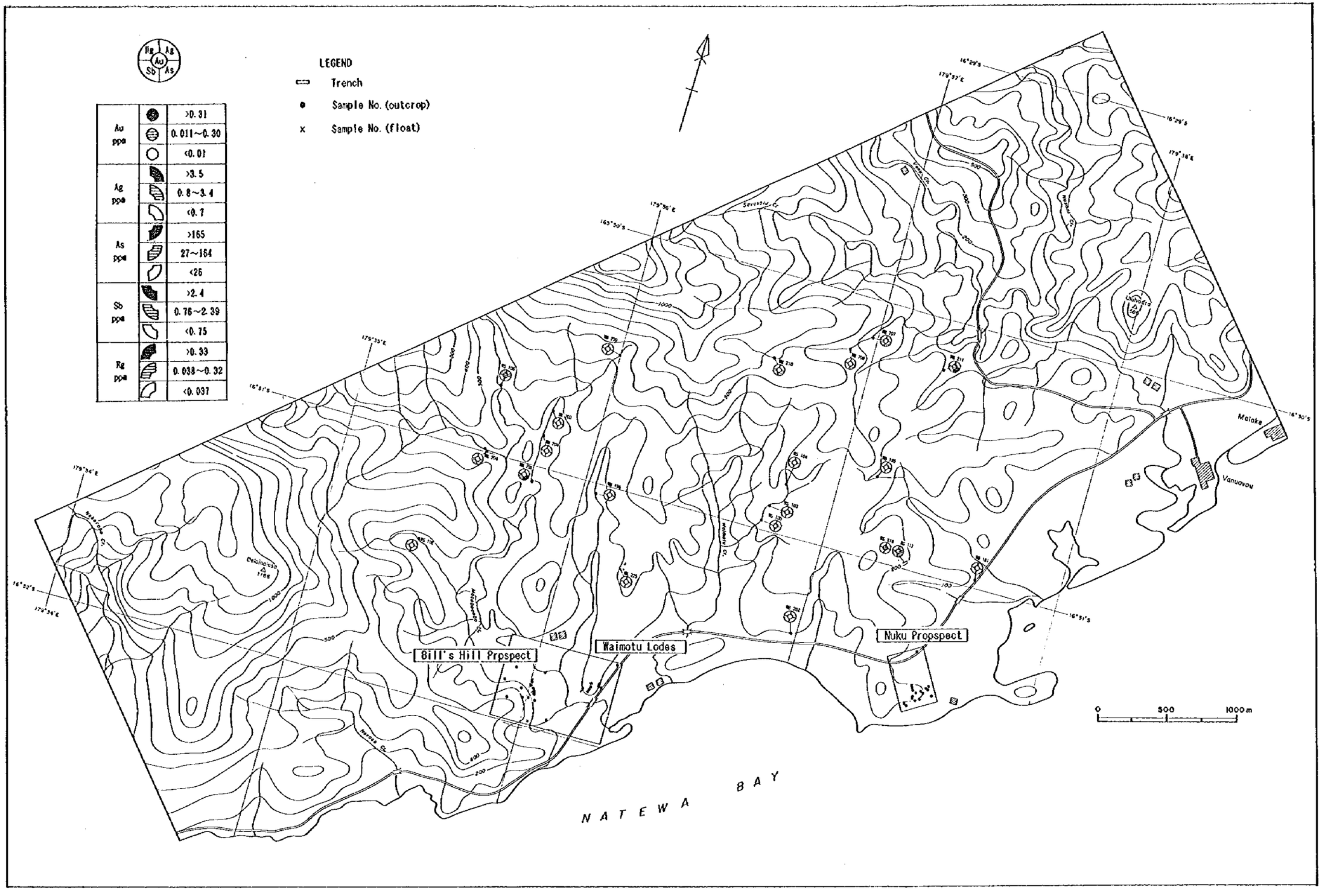

Fig. 2-4-6 Geochemical Survey Results of the Waimotu Area

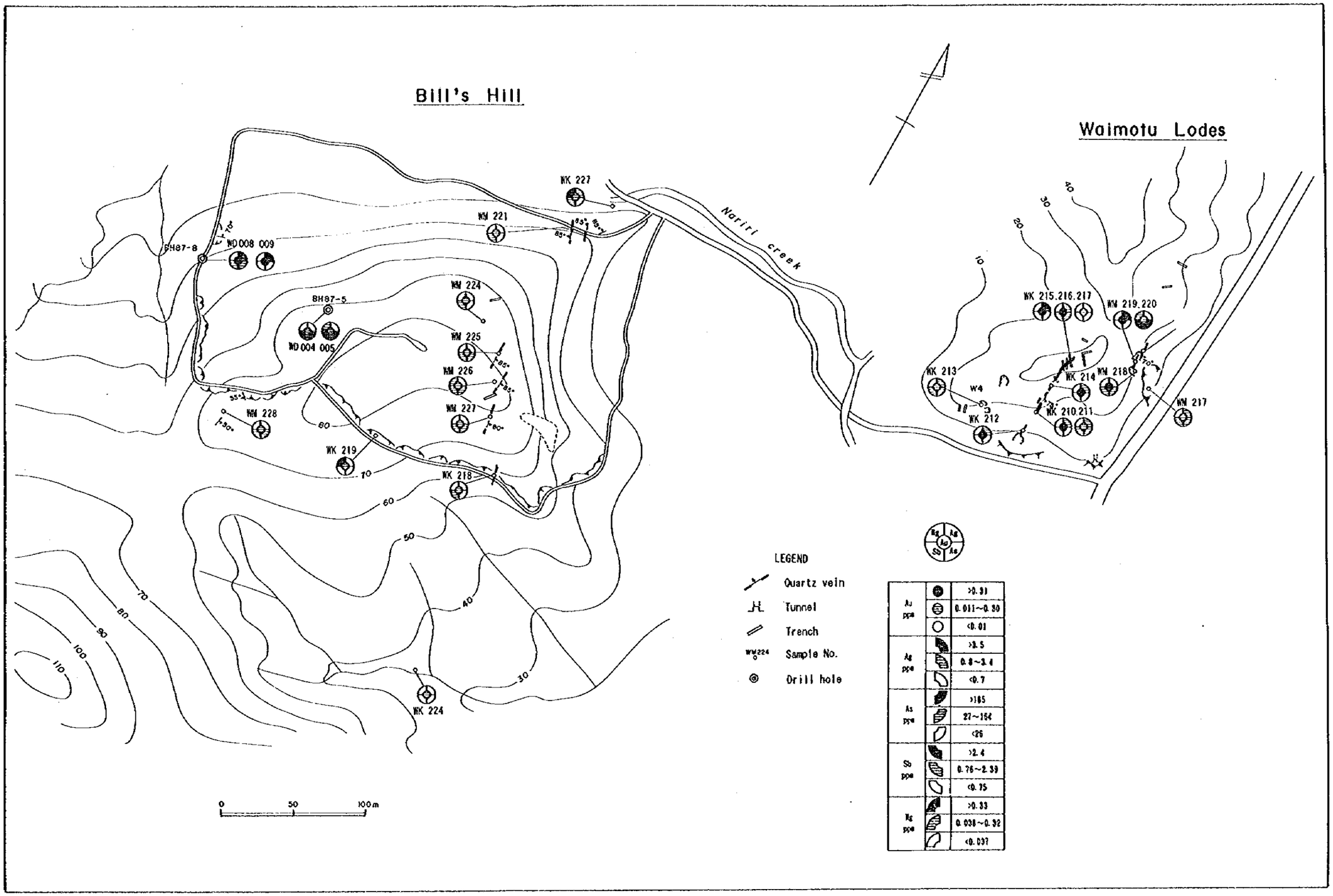

Fig. 2-4-7 Geochemical Survey Results of the Waimotu Lodes and Bill's Hill Area

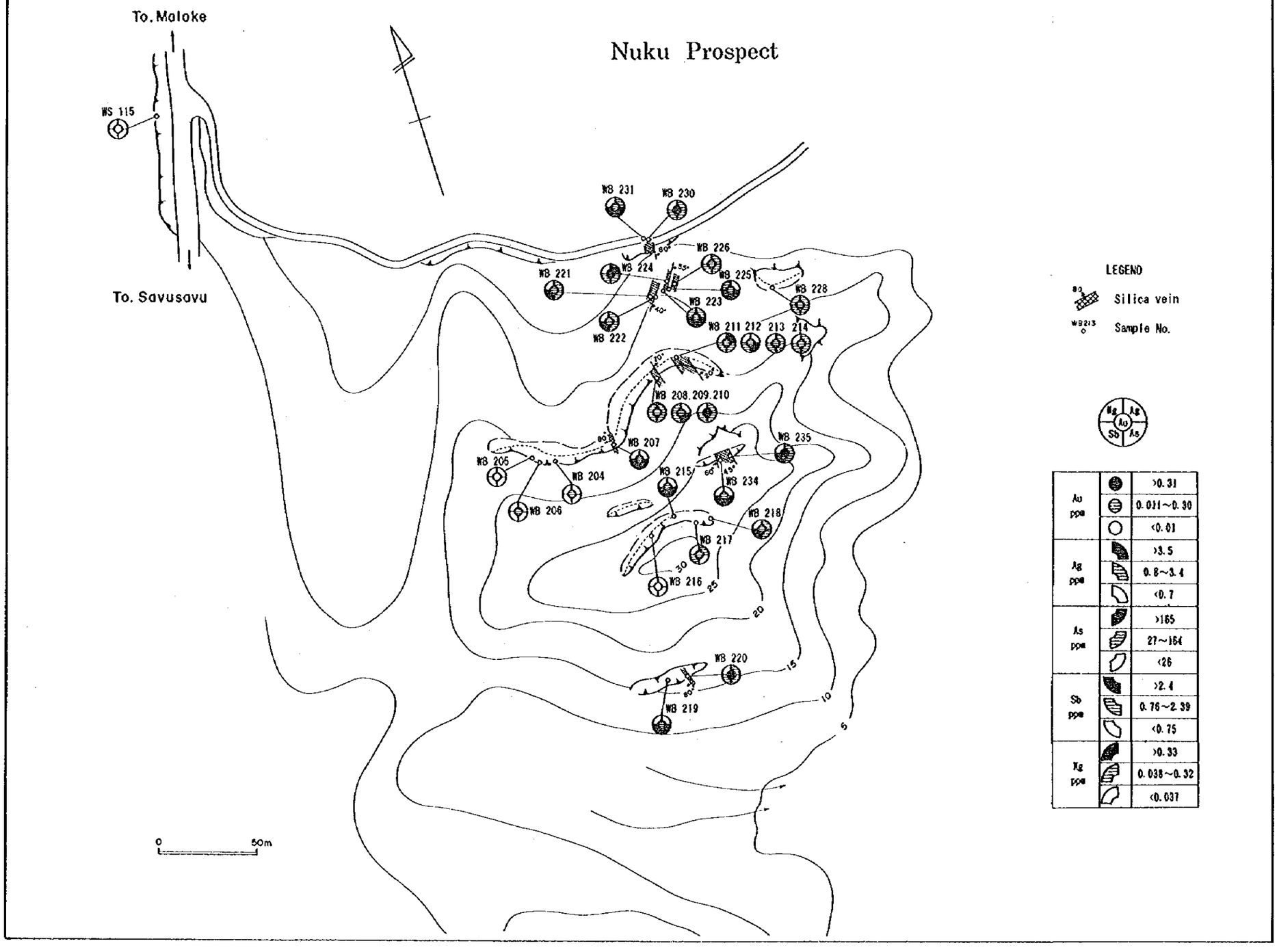

Fig. 2-4-8 Geochemical Survey Results of the Nuku Prospect Area

Waimotu Lodes Prospect

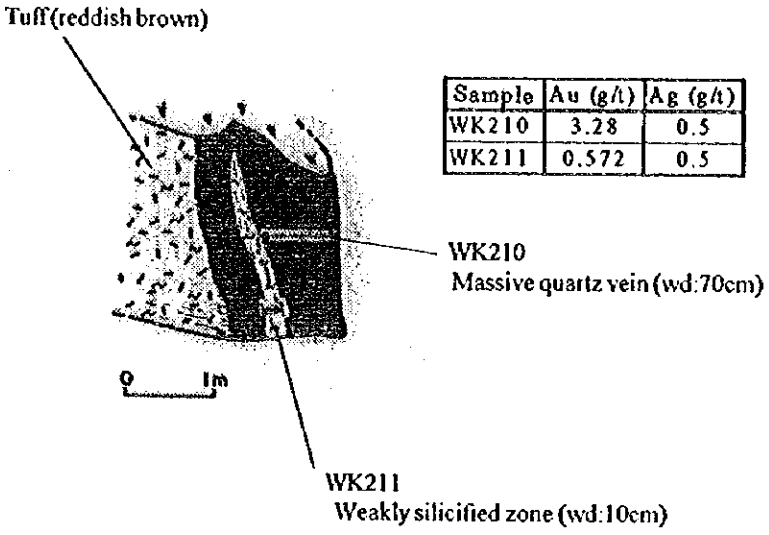

Sample	Au (g/t)	Ag (g/t)
WK210	3.28	0.5
WK211	0.572	0.5

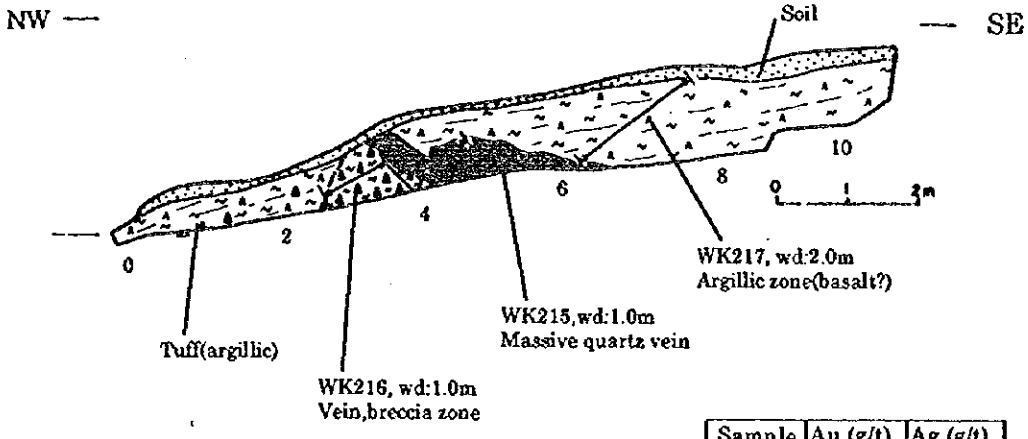

Sample	Au (g/t)	Ag (g/t)
WK215	24.2	2.5
WK216	10.6	1.0
WK217	0.147	<0.4

Fig. 2-4-9 Sketch of Trenches at the Waimotu Lodes

Nuku Prospect

Costean No.2

Sample	width(m)	Au (g/t)	Ag (g/t)
WB221	1.5	0.593	0.5
WB222	1.2	1.900	0.5
WB223	(1.5)	0.921	1.5
WB224	0.7	2.510	3.5
WB225	1.5	0.517	<0.4
WB226	1.5	1.100	0.5

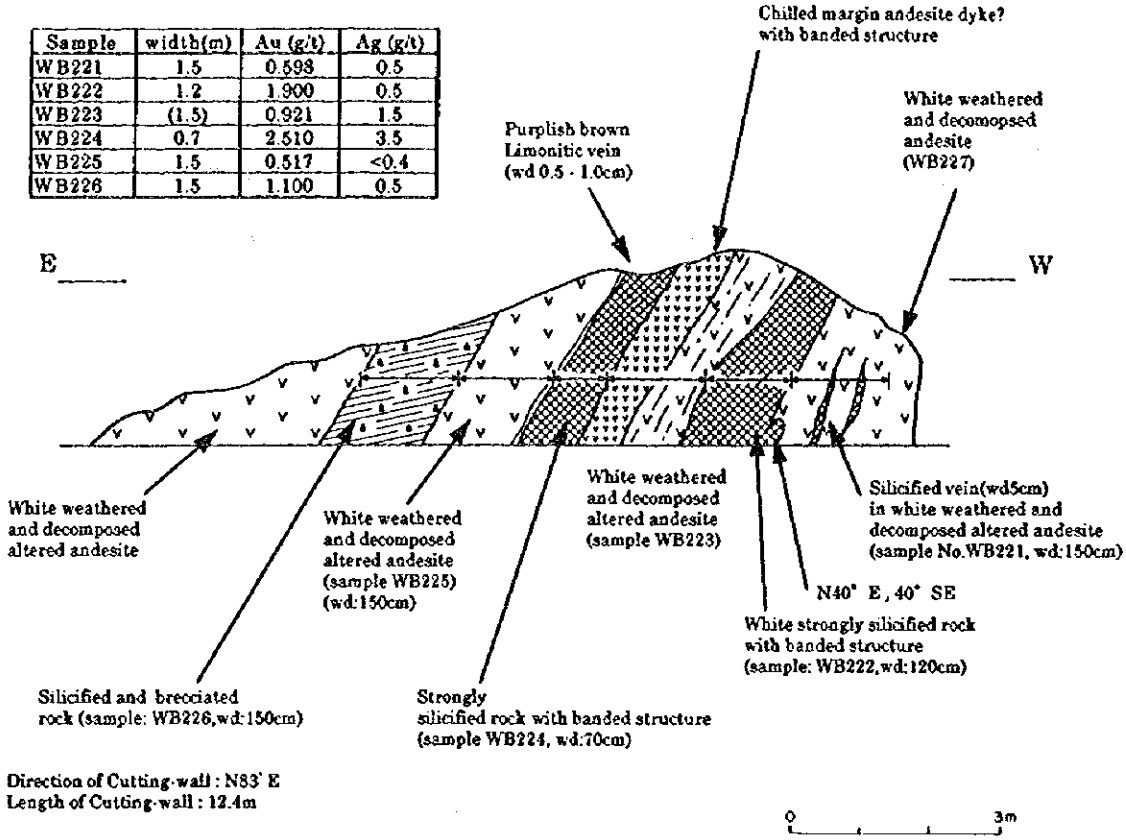

Fig. 2-4-10 Sketch of a Trench at the Nuku Prospect

Figures and Tables

for

Chapter 2 ~ 4

Au

MEAN(M)= .0138615

STANDARD DEVIATION(σ)= .756216

MINIMUM= .005 M+σ= .0790724

MAXIMUM= 12.9 M+2σ= .451067

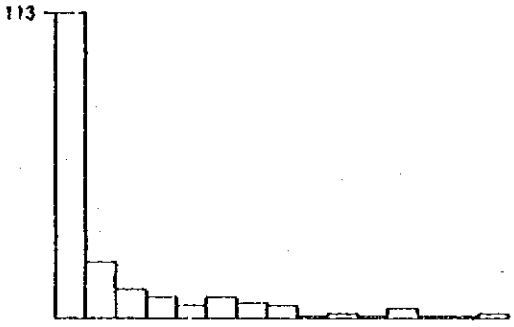

Hg

MEAN(M)= .036973

STANDARD DEVIATION(σ)= .406146

MINIMUM= .007 M+σ= .0941955

MAXIMUM= 92 M+2σ= .239981

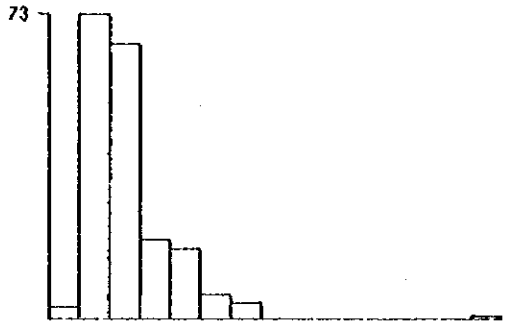

Ag

MEAN(M)= .355778

STANDARD DEVIATION(σ)= .470887

MINIMUM= .2 M+σ= 1.05212

MAXIMUM= 14.9 M+2σ= 3.11138

As

MEAN(M)= 2.61952

STANDARD DEVIATION(σ)= .768409

MINIMUM= .5 M+σ= 15.3685

MAXIMUM= 210 M+2σ= 90.1655

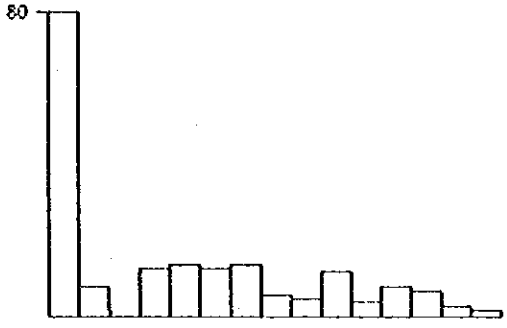

Sb

MEAN(M)= .36043

STANDARD DEVIATION(σ)= .327388

MINIMUM= .25 M+σ= .765965

MAXIMUM= 14.3 M+2σ= 1.62779

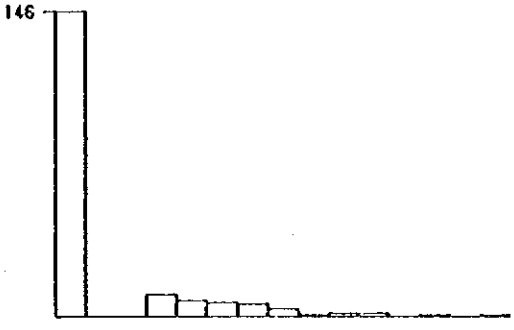

Fig. 2-A-1 Histogram of Assay Values(the Nakoroutari Area)

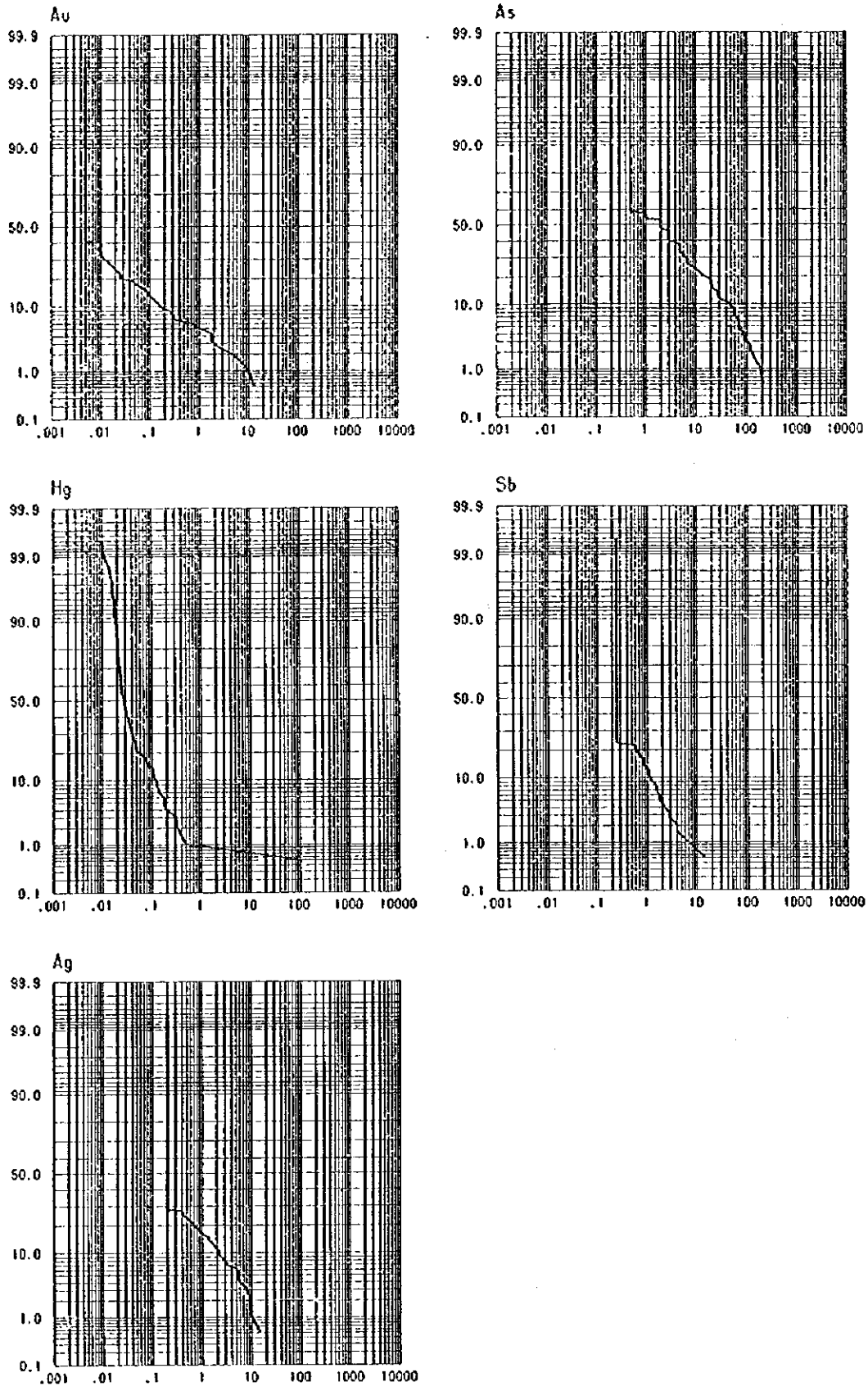

Fig. 2-A-2 Cumulative Frequency Distribution of Assay Values
(the Nakoroutari Area)

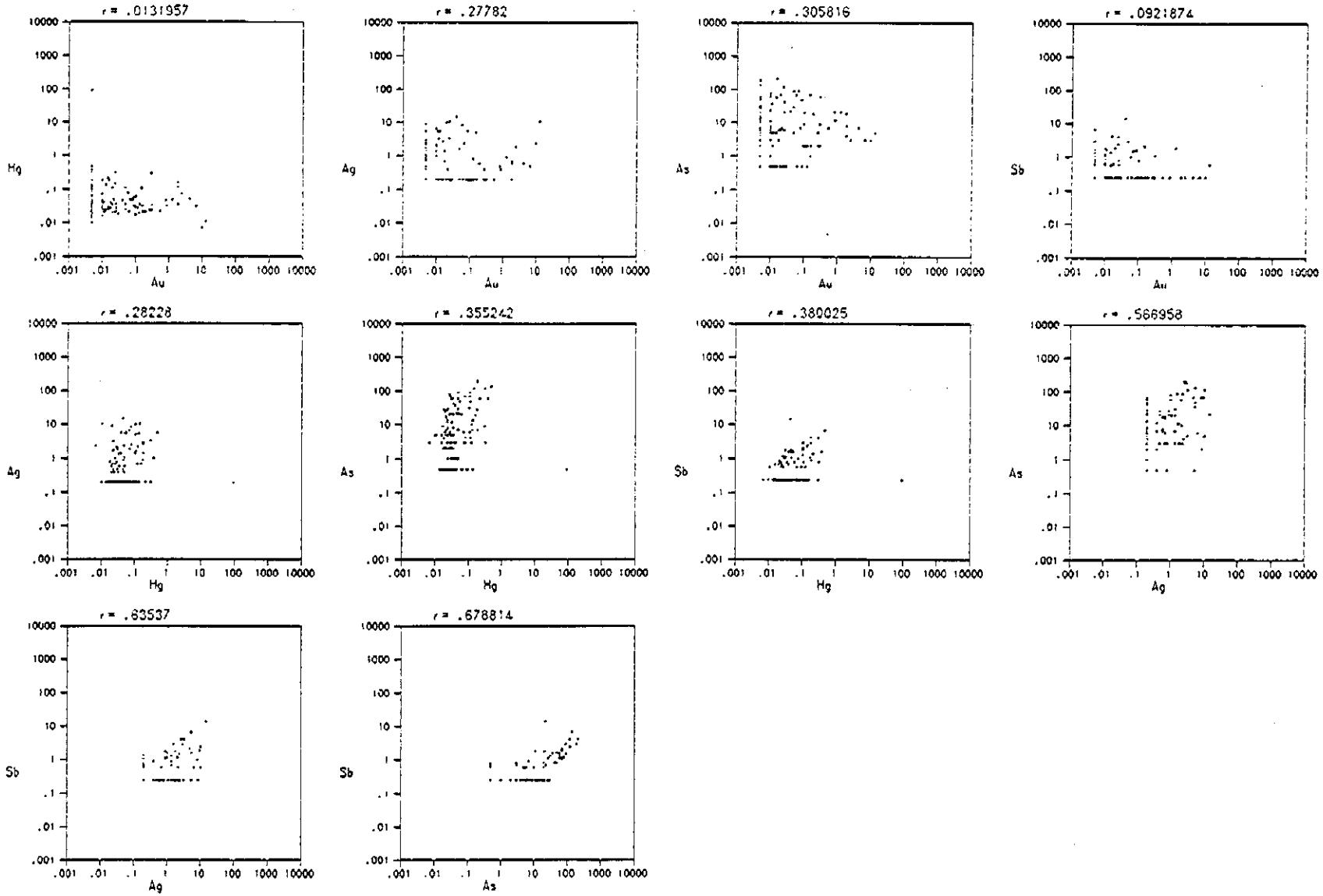

Fig. 2-A-3 Correlation between Elements (the Nakoroutari Area)

Au

MEAN(M)= .035944

STANDARD DEVIATION(σ)= .929507

MINIMUM= .005 M+σ= .305586

MAXIMUM= 16.1 M+2σ= 2.59801

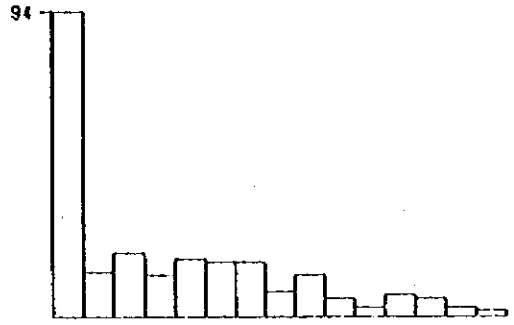

Hg

MEAN(M)= .0370741

STANDARD DEVIATION(σ)= .47269

MINIMUM= .006 M+σ= .110093

MAXIMUM= 3.16 M+2σ= .326928

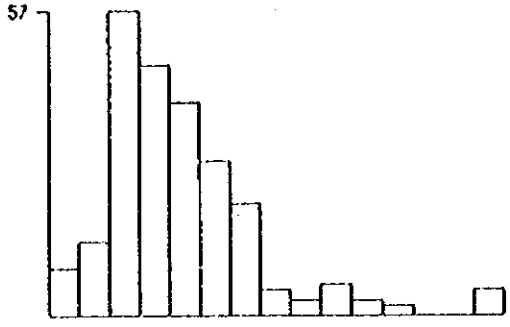

Ag

MEAN(M)= .699243

STANDARD DEVIATION(σ)= .703515

MINIMUM= .2 M+σ= 3.53299

MAXIMUM= 151 M+2σ= 17.8508

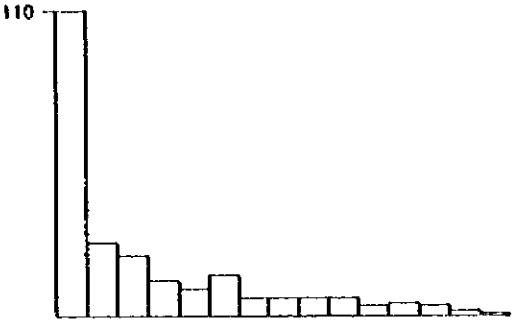

As

MEAN(M)= 25.8108

STANDARD DEVIATION(σ)= .806642

MINIMUM= .5 M+σ= 165.365

MAXIMUM= 1590 M+2σ= 1059.46

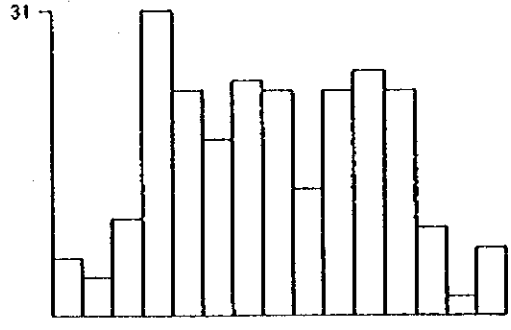

Sb

MEAN(M)= .752603

STANDARD DEVIATION(σ)= .497802

MINIMUM= .25 M+σ= 2.36793

MAXIMUM= 28.3 M+2σ= 7.45024

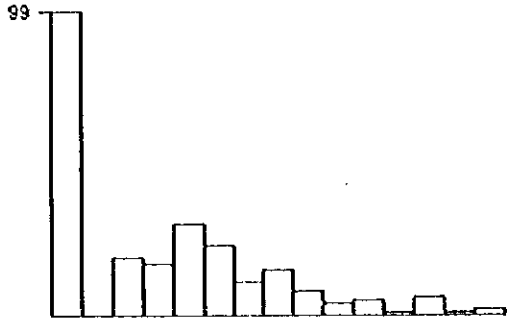

Fig. 2-A-4 Histogram of Assay Values(the Dakuniba Area)

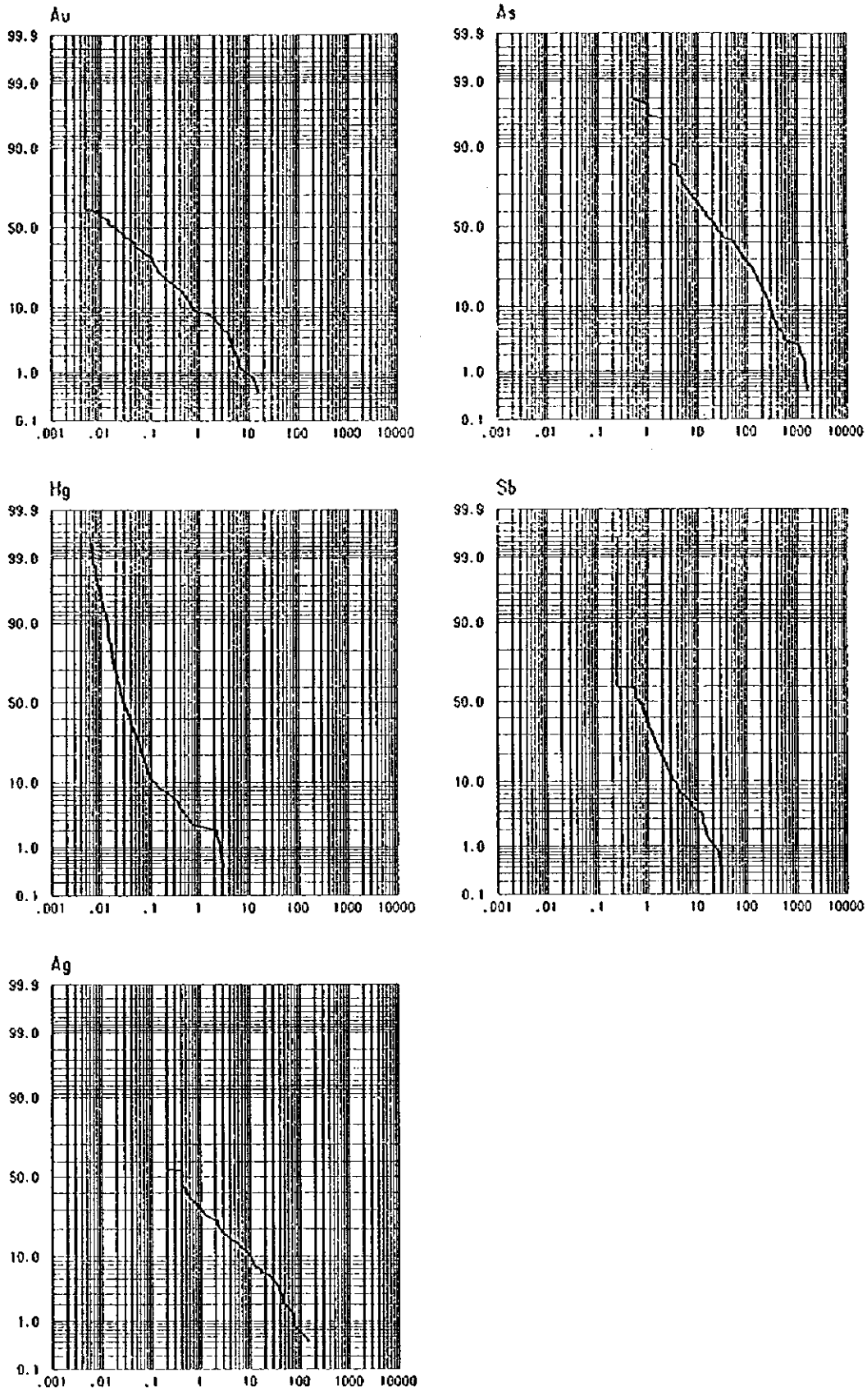

Fig. 2-A-5 Cumulative Frequency Distribution of Assay Values (the Dakuniba Area)

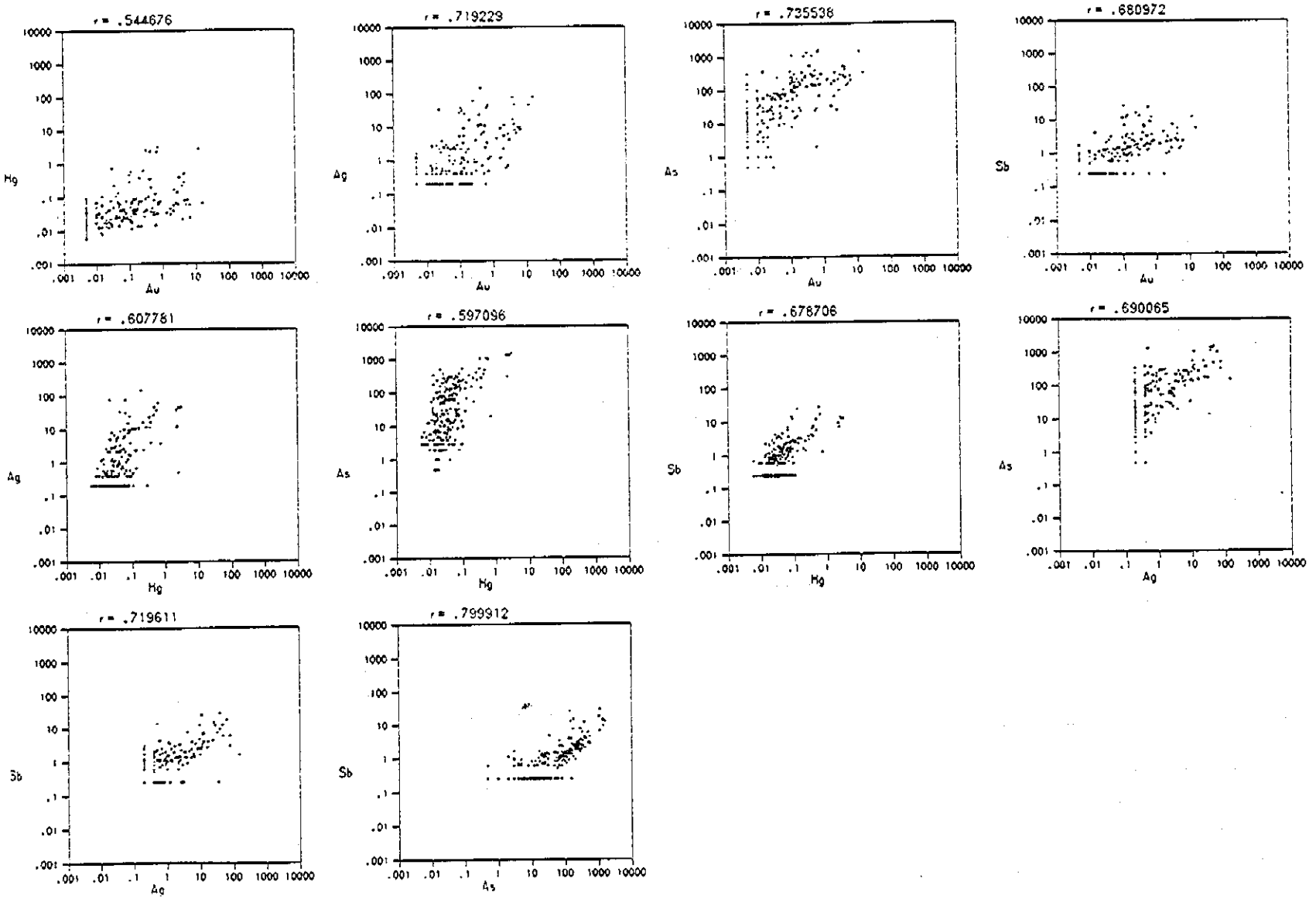

Fig. 2-A-6 Correlation between Elements (the Dakuniba Area)

Au

MEAN(M)= .156692

STANDARD DEVIATION(σ)= 1.14397

MINIMUM= .004 M+σ= 2.18281

MAXIMUM= 42.5 M+2σ= 30.4079

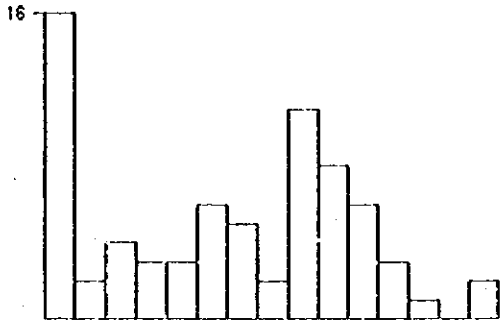

Hg

MEAN(M)= .014362

STANDARD DEVIATION(σ)= .495827

MINIMUM= .0025 M+σ= .0449616

MAXIMUM= .257 M+2σ= .140757

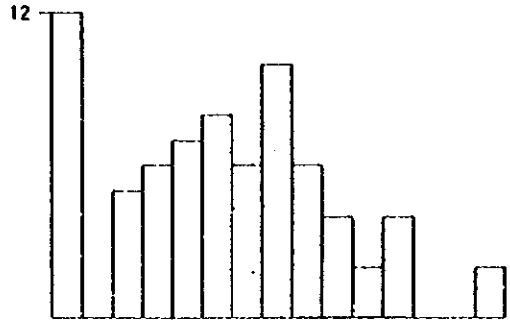

Ag

MEAN(M)= .376759

STANDARD DEVIATION(σ)= .391602

MINIMUM= .2 M+σ= .928251

MAXIMUM= 7 M+2σ= 2.28701

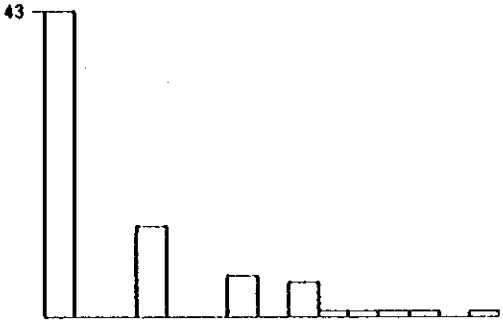

As

MEAN(M)= 18.5797

STANDARD DEVIATION(σ)= .719047

MINIMUM= .5 M+σ= 97.2937

MAXIMUM= 460 M+2σ= 509.485

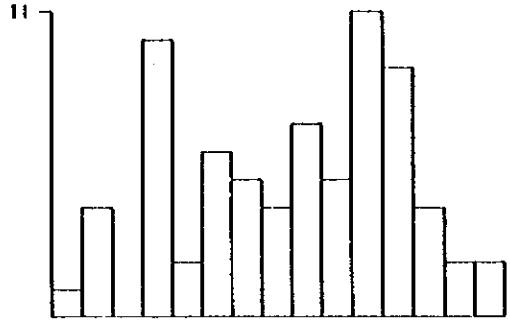

Sb

MEAN(M)= .656245

STANDARD DEVIATION(σ)= .314184

MINIMUM= .25 M+σ= 1.35285

MAXIMUM= 2.4 M+2σ= 2.78891

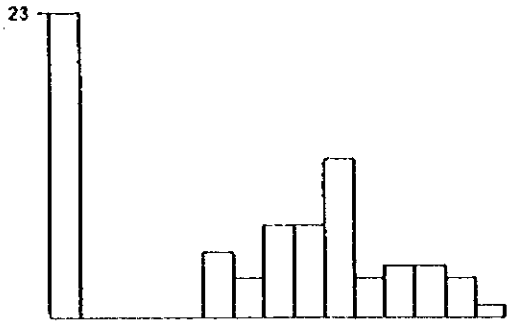

Fig. 2-A-7 Histogram of Assay Values(the Waimotu Area)

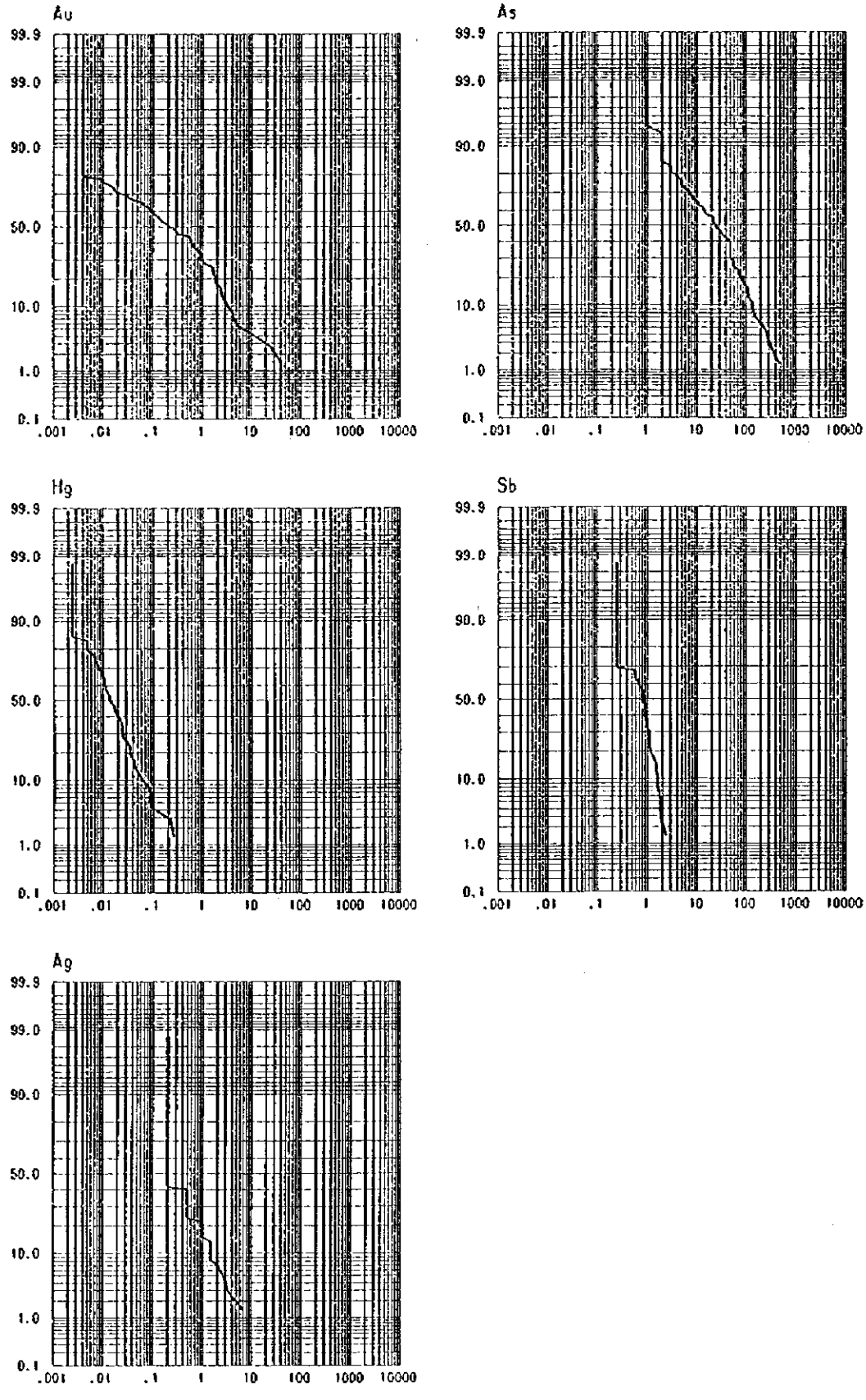

Fig. 2-A-8 Cumulative Frequency Distribution of Assay Values (the Waimotu Area)

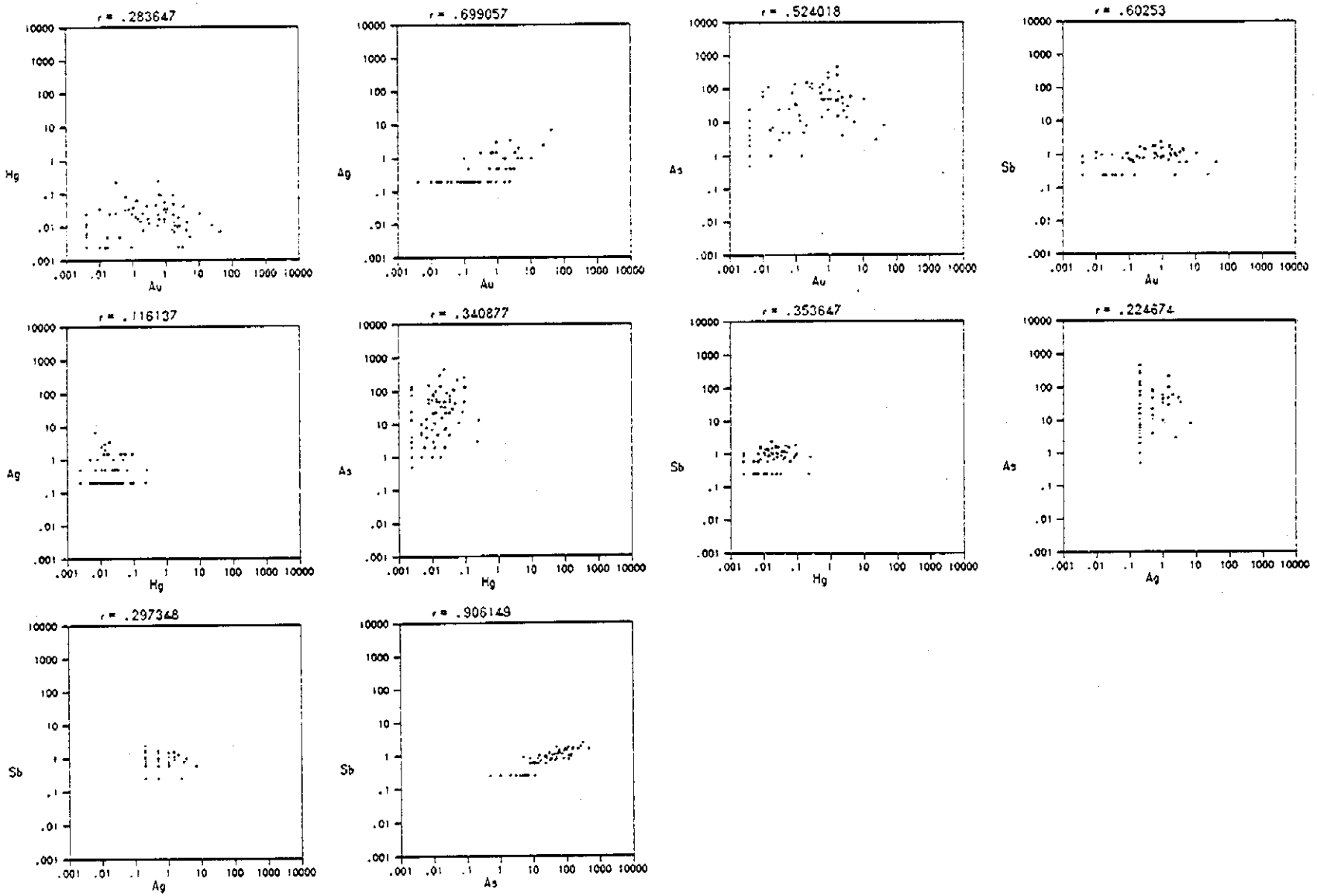

Fig. 2-A-9 Correlation between Elements (the Waimotu Area)

Tables 2-A-1 Results of Microscopic Observation of Thin Section

Sample No.	Rock type	Texture	Phenocryst						Groundmass (including microphenocryst)									Alteration
			ol	cpx	opx	pl	op	others	ol	cpx	opx	hb	pl	kf	qz	gl	op	others	
NS008	lapilli tuff	clastic							(△)				◎		·	◎	○		ol totally→idd, gl partly→carb +smec
NS045	basalt	porphyritic	(·)	◎		◎				○	·		○			◎	○		ol→idd
NM003	basalt	porphyritic	(○)	◎		◎				○			◎			○	○		ol→idd
NM004	basalt	porphyritic	(△)	◎	△	◎	△		(·)	·			◎			◎	○		ol→idd, opx→smec
NK009	andesite	glomeroporphyritic			(△)	◎				○	(○)		◎			◎	○		opx→idd
NK057	tuff breccia	clastic	(○)			◎	○						◎			◎	○		ol→smec, pl partly→carb, gl→druse patly→epi
NK060	andesite	aphyric		△	(△)	△					(△)		○			◎	○		opx→smec
NB005	andesite	porphyritic		(○)	(△)	◎	○			(△)	(△)		◎			◎	○		pl partly→carb, cpx→carb, opx→carb
NB035	basalt	porphyritic	(○)	○	△	○				○	△		◎			(◎)	○		ol→smec, gl→smec
NB084	basalt	glomeroporphyritic	(○)			◎				○			◎			○	△		ol→smec
NB085	basalt	porphyritic	(○)	○		◎	○			○			◎			◎	△		ol→smec
DM077	tuff	clastic		◎		○	·			·			◎		○	(◎)			gl→smec+chl+epi
DM089	picrite	porphyritic	◎	○		△	·		△	◎			○			◎	·		ol→smec
DK069	andesite	porphyritic		(○)		◎	·			△			○			(◎)			opx→smec, gl→smec
DK075	basalt	porphyritic	(○)	◎		○							◎			(◎)	○		ol→carb, pl partly→carb+alb, gl→smec
DK084	tuff breccia	clastic	(◎)	◎						△			◎			(◎)	·		ol→smec, gl→smec, druse→ca qz+carb
DK145	basalt	porphyritic	(◎)	◎		△				○			◎			(◎)	·		ol→smec, gl→smec, druse→smec+carb+epi
DB122	basalt	porphyritic	(◎)	◎		○				○			◎			(◎)	·		ol→smec, gl→smec
DB131	basalt	glomeroporphyritic	(○)			○			(○)	○			◎			◎	○		ol→smec, druse→carb pool
DB136	basalt	porphyritic	(○)	◎		◎			(○)	◎			◎			◎	·		ol→smec
DS060	picritic basalt	porphyritic	◎	○		△	·			○			◎			◎	·		ol→smec
WB184	basalt	porphyritic	(△)	◎	△	◎	△			○			○			◎	·		ol→smec
WB191	basalt	porphyritic				○			(△)	(○)			◎			(◎)			carb vein, ol→smec+carb, cpx→carb, pl partly→carb, gl→ clay
WB192	basalt	porphyritic	○	△	○	◎				△	△		○			○	·		
WK207	basalt	porphyritic	(○)		△	◎				○			◎			◎	·		ol→smec, pl partly→carb
WK223	andesite	glomeroporphyritic		○	○	◎	○			△	○		◎			◎	·		opx→clay
WM201	lapilli tuff	clastic		△		○				△			◎			◎	·		pl partly→alb
WM206	tuff breccia	clastic		△		○		qz ·		△			◎			◎	·		
WM209	andesite	porphyritic				○	·						◎	○		◎	·	ap ·	pl partly→alb
WS113	andesite	porphyritic		◎	△	◎	△			·	△		◎			(◎)	·		gl→smec, druse→qz+smec
ND018	andesite	porphyritic		(○)		◎	·			(△)			◎			◎	·		cpx→chl, druse→chl+epi, gl partly→carb

◎ abundant
○ common
△ small
· rare
() totally decomposed

ol=olivine, cpx=clinopyroxene, opx=orthopyroxene, pl=plagioclase, op=opaque minerals, qz=quartz, hb=hornblende, kf=K-feldspar
gl=glass or microcrystalline aggregate, ap=apatite, carb=carbonate, smec=smectite, idd=iddingsite, epi=epidote, ca=calcedonic
chl=chlorite

Tables 2-A-2 Results of Microscopic Observation of Thin Section

Sample No.	Rock type		Ore minerals						Gangue minerals										
	Name	Texture under microscope	Py	Cha	Sph	Aca	Gal	others	qz	kf	pl	goe	clay	smc	apa	carb	bar	ser	others
NB034	Quartz vein		△				·		◎		○		△		·	△			epi(·)
NB099	Quartz vein	Dolomite rock						chcc(·)				△	△			◎			
NK033	Quartz vein	Quartz vein		·	△		·		◎			·	·						
NK042	Quartz vein	Quartz vein	·	·					◎			·	△				·		
NM068	Quartz vein	silicified tuff breccia							◎	○		△					△		hema(·)
NM071	Quartz vein	quartz vein	·				·		◎			·					·		
DK117	Quartz vein	silicified volcanic breccia	·						◎			△	△				△	·	
DK127	Quartz vein	silicified volcanic breccia							◎		△	△					△		
DK154	Quartz vein	silicified volcanic breccia	△	·					◎		○	△						△	
DB110	Quartz vein	silicified volcanic breccia	△		·		·		◎	◎		△							
DB111	Quartz vein	silicified tuff							◎	○		△					△	△	
DB118	Quartz vein	silicified volcanic breccia	△	·			·		◎	○							·	·	
DB119	Quartz vein	silicified volcanic breccia	△	·	·		·		◎	△		·							
DB148	Quartz vein	silicified volcanic breccia	△		·	·	·	Ars(·)	◎	◎	△	·							
DB153	Quartz vein	silicified volcanic breccia	△	·					◎	○		·							
DM102	Quartz vein	carbonatised tuff	·						◎	△	○		△			◎			
DM125	Quartz vein	silicified tuff	○				·		◎			△	△						chl(·), Pyro(△)
DM131	Quartz vein	quartz aggregate					·		◎						·				
WB218	Quartz vein	silicified tuff breccia							◎				△	△					
WB222	Quartz vein	silicified tuff	·			·			◎	△		·							
WB231	Quartz vein	opal	△									△	△						opal(◎)
WK210	Quartz vein	silicified tuff	·						◎	△									
WK212	Quartz vein	silicified tuff breccia	·						◎	·		·							
WK214	Quartz vein	silicified tuff	·						◎	△		·							
WK218	Quartz vein	silicified tuff							◎			·	△						
WK224	Quartz vein	silicified tuff		·					◎			·							
WM217	Quartz vein	silicified tuff							◎			·	·						
WM219	Quartz vein	silicified tuff breccia							◎			·	·						
WM221	Quartz vein	quartz vein							◎			·	△	△					
WS105	Quartz vein	silicified tuff breccia	·						◎		○	·		△					cpx(·)
WD013	Quartz vein	altered quenched basalt	○						△		◎		·	◎					

Py=pyrite, Cha=chalcopyrite, Sph=sphalerite, Aca=acanthite, Gal=galena, chcc=chalcocite, Ars=arsenopyrite

qz=quartz, kf=K-feldspar, pl=plagioclase, goe=goethite, clay= clay minerals, smc=smectite, apa=apatite, cb=carbonate
ba=barite, epi=epidote, hema=hematite, ser=sericite, chl=chlorite, pyro=pyrolusite, cpx=clinopyroxene
◎= abundant, ○=common, △ =small, · = rare

Tables 2-A-3 Results of Chemical Analysis (1)

Sample No.	Field description	Clay mineral					Silica		Feldspar		Zeolite						Carbonate		Sulfate			Others					
		Sm	Ch	Ka	Se	Tr	Cr	Qz	Pl	Kf	Cb	St	Wa	La	Na	An	Ca	Do	Al	Ja	Gy	Ap	Py	Mg	He	Gb	Others
NS 010	Lapilli tuff	△		·				○		○												○	·				
NS 011	Lapilli tuff	△						◎		○										·							
NS 012	Tuff(light gray)	△		·				○		○										·							
NS 013	Lapilli tuff			△				◎									○						○				
NS 022	Andesitic volcanic breccia			·			◎																△				
NS 028	Clay-quartz vein			·				◎											·								
NS 033	Lapilli tuff			△				○																			
NS 035	Lapilli tuff			△			○	△																			
NS 036	Volcanic breccia			·			◎																△				
NS 049	Andesite?	△																									
NS 051	Lapilli tuff	○						·																			
NM 007	Basaltic andesite(pale green)	○						·													· ?			△			
NM 010	Porphyritic basalt			·			○																				
NM 016	Coarse tuff							○		○					·								○				
NM 021	Tuff(dark green)	○							○								△										
NM 034	Basalt(pale green)	○						△		△							△										
NM 018	Coarse tuff		△					◎	○	△																	
NK 022	Silicified, argillic rock		△					◎		○																	
NK 036	Lapilli tuff		△					◎		○																	
NK 038	Silifified rock		△					◎		△																	
NK 039	Lapilli tuff~tuff breccia		○					◎		△																	
NK 040	Lapilli tuff(clayey)	○						○		○																	
NK 043	Silicified rock	△						◎		·															·		
NK 050	Lapilli tuff	○		·																							△Te?
NK 052	Lapilli tuff	○							△																		
NK 054	Lapilli tuff	○																									
NK 057	Tuff breccia(greenish)	○	△					◎	○	△			△				○						·				
NK 058	Tuff(clayey)	○		·																							
NB 012	Argillic rock			△				◎											· ?				·				
NB 016	Argillic rock																										
NB 019	Argillic rock			△				◎															·				
NB 021	Argillic rock			△			◎																·				
NB 022	Weakly argillic basalt	△							◎	○													·				
NB 026	Argillic rock	·		△			○	○																			
NB 030	Argillic volcanic breccia			△			◎																·				· Te?
NB 031	Decomposed volcanic breccia			△																			·				
NB 034	Silicified zone /quartz vein	◎						◎	△												△		·		·		
NB 043	Argillic rock			○			○	○																	·		
NB 053	Argillic rock			○				◎											·				·		·		

Tables 2-A-3 Results of Chemical Analysis (2)

Sample No.	Field description	Clay mineral					Silica	Feldspar		Zeolite						Carbonate		Sulfate			Others				
		Sm	Ch	Ka	Se	Tr	Qz	Pl	Kf	Cb	St	Wa	La	Na	An	Ca	Do	Al	Ja	Gy	Ap	Py	Mg	He	Gb	Others
NB 058	Argillic rock			△			○	○														·		·		
NB 090	Argillic altered volcanic breccia			△		◎		△														△				
ND 020	Andesitic vocanic breccia		△					○		·	·															
DS 086	Clay zone (0.3m)	○						◎	△																	
DS 068	Clay zone (0.1m)	△						◎																		· Sp?
DS 080	Clay zone (0.2m)				·			◎	·																	
DS 084	Clay zone (0.25m)	△						◎	△																	
DS 090	Brecciated zone	△	△					◎	△													△				
DS 096	Silicified, brecciated rock	·						◎	○													·				
DM 080	Argilli rock		·					○	◎													○				
DM 081	Argillic basalt	△	△					◎	·													○				
DM 086	Bleached (basalt?)	○						○	○													△	△			
DM 095	Silicified, argillic rock		○					○	○	○												○				
DM 103	Quartz, argillic zone (5cm)			·				◎									◎									· Ma?
DM 106	Argillic zone with quartz veinlets	○		△				◎									◎					·				
DM 179	Argillic zone (2m)	△	·					◎	○																	
DM 187	Argillic zone (1m)	○	△					◎	·													△				
DM 188	Argillic zone (3m)	△						◎	△													·		·		
DM 191	Tuff breccia (2m)	○		·					○													△				
DK 073	Quartz vein		△					◎	△							◎						·		·		
DK 074	Clay	○	△					○	△								○									
DK 076	Weakly silicified rock	○	△					◎	· ?							○						·				
DK 078	Strongly argillic rock		○					○	○							△						·				
DK 082	Weakly argillic rock		○					◎	· ?							◎						△				
DK 083	Basaltic tuff breccia(light blue)	△					△	△	·							◎	◎					·				
DK 086	Weakly silicified rock		△					◎	·	△						△						△				
DK 088	Breccia zone in basalt		○		○			◎														·				
DK 133	Silicified rock(float)	○	△		△			◎								◎										
DB 112	White clay	△						◎	○																	
DB 114	Leached (clay) zone			△				○																·		
DB 120	Clay zone (whitish-brownish)				△			◎	○																	
WM 200	Clay (pale green,0.8m)	○						◎	○						·											
WM 205	Quartz stringer (0.1m)			△				○														·		·		
WM 211	White clay (0.1m)				△			◎														·		·		
WM 217	Quartz vein (Waimotu lode)							◎																		
WM 222	Argillic andesite(pinky)			·				◎	△													·			·	
WM 223	Quartz, argillic zone(gray-purplish)			△				◎	△													·		·		
WM 226	Argillic zone							◎	○															△		
WM 227	Silicified, brecciated basalt							◎	○															△		

Tables 2-A-3 Results of Chemical Analysis (3)

Sample No.	Field description	Clay mineral					Silica	Feldspar		Zeolite						Carbonate		Sulfate			Others					
		Sm	Ch	Ka	Se	Tr	Cr	Qz	Pl	Kf	Cb	St	Wa	La	Na	An	Ca	Do	Al	Ja	Gy	Ap	Py	Mg	He	Gb	Others
WM 228	Quartz stringer bearing tuff breccia							◎																	·		
WM 229	Soapy tuff breccia	○						○																			
WK 200	Lapilli tuff		○					◎	○														·		·		
WK 204	Basalt with quartz vein		·					◎				△		○			◎										
WK 205	Weakly silicified rock		·					◎						△									·				
WK 206	Lapilli tuff		○					◎						○													
WK 211	Weakly silicified, limonitic zone	△						○		○																	
WK 213	Weakly silicified rock			△				◎		△									·								
WK 219	Quartz vein with iron oxide			· ?				◎															·				
WK 220	Clayey tuff	△						◎															△				
WK 227	Silicified rock							◎		△													△				
WB 205	Limonitic veinlet in andesite			△				○															·				
WB 207	Silicified, brecciated rock			·				◎																	·		
WB 208	Silicified, brecciated rock			·				◎															·		·		
WB 209	White clay (0.5m)			△				◎															·		·		
WB 210	Silicified, brecciated rock			·				◎																	·		
WB 211	Strongly silicified rock			·				◎																			
WB 212	Andesite(whitisch)			○				◎															·				
WB 213	Strongly silicified rock			· ?				◎																			
WB 214	Strongly silicified rock			·				◎																	·		
WB 215	Weakly silicified rock			·				◎															·		·		
WB 217	Strongly silicified, clay zone			△				◎															·				
WB 219	Strongly silicified, brecciated zone			· ?				◎		○																	
WB 224	Strongly silicified rock			·				◎															·		·		
WB 226	Strongly silicified, brecciated rock			·				◎															·		·		
WB 227	Andesite?(white, decomposed)			○																							
WB 234	Silicified, brecciated rock			△				○															·				
WD 006	Tuff breccia (weakly silicified)	○						○		△													◎				
WD 007	Shear zone			·				◎		○													○				
WD 008	Tuff breccia							◎		△																	

◎= abundant, ○=common, △=small, ·=rare

Sm:smectite, Ch:chrolite, Ka:kaolin, Se:sericite, Tr:tridymite, Cr:cristobalite, Qz:quartz
Pl:plagioclase, Kf:K-feldspar, Al:alunite, Ja:jarosite, Ca:calcite, Do:dolomite, Gy:gypsum, Ap:apatite, An:anatase
Cb:chabasite, St:stibite, Wa:wairakite, Na:natrolite, La:laumontite
Py:pyrite, Mag:magnetite, He:hematite, Gb:gibbsite, Te:tennantite, Sp:sphalerite, Ma:malachite

Tables 2-A-4 Results of X-ray Diffraction Analysis (1)

Element Unit	Au (ppm)	Ag (ppm)	As (ppm)	Sb (ppm)	Hg (ppm)
Detection	0.01(0.008)	0.4	1	0.5	0.005
DB 107	5.72	9.8	160	1.6	0.08
DB 108	5.11	6.5	140	1.4	0.061
DB 109	4	16.5	280	2.8	0.219
DB 110	4.55	47	500	5.8	0.483
DB 111	2.89	6.4	100	1.5	0.061
DB 113	0.38	11.1	560	2.7	0.104
DB 114	0.1	<0.4	250	3.1	0.288
DB 115	0.318	0.5	1360	14.4	2.57
DB 116	0.13	1.2	310	3.4	0.041
DB 117	4.45	12.3	410	3.9	0.276
DB 118	6.7	8.5	200	2.5	0.025
DB 119	6.56	10.4	265	2.4	0.06
DB 123	<0.01	<0.4	3	<0.5	0.016
DB 124	<0.01	<0.4	4	<0.5	0.022
DB 125	<0.01	<0.4	3	<0.5	0.018
DB 126	0.62	<0.4	2	<0.5	0.015
DB 130	<0.01	<0.4	4	<0.5	0.026
DB 132	<0.01	<0.4	2	<0.5	0.02
DB 134	<0.01	<0.4	6	<0.5	0.011
DB 137	0.02	2.8	24	<0.5	0.017
DB 139	0.12	1.2	55	<0.5	0.012
DB 140	0.2	<0.4	25	<0.5	0.014
DB 141	0.03	<0.4	<1	<0.5	0.014
DB 142	1.77	1.2	155	<0.5	0.031
DB 143	<0.01	<0.4	3	<0.5	0.014
DB 144	0.11	0.4	8	<0.5	0.02
DB 145	<0.01	<0.4	4	<0.5	0.014
DB 146	0.69	38.7	1430	9.4	2.25
DB 147	0.71	47	1590	12.6	3.16
DB 148	12.4	46	1420	12.7	2.7
DB 149	2.18	5.6	190	2.3	0.057
DB 150	0.045	2.4	70	3.3	0.136
DB 151	1.33	4.6	210	2	0.034
DB 152	0.54	7.2	280	3.4	0.03
DB 153	2.28	11.3	345	3.3	0.165
DB 154	4.61	8.3	240	2.4	0.08
DB 155	16.1	78	330	6	0.065
DB 156	<0.01	<0.4	5	<0.5	0.022
DB 158	<0.01	0.4	3	<0.5	0.096
DB 159	<0.01	<0.4	155	1.7	0.065
DB 160	<0.01	<0.4	8	<0.5	0.044
DB 161	<0.01	<0.4	4	<0.5	0.024
DB 162	<0.01	<0.4	21	<0.5	0.077
DB 163	<0.01	0.4	<1	<0.5	0.016
DB 164	<0.01	<0.4	7	<0.5	0.03
DB 165	<0.01	<0.4	2	<0.5	0.032
DB 166	<0.01	<0.4	3	1	0.039
DB 167	<0.01	<0.4	3	1.6	0.024
DB 168	<0.01	<0.4	2	1.1	0.028
DB 169	<0.01	<0.4	8	0.6	0.017
DB 171	<0.01	<0.4	3	0.9	0.017
DB 172	<0.01	<0.4	20	<0.5	0.022
DB 173	0.02	0.4	4	<0.5	0.022
DB 174	0.01	<0.4	3	<0.5	0.026
DB 175	0.015	<0.4	11	<0.5	0.027
DB 176	<0.01	<0.4	3	<0.5	0.021
DB 177	0.02	<0.4	23	<0.5	0.017
DB 178	<0.01	<0.4	7	<0.5	0.016
DK 063	<0.01	<0.4	10	0.8	0.022
DK 064	<0.01	<0.4	5	0.9	0.022
DK 065	<0.01	<0.4	7	<0.5	0.014
DK 066	<0.01	<0.4	5	0.7	0.017
DK 067	<0.01	0.4	5	<0.5	0.018
DK 068	<0.01	<0.4	1	<0.5	0.016
DK 073	<0.01	<0.4	17	0.8	0.018

Element Unit	Au (ppm)	Ag (ppm)	As (ppm)	Sb (ppm)	Hg (ppm)
Detection	0.01(0.008)	0.4	1	0.5	0.005
DK 074	<0.01	<0.4	2	<0.5	0.025
DK 086	<0.01	<0.4	5	0.7	0.006
DK 088	<0.01	<0.4	4	0.6	0.01
DK 089	<0.01	0.4	3	0.6	0.009
DK 092	0.11	38.5	1130	28.3	0.575
DK 093	0.26	62	1050	17.4	0.63
DK 095	0.015	0.6	380	4.3	0.028
DK 096	<0.01	1.6	310	1.9	0.048
DK 097	0.1	27.2	380	12.3	0.465
DK 100	<0.01	<0.4	16	1	0.034
DK 101	0.12	<0.4	24	1.3	0.075
DK 102	2.55	0.6	26	1.1	0.065
DK 103	0.07	0.4	70	1	0.025
DK 104	0.015	<0.4	4	<0.5	0.06
DK 105	0.19	2.2	31	0.9	0.063
DK 106	0.14	1	15	0.6	0.041
DK 107	0.56	0.4	25	1.3	0.037
DK 108	0.05	<0.4	21	0.7	0.067
DK 109	0.052	<0.4	17	<0.5	0.063
DK 110	0.049	<0.4	15	<0.5	0.06
DK 111	0.173	<0.4	130	1.6	0.046
DK 112	0.049	<0.4	35	<0.5	0.064
DK 113	0.435	12.2	310	7.4	2.33
DK 114	0.04	<0.4	246	2.6	0.111
DK 115	0.162	1.7	226	2.9	0.09
DK 116	0.12	0.4	90	1.3	0.069
DK 117	0.204	16.1	160	2.6	0.076
DK 118	0.01	<0.4	5	<0.5	0.033
DK 119	0.012	<0.4	6	<0.5	0.034
DK 120	<0.01	<0.4	16	<0.5	0.012
DK 121	<0.01	0.4	23	<0.5	0.027
DK 122	0.012	<0.4	37	<0.5	0.013
DK 123	<0.01	0.6	31	<0.5	0.025
DK 126	<0.01	<0.4	50	0.6	0.022
DK 127	<0.01	1.2	25	<0.5	0.025
DK 128	0.01	0.4	60	0.5	0.031
DK 129	0.01	<0.4	60	0.8	0.029
DK 130	0.01	<0.4	50	<0.5	0.029
DK 131	<0.01	<0.4	11	<0.5	0.03
DK 132	<0.01	<0.4	20	<0.5	0.016
DK 133	0.02	0.8	8	<0.5	0.036
DK 134	0.07	2.4	70	1.1	0.045
DK 136	0.136	5.5	130	3.9	0.034
DK 140	<0.01	<0.4	7	<0.5	0.021
DK 144	<0.01	<0.4	3	<0.5	0.018
DK 146	<0.01	<0.4	7	<0.5	0.019
DK 147	1.7	9.2	34	4.7	0.045
DK 148	0.6	10.8	140	25.4	0.128
DK 149	0.141	25.4	180	14.8	0.088
DK 150	0.134	9.5	145	12.7	0.09
DK 151	0.117	32.3	175	7.4	0.065
DK 152	0.015	2.7	60	<0.5	0.058
DK 153	0.113	0.9	200	0.9	0.028
DK 154	0.04	3	80	<0.5	0.03
DK 155	0.024	34.7	14	<0.5	0.044
DM 078	<0.01	<0.4	6	1.2	0.061
DM 079	<0.01	<0.4	10	0.8	0.037
DM 080	<0.01	0.6	13	0.6	0.017
DM 081	0.07	2.8	155	0.6	0.013
DM 083	<0.01	0.4	3	<0.5	0.011
DM 085	<0.01	0.4	15	0.6	0.095
DM 086	<0.01	<0.4	6	<0.5	0.016
DM 091	0.405	23.6	550	4.3	0.342
DM 095	0.03	0.5	15	<0.5	0.016
DM 096	<0.01	0.4	3	<0.5	0.008

Tables 2-A-4 Results of X-ray Diffraction Analysis (2)

Element Unit	Au (ppm)	Ag (ppm)	As (ppm)	Sb (ppm)	Hg (ppm)
Detection	0.01(0.008)	0.4	1	0.5	0.005
DM 097	<0.01	<0.4	11	<0.5	0.021
DM 098	<0.01	<0.4	110	0.7	0.031
DM 099	<0.01	<0.4	15	0.6	0.023
DM 101	<0.01	0.4	4	<0.5	0.013
DM 102	0.065	0.8	10	<0.5	0.028
DM 103	<0.01	0.9	25	0.8	0.026
DM 104	<0.01	<0.4	2	<0.5	0.08
DM 106	<0.01	<0.4	5	<0.5	0.018
DM 107	<0.01	<0.4	5	<0.5	0.02
DM 108	0.018	<0.4	1	<0.5	0.018
DM 109	<0.01	<0.4	6	<0.5	0.011
DM 110	<0.01	<0.4	4	<0.5	0.034
DM 111	<0.01	0.4	15	0.6	0.017
DM 112	0.112	2.2	110	1	0.022
DM 113	<0.01	<0.4	3	<0.5	0.054
DM 114	0.077	2.2	31	0.6	0.034
DM 115	<0.01	0.6	4	0.7	0.026
DM 116	<0.01	<0.4	3	<0.5	0.006
DM 117	<0.01	0.4	13	0.6	0.01
DM 118	<0.01	<0.4	6	<0.5	0.01
DM 119	0.025	2.2	70	0.9	0.019
DM 120	<0.01	<0.4	5	<0.5	0.008
DM 121	<0.01	<0.4	7	<0.5	0.007
DM 122	<0.01	<0.4	13	<0.5	0.025
DM 123	<0.01	<0.4	7	<0.5	0.037
DM 124	<0.01	<0.4	10	0.8	0.038
DM 125	0.063	2.2	110	1.3	0.043
DM 126	0.085	2.9	50	0.8	0.024
DM 127	0.06	<0.4	80	0.8	0.021
DM 128	0.288	0.9	240	1.9	0.038
DM 129	0.028	0.5	25	<0.5	0.017
DM 130	0.557	0.4	390	2	0.083
DM 131	2.85	0.7	210	2.4	0.136
DM 132	0.072	1	80	1.5	0.04
DM 133	<0.01	<0.4	<1	0.6	0.019
DM 134	0.137	<0.4	90	0.9	0.044
DM 135	0.327	0.9	130	1.3	0.042
DM 136	0.11	0.8	95	1.1	0.052
DM 137	0.027	0.4	55	0.8	0.023
DM 138	2.11	2.2	65	1	0.039
DM 139	0.112	0.5	105	1.1	0.018
DM 140	4.05	78	520	2.9	0.022
DM 141	0.5	0.7	135	1.8	0.047
DM 142	3.2	4.1	285	7.6	0.382
DM 143	0.75	0.5	70	2.3	0.059
DM 144	<0.01	<0.4	5	0.6	0.041
DM 145	0.05	1.4	55	1	0.026
DM 146	0.08	0.4	50	1.5	0.079
DM 147	0.77	1.1	150	3.8	0.068
DM 148	0.86	1.3	305	2.4	0.075
DM 149	0.135	0.6	115	1.6	0.088
DM 150	0.23	0.4	205	1.8	0.077
DM 151	0.01	<0.4	31	1	0.068
DM 152	<0.01	<0.4	12	0.6	0.043
DM 153	<0.01	<0.4	23	1	0.014
DM 154	0.05	0.5	15	<0.5	0.015
DM 155	0.03	0.6	65	1	0.014
DM 156	0.23	<0.4	345	2.3	0.014
DM 157	<0.01	1.3	23	1.1	0.014
DM 158	0.01	<0.4	20	1.2	0.017
DM 159	0.015	<0.4	31	0.9	0.013
DM 160	0.01	0.4	100	0.8	0.017
DM 161	0.02	0.6	75	1.2	0.018
DM 162	0.12	0.5	245	2.1	0.018
DM 163	0.18	0.9	180	1.1	0.014

Element Unit	Au (ppm)	Ag (ppm)	As (ppm)	Sb (ppm)	Hg (ppm)
Detection	0.01(0.008)	0.4	1	0.5	0.005
DM 164	0.05	1	75	1	0.014
DM 165	<0.01	0.7	13	0.8	0.054
DM 166	<0.01	<0.4	8	0.6	0.015
DM 167	0.13	3.4	140	1.4	0.044
DM 168	0.31	4	130	0.9	0.091
DM 169	0.454	151	155	1.6	0.198
DM 170	0.1	5.3	160	1.3	0.022
DM 171	0.053	2.2	60	1.4	0.041
DM 172	0.039	0.5	85	1.1	0.024
DM 173	0.027	1.8	33	1.3	0.08
DM 174	0.033	2.6	85	2.2	0.051
DM 175	0.034	2.5	55	1.4	0.225
DM 176	0.03	3.9	20	1.3	0.735
DM 179	0.01	<0.4	1	<0.5	0.019
DM 180	0.014	0.7	13	<0.5	0.009
DM 181	0.024	<0.4	28	<0.5	0.013
DM 184	0.2	16.7	145	3.9	0.379
DM 185	<0.01	0.5	9	<0.5	0.04
DM 186	<0.01	<0.4	3	<0.5	0.007
DM 187	<0.01	<0.4	2	<0.5	0.01
DM 188	0.16	0.4	17	1.6	0.039
DM 190	0.63	2.4	29	1.4	0.127
DM 192	<0.01	<0.4	2	<0.5	0.022
DM 193	<0.01	<0.4	3	<0.5	0.052
DS 061	0.01	0.4	<1	<0.5	0.018
DS 065	<0.01	<0.4	2	<0.5	0.021
DS 067	<0.01	0.4	<1	<0.5	0.016
DS 069	0.01	<0.4	10	<0.5	0.052
DS 070	0.045	<0.4	9	<0.5	0.073
DS 071	0.015	<0.4	3	<0.5	0.058
DS 074	0.02	<0.4	2	<0.5	0.014
DS 076	0.688	3.4	220	1.9	0.033
DS 079	0.157	<0.4	70	1	0.032
DS 080	0.282	1.1	285	1.5	0.027
DS 081	0.015	<0.4	24	0.7	0.026
DS 082	0.04	0.4	80	0.6	0.025
DS 083	<0.01	<0.4	4	<0.5	0.026
DS 084	0.466	6.1	270	1.7	0.038
DS 085	<0.01	<0.4	4	<0.5	0.038
DS 086	0.05	<0.4	65	0.6	0.052
DS 088	0.024	<0.4	1	<0.5	0.041
DS 089	0.015	0.5	10	<0.5	0.106
DS 092	<0.01	<0.4	<1	<0.5	0.015
DS 093	<0.01	<0.4	12	<0.5	0.015
DS 094	0.015	0.4	3	<0.5	0.008
DS 096	0.45	11.8	1100	6.6	0.36
NB 006	0.018	1.4	3	0.7	0.039
NB 008	0.296	<0.4	9	<0.5	0.307
NB 009	0.545	<0.4	7	<0.5	0.022
NB 012	0.01	<0.4	<1	<0.5	0.042
NB 016	<0.01	<0.4	<1	<0.5	0.025
NB 019	<0.01	<0.4	<1	<0.5	0.023
NB 021	<0.01	<0.4	<1	<0.5	0.026
NB 023	<0.01	<0.4	<1	<0.5	0.021
NB 027	<0.01	<0.4	<1	<0.5	0.088
NB 028	<0.01	<0.4	<1	<0.5	0.022
NB 029	<0.01	<0.4	<1	<0.5	0.038
NB 030	<0.01	<0.4	<1	<0.5	0.036
NB 031	<0.01	<0.4	<1	<0.5	0.021
NB 033	<0.01	<0.4	2	<0.5	0.031
NB 034	<0.01	<0.4	6	<0.5	0.112
NB 037	<0.01	<0.4	2	<0.5	0.029
NB 043	0.01	<0.4	5	<0.5	0.016
NB 045	<0.01	<0.4	29	<0.5	0.048
NB 048	<0.01	<0.4	<1	<0.5	0.022

Tables 2-A-4 Results of X-ray Diffraction Analysis (3)

Element Unit	Au (ppm)	Ag (ppm)	As (ppm)	Sb (ppm)	Hg (ppm)
Detection	0.01(0.008)	0.4	1	0.5	0.005
NB 050	<0.01	<0.4	<1	<0.5	0.025
NB 053	<0.01	<0.4	3	<0.5	0.041
NB 055	<0.01	<0.4	5	<0.5	0.01
NB 058	<0.01	<0.4	14	<0.5	0.023
NB 061	0.02	<0.4	<1	<0.5	0.034
NB 065	<0.01	<0.4	3	0.7	0.016
NB 067	0.01	<0.4	<1	<0.5	0.027
NB 070	<0.01	<0.4	<1	<0.5	0.025
NB 073	<0.01	<0.4	1	<0.5	0.039
NB 077	0.01	<0.4	<1	<0.5	0.035
NB 080	<0.01	<0.4	<1	<0.5	0.042
NB 081	<0.01	<0.4	4	<0.5	0.019
NB 087	<0.01	<0.4	<1	0.7	0.025
NB 088	<0.01	<0.4	<1	<0.5	0.034
NB 089	<0.01	<0.4	1	<0.5	0.036
NB 090	<0.01	<0.4	<1	<0.5	0.021
NB 091	<0.01	<0.4	<1	<0.5	0.029
NB 092	<0.01	<0.4	<1	<0.5	0.036
NB 093	<0.01	0.4	<1	<0.5	0.024
NB 094	0.01	<0.4	3	<0.5	0.075
NB 096	<0.01	0.7	3	<0.5	0.123
NB 097	<0.01	<0.4	3	<0.5	0.029
NB 099	0.013	5.3	<1	<0.5	0.138
NB 100	<0.01	<0.4	2	<0.5	0.02
NB 101	0.01	<0.4	3	<0.5	0.039
NB 102	<0.01	<0.4	<1	<0.5	0.032
NB 103	0.012	<0.4	<1	<0.5	0.025
NB 104	<0.01	0.8	3	<0.5	0.029
NB 105	<0.01	<0.4	<1	<0.5	0.063
NK 001	0.1	<0.4	9	<0.5	0.017
NK 002	<0.01	<0.4	28	<0.5	0.019
NK 003	<0.01	<0.4	5	<0.5	0.02
NK 018	<0.01	<0.4	5	<0.5	0.025
NK 019	0.026	<0.4	6	<0.5	0.021
NK 020	0.127	0.8	<1	<0.5	0.019
NK 021	0.02	<0.4	6	<0.5	0.02
NK 022	0.192	0.6	18	<0.5	0.021
NK 026	0.022	0.4	7	<0.5	0.048
NK 027	0.08	<0.4	7	<0.5	0.047
NK 029	12.9	10.4	5	0.6	0.011
NK 030	1.89	0.6	8	<0.5	0.035
NK 031	0.096	<0.4	2	<0.5	0.029
NK 032	0.064	<0.4	<1	<0.5	0.021
NK 033	9.78	2.3	3	<0.5	0.007
NK 034	0.01	<0.4	23	0.7	0.02
NK 035	0.115	<0.4	2	<0.5	0.028
NK 037	6.69	0.5	3	<0.5	0.031
NK 038	4.24	0.6	7	<0.5	0.051
NK 039	1.84	0.7	19	<0.5	0.161
NK 040	0.86	0.4	12	<0.5	0.032
NK 041	0.07	2.3	90	1.5	0.049
NK 042	0.01	1.8	11	1.8	0.032
NK 043	0.011	5.4	37	1.6	0.04
NK 044	0.04	14.9	22	14.3	0.045
NK 045	0.025	10.4	120	2.4	0.145
NK 046	0.049	1.6	90	2.9	0.109
NK 047	0.086	5.4	50	1.6	0.054
NK 048	0.01	<0.4	1	<0.5	0.046
NK 049	0.06	8.2	70	1	0.079
NK 050	<0.01	<0.4	<1	0.6	0.098
NK 051	<0.01	<0.4	<1	<0.5	92
NK 052	<0.01	<0.4	2	<0.5	0.024
NK 053	<0.01	<0.4	<1	<0.5	0.021
NK 054	<0.01	0.4	<1	<0.5	0.022
NK 056	<0.01	<0.4	<1	<0.5	0.067

Element Unit	Au (ppm)	Ag (ppm)	As (ppm)	Sb (ppm)	Hg (ppm)
Detection	0.01(0.008)	0.4	1	0.5	0.005
NK 058	<0.01	<0.4	14	<0.5	0.141
NK 059	<0.01	<0.4	50	0.8	0.114
NM 002	<0.01	<0.4	<1	<0.5	0.014
NM 003	<0.01	<0.4	<1	<0.5	0.016
NM 005	<0.01	<0.4	<1	<0.5	0.018
NM 006	<0.01	<0.4	<1	<0.5	0.019
NM 007	<0.01	<0.4	<1	<0.5	0.026
NM 008	<0.01	<0.4	<1	<0.5	0.015
NM 009	<0.01	<0.4	<1	<0.5	0.021
NM 010	<0.01	<0.4	<1	<0.5	0.018
NM 012	<0.01	<0.4	1	<0.5	0.024
NM 014	<0.01	<0.4	2	<0.5	0.018
NM 017	<0.01	0.5	27	<0.5	0.023
NM 018	<0.01	<0.4	3	<0.5	0.081
NM 024	<0.01	0.4	7	0.9	0.021
NM 025	<0.01	<0.4	1	<0.5	0.037
NM 026	<0.01	<0.4	<1	<0.5	0.018
NM 027	<0.01	<0.4	<1	<0.5	0.022
NM 028	<0.01	<0.4	5	<0.5	0.03
NM 029	<0.01	<0.4	<1	<0.5	0.022
NM 030	<0.01	<0.4	<1	<0.5	0.016
NM 033	<0.01	<0.4	3	0.8	0.323
NM 034	<0.01	1.7	12	<0.5	0.023
NM 035	<0.01	<0.4	<1	<0.5	0.025
NM 036	<0.01	8.9	2	<0.5	0.021
NM 037	<0.01	0.7	16	<0.5	0.022
NM 038	0.012	<0.4	2	<0.5	0.021
NM 040	<0.01	<0.4	<1	<0.5	0.02
NM 041	<0.01	<0.4	<1	<0.5	0.021
NM 042	<0.01	<0.4	<1	<0.5	0.021
NM 043	0.05	<0.4	29	<0.5	0.025
NM 044	0.103	<0.4	20	0.8	0.061
NM 045	0.01	<0.4	8	<0.5	0.024
NM 046	0.015	<0.4	60	1.4	0.218
NM 047	0.026	<0.4	42	0.8	0.036
NM 048	0.01	6.5	6	0.6	0.071
NM 049	0.018	0.7	6	0.6	0.028
NM 050	0.026	<0.4	20	0.6	0.027
NM 051	0.01	2.1	60	1.2	0.03
NM 052	0.01	<0.4	70	1.1	0.029
NM 053	<0.01	<0.4	60	1.1	0.049
NM 054	0.012	3.2	5	<0.5	0.023
NM 055	<0.01	<0.4	3	<0.5	0.023
NM 056	<0.01	1.4	31	1.3	0.107
NM 057	0.015	<0.4	5	0.6	0.024
NM 058	0.05	<0.4	5	<0.5	0.034
NM 059	0.266	<0.4	5	<0.5	0.024
NM 060	1.26	0.9	21	1.8	0.048
NM 061	0.316	<0.4	60	1.1	0.033
NM 062	2.46	1.9	3	<0.5	0.074
NM 063	0.305	<0.4	2	<0.5	0.024
NM 064	1.83	<0.4	4	<0.5	0.116
NM 065	0.016	<0.4	<1	<0.5	0.026
NM 066	0.025	3.3	120	4	0.312
NM 067	<0.01	5.4	140	6.7	0.485
NM 068	0.02	9.8	70	1.9	0.108
NM 069	<0.01	2.9	190	2.9	0.184
NM 070	0.152	5	70	2.1	0.108
NM 071	0.016	2.7	210	4.1	0.184
NM 072	0.01	1.4	7	0.9	0.188
NM 073	<0.01	2.2	10	0.6	0.128
NM 074	<0.01	2.5	4	<0.5	0.08
NM 075	<0.01	1.4	20	<0.5	0.034
NM 076	<0.01	1	60	1.6	0.388
NS 010	<0.01	0.9	28	1.1	0.181

Tables 2-A-4 Results of X-ray Diffraction Analysis (4)

Element / Unit	Au (ppm)	Ag (ppm)	As (ppm)	Sb (ppm)	Hg (ppm)
Detection	0.01(0.008)	0.4	1	0.5	0.005
NS 012	<0.01	1.1	20	<0.5	0.05
NS 013	0.01	1	80	1.2	0.027
NS 018	<0.01	<0.4	<1	<0.5	0.042
NS 019	0.01	<0.4	<1	<0.5	0.03
NS 020	<0.01	<0.4	<1	<0.5	0.02
NS 021	<0.01	<0.4	<1	0.8	0.022
NS 022	<0.01	<0.4	<1	0.8	0.024
NS 023	<0.01	<0.4	<1	<0.5	0.043
NS 024	<0.01	<0.4	<1	<0.5	0.039
NS 025	<0.01	<0.4	<1	<0.5	0.024
NS 026	0.27	0.4	2	<0.5	0.023
NS 027	<0.01	<0.4	1	<0.5	0.031
NS 028	0.83	0.5	21	<0.5	0.046
NS 029	<0.01	<0.4	1	<0.5	0.048
NS 030	<0.01	<0.4	<1	<0.5	0.021
NS 031	<0.01	<0.4	<1	<0.5	0.024
NS 032	<0.01	<0.4	<1	<0.5	0.043
NS 033	<0.01	<0.4	<1	<0.5	0.024
NS 034	<0.01	<0.4	<1	<0.5	0.018
NS 035	<0.01	<0.4	<1	<0.5	0.025
NS 036	0.025	<0.4	<1	<0.5	0.02
NS 037	<0.01	<0.4	<1	<0.5	0.02
NS 038	<0.01	<0.4	<1	<0.5	0.018
NS 039	0.015	<0.4	<1	<0.5	0.029
NS 040	0.163	<0.4	2	<0.5	0.021
NS 041	0.09	<0.4	<1	<0.5	0.032
NS 042	<0.01	<0.4	<1	<0.5	0.023
NS 043	<0.01	<0.4	<1	<0.5	0.024
NS 044	<0.01	<0.4	<1	<0.5	0.03
NS 046	<0.01	<0.4	<1	<0.5	0.025
NS 049	<0.01	<0.4	7	<0.5	0.128
NS 050	<0.01	<0.4	13	<0.5	0.131
NS 051	<0.01	<0.4	<1	<0.5	0.021
NS 052	<0.01	<0.4	<1	<0.5	0.026
NS 053	<0.01	<0.4	<1	<0.5	0.024
NS 054	<0.01	<0.4	<1	<0.5	0.02
NS 055	<0.01	<0.4	<1	<0.5	0.023
NS 056	0.03	<0.4	<1	<0.5	0.018
NS 057	0.16	<0.4	1	<0.5	0.031
NS 058	0.13	<0.4	2	<0.5	0.034
WB 181	<0.008	<0.4	1	<0.5	0.01
WB 185	<0.008	<0.4	2	<0.5	<0.005
WB 202	<0.008	<0.4	1	<0.5	0.005
WB 204	0.02	<0.4	7	<0.5	0.024
WB 205	<0.008	<0.4	11	<0.5	0.012
WB 206	0.063	<0.4	5	<0.5	0.033
WB 207	1.68	<0.4	460	1.6	0.023
WB 208	1.71	1	43	1.1	0.049
WB 209	0.641	<0.4	135	1	0.097
WB 210	3.45	1.5	30	1.2	0.042
WB 211	0.921	3	50	0.8	0.014
WB 212	0.274	<0.4	115	0.8	0.043
WB 213	1.57	1	45	0.7	0.008
WB 214	0.637	1.5	50	1.1	0.017
WB 215	0.212	<0.4	155	1.7	0.008
WB 216	<0.008	<0.4	<1	<0.5	<0.005
WB 217	1.78	0.5	15	1	0.007
WB 218	1.02	0.5	90	1.6	0.028
WB 219	0.297	<0.4	145	1.5	0.018

Element / Unit	Au (ppm)	Ag (ppm)	As (ppm)	Sb (ppm)	Hg (ppm)
Detection	0.01(0.008)	0.4	1	0.5	0.005
WB 220	2.67	0.5	22	0.9	0.011
WB 221	0.598	0.5	50	1.8	0.023
WB 222	1.9	0.5	85	1.4	0.011
WB 223	0.921	1.5	220	1.6	0.057
WB 224	2.51	3.5	36	1	0.019
WB 225	0.517	<0.4	110	1.8	0.046
WB 226	1.1	0.5	50	0.9	0.035
WB 228	0.711	1.5	50	0.9	0.092
WB 230	4.3	2	60	1.3	0.014
WB 231	0.314	1.5	100	1.5	0.013
WB 234	0.915	<0.4	315	2.4	0.017
WB 235	4.22	1	60	1.5	0.008
WD 004	3.65	4	33	0.8	<0.005
WD 005	4.03	2.5	15	0.6	<0.005
WD 008	0.347	<0.4	190	2.3	0.02
WD 009	1.55	<0.4	210	1.6	0.066
WD 011	<0.008	<0.4	2	<0.5	<0.005
WK 204	<0.008	<0.4	25	0.9	<0.005
WK 210	3.28	0.5	14	0.6	<0.005
WK 211	0.572	0.5	75	1.1	0.011
WK 212	2.41	0.5	4	<0.5	<0.005
WK 213	0.917	0.5	23	0.9	0.034
WK 214	5.45	1	10	0.6	0.005
WK 215	24.2	2.5	3	<0.5	0.011
WK 216	10.6	1	50	1.1	0.025
WK 217	0.147	<0.4	1	<0.5	0.018
WK 218	0.173	<0.4	5	0.9	0.015
WK 219	0.032	<0.4	3	<0.5	0.232
WK 224	0.017	<0.4	6	<0.5	0.005
WK 225	<0.008	<0.4	3	<0.5	<0.005
WK 227	0.591	0.5	14	0.8	0.257
WM 196	<0.008	<0.4	2	<0.5	0.024
WM 200	<0.008	<0.4	2	<0.5	0.025
WM 203	<0.008	<0.4	2	<0.5	<0.005
WM 204	<0.008	<0.4	2	<0.5	0.012
WM 205	0.092	<0.4	140	1	<0.005
WM 207	0.01	<0.4	80	0.8	<0.005
WM 208	<0.008	<0.4	23	0.6	0.013
WM 210	0.01	<0.4	60	1.2	0.035
WM 211	0.015	<0.4	115	1	<0.005
WM 217	1.78	0.5	50	0.9	0.014
WM 218	2.39	<0.4	55	1.1	0.01
WM 219	42.5	7	8	0.6	0.007
WM 220	1.66	<0.4	265	1.9	0.093
WM 221	0.207	<0.4	8	0.8	0.026
WM 224	0.127	<0.4	16	0.7	0.02
WM 225	0.079	<0.4	75	1.1	0.035
WM 226	0.064	<0.4	25	0.8	0.082
WM 227	0.031	<0.4	23	1	0.026
WM 228	0.107	<0.4	32	0.7	0.039
WS 103	<0.008	<0.4	2	<0.5	0.006
WS 104	<0.008	<0.4	4	<0.5	0.007
WS 105	0.017	<0.4	1	<0.5	<0.005
WS 106	0.132	0.5	11	0.6	0.064
WS 108	<0.008	<0.4	2	<0.5	<0.005
WS 115	<0.008	<0.4	7	<0.5	0.01
WS 116	0.04	<0.4	5	<0.5	0.005
WS 117	0.097	1	34	0.8	0.025

Navakuru

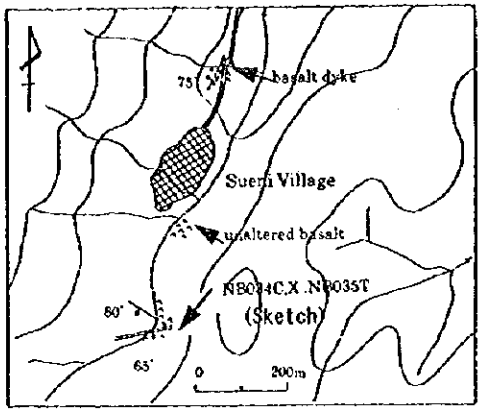

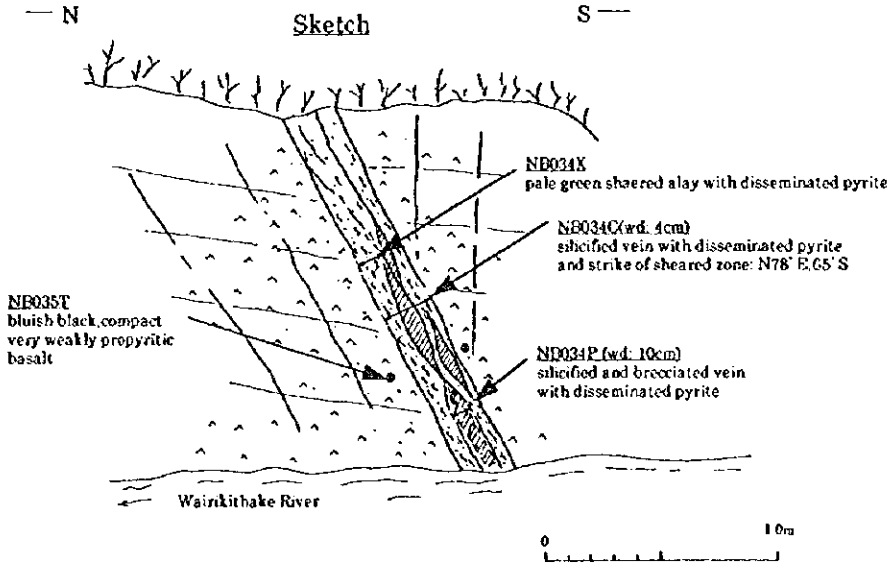

Fig. 2-A-10 Sketch of Trenches in the Nakoroutari Area (1)

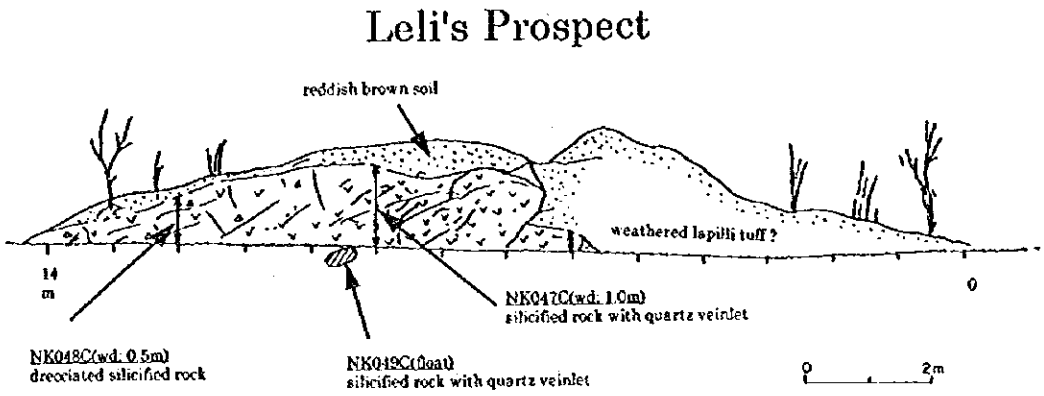

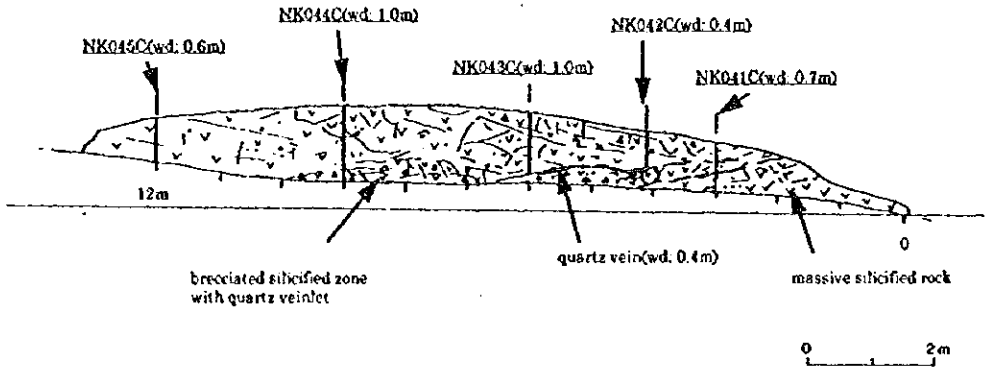

Fig. 2-A-11 Sketch of Trenches in the Nakoroutari Area (2)

Dakuniba Prospect(Trench 1)

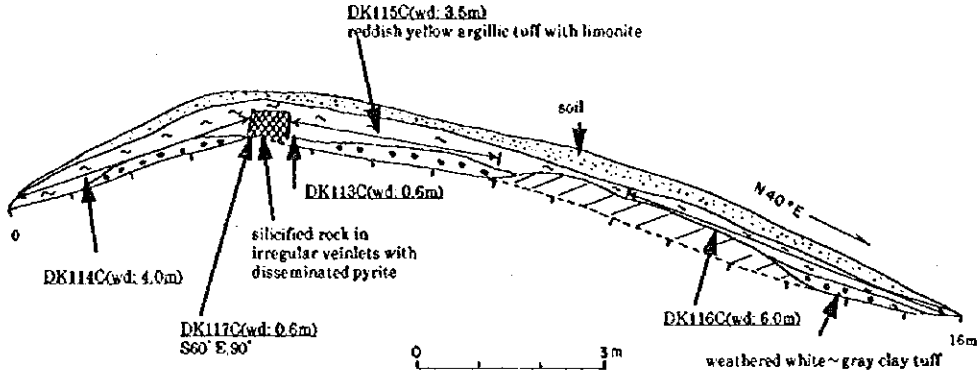

Dakuniba Prospect(Trench 3)

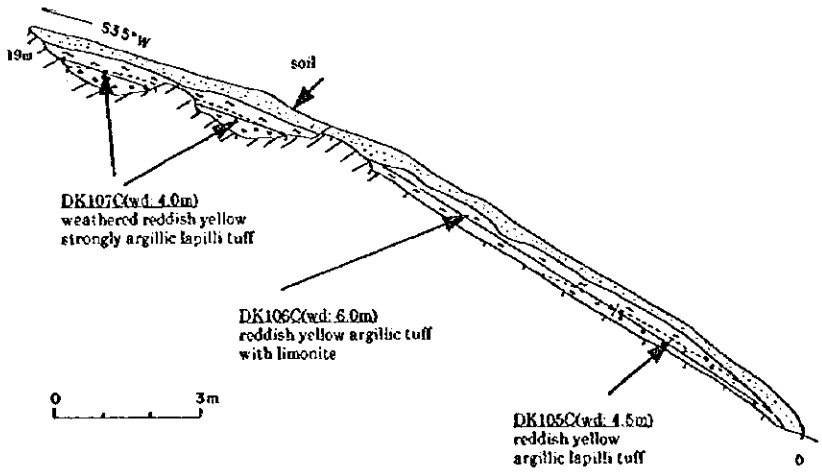

Dakuniba Prospect(Trench 4)

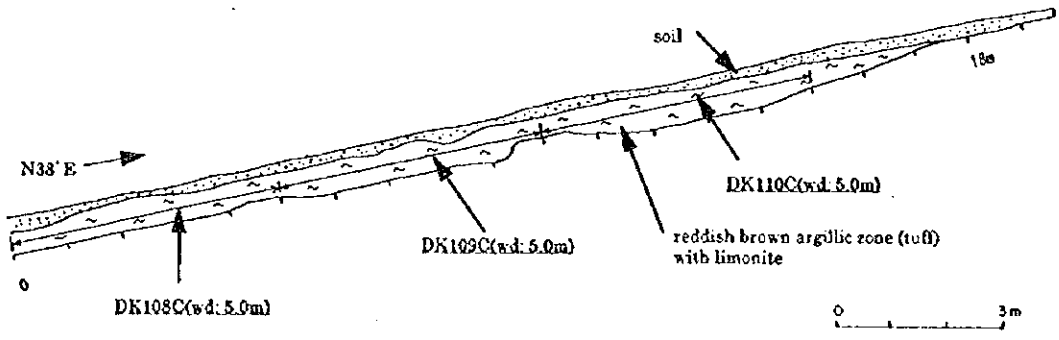

Fig. 2-A-12 Sketch of Trenches in the Dakuniba Area (1)

Dakuniba Prospect(Trench 5)

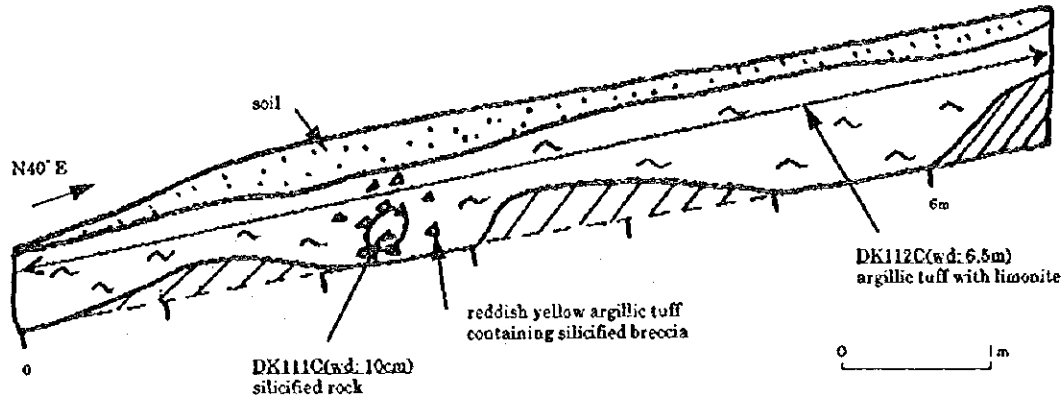

Dakuniba Prospect(Trench 6)

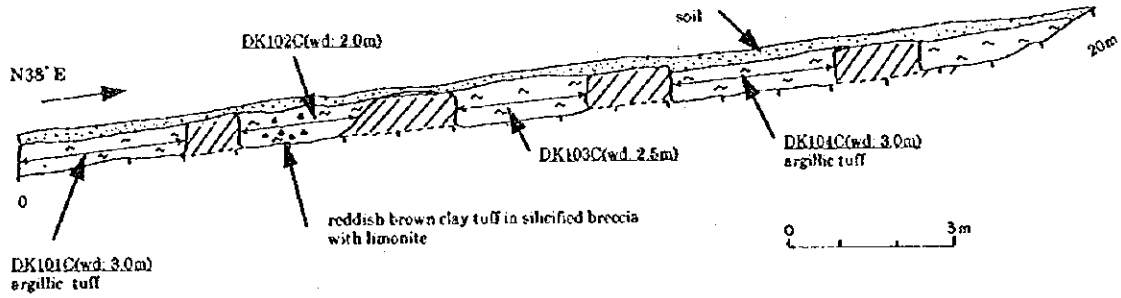

Dakuniba Prospect(Trench 7)

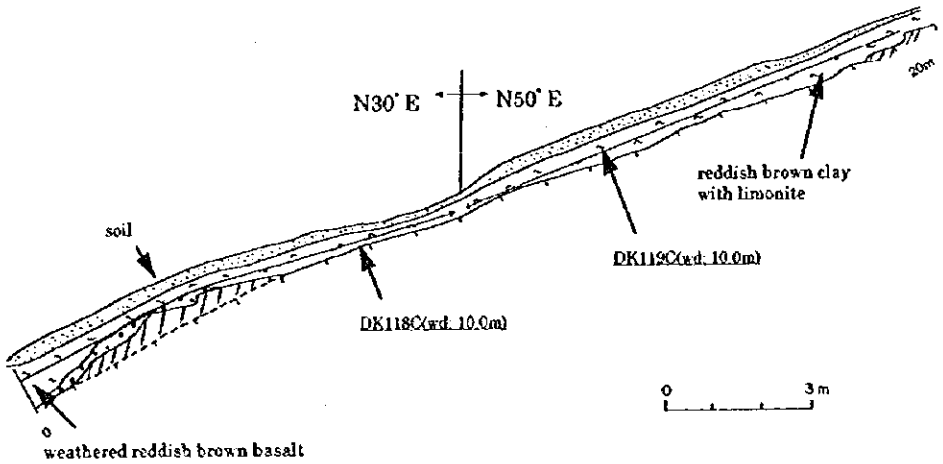

Fig. 2-A-13 Sketch of Trenches in the Dakuniba Area (2)

Dakuniba Prospect(Trench 8)

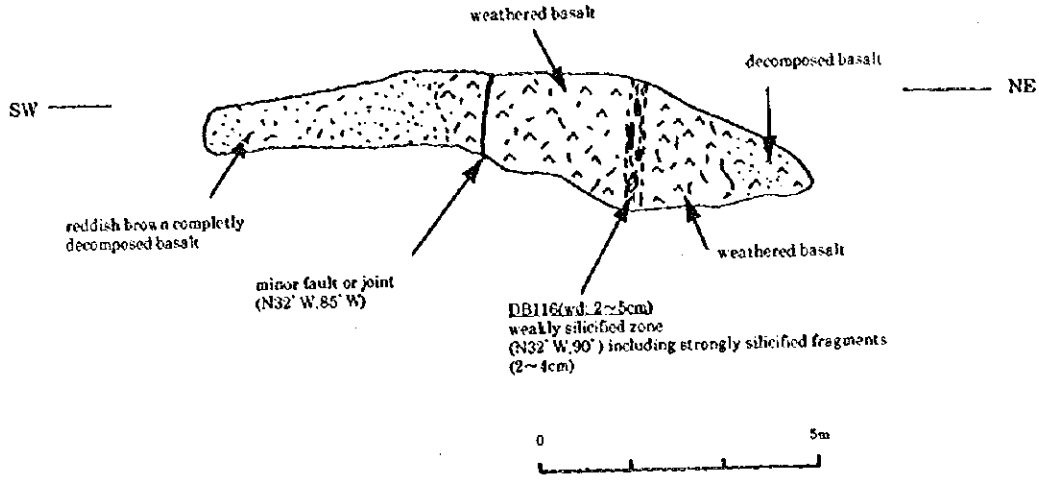

Dakuniba Prospect(Trench 10)

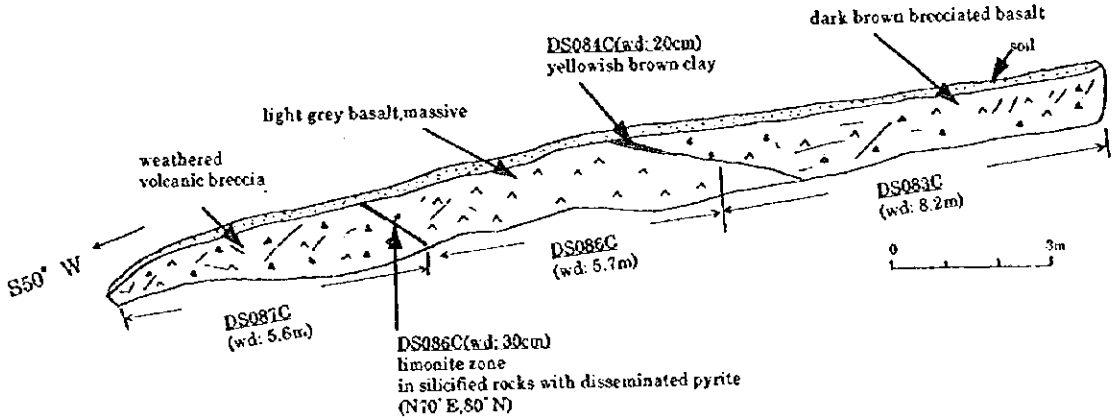

Dakuniba Prospect(Trench 12)

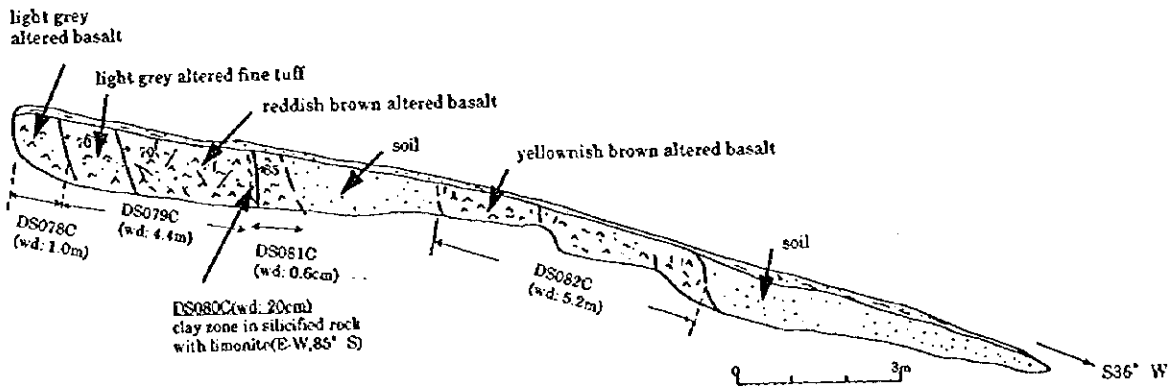

Fig. 2-A-14 Sketch of Trenches in the Dakuniba Area (3)

Dakuniba Prospect(Trench 13)

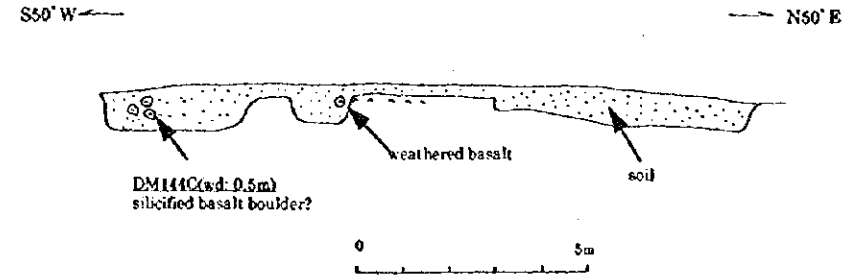

Dakuniba Prospect(Trench 14)

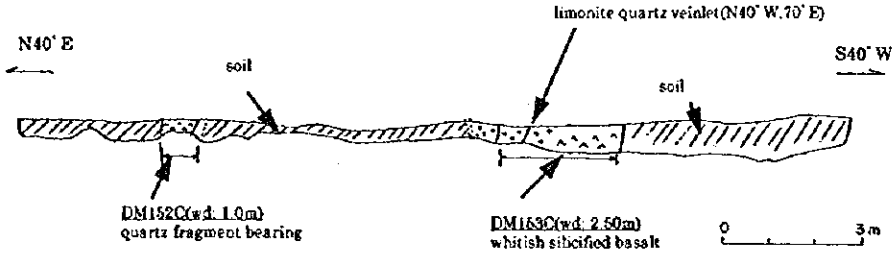

Dakuniba Prospect(Trench 15)

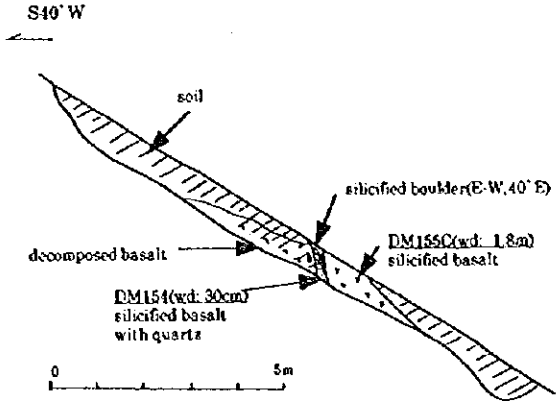

Fig. 2-A-15 Sketch of Trenches in the Dakuniba Area (4)

Dakuniba Prospect(Trench 16)

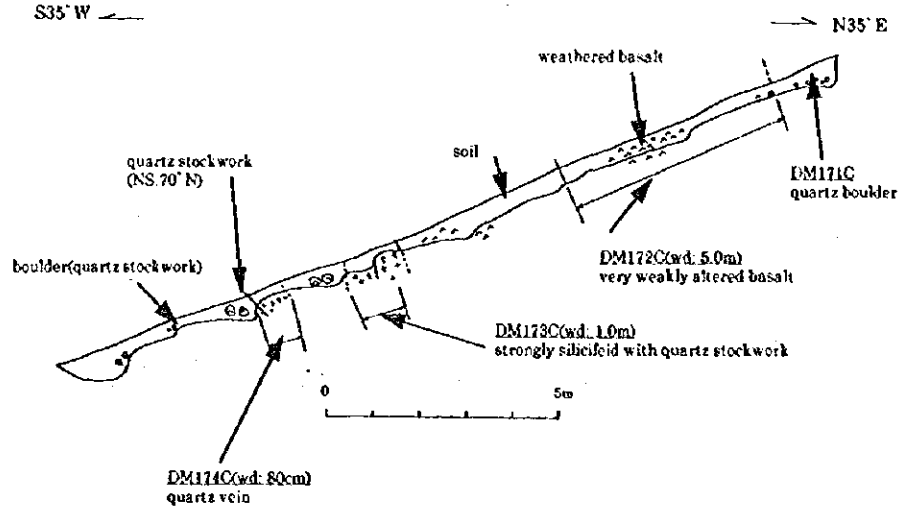

Dakuniba Prospect(Trench 21)

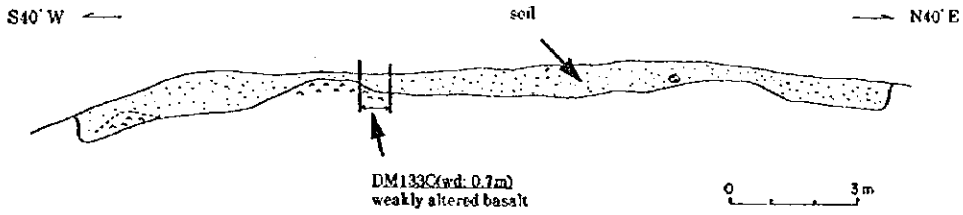

Dakuniba Prospect(Trench 22)

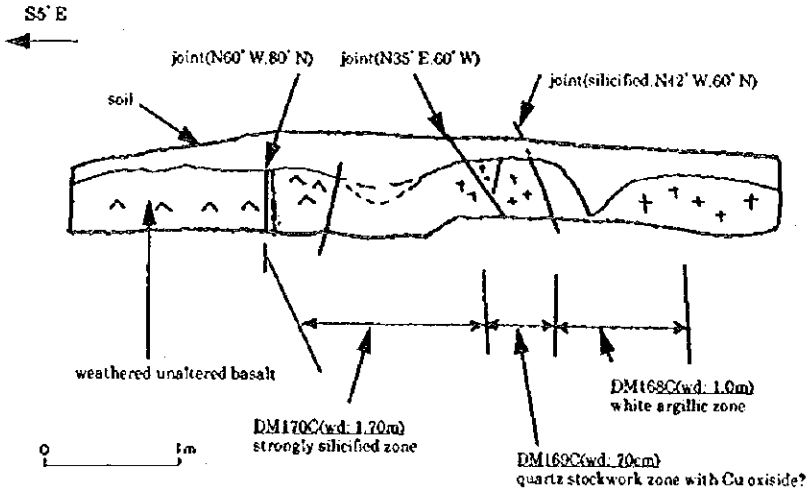

Fig. 2-A-16 Sketch of Trenches in the Dakuniba Area (5)

Dakuniba Prospect(Trench 23)

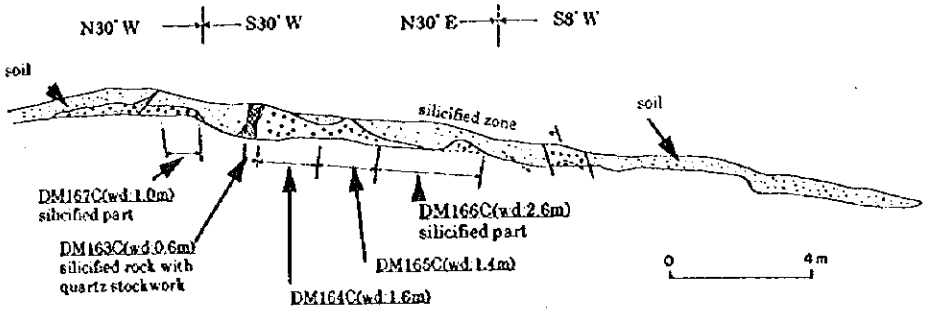

Dakuniba Prospect(Trench 24)

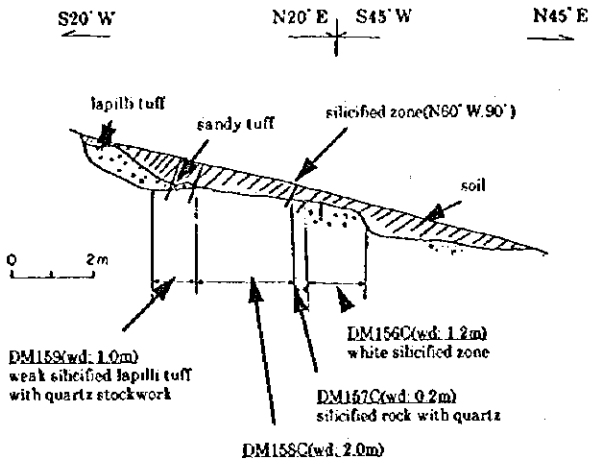

Dakuniba Prospect(Trench 27)

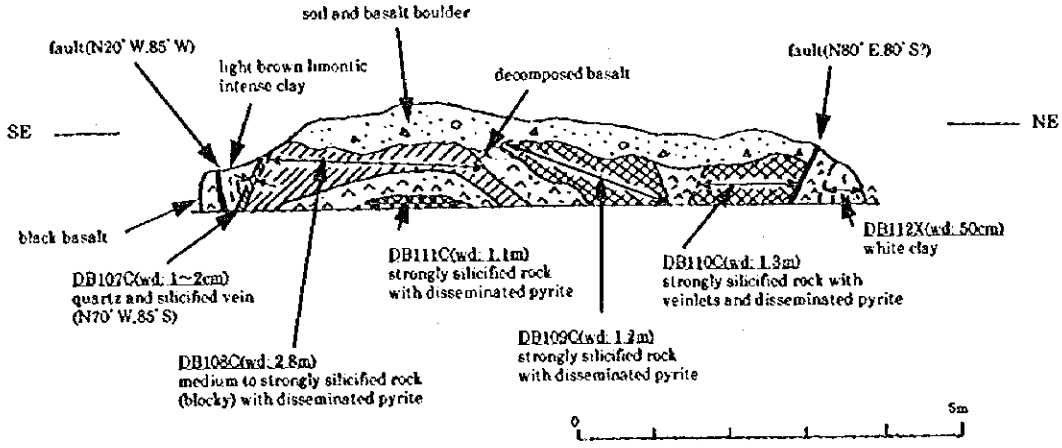

Fig. 2-A-17 Sketch of Trenches in the Dakuniba Area (6)

Dakuniba Prospect(Trench 29)

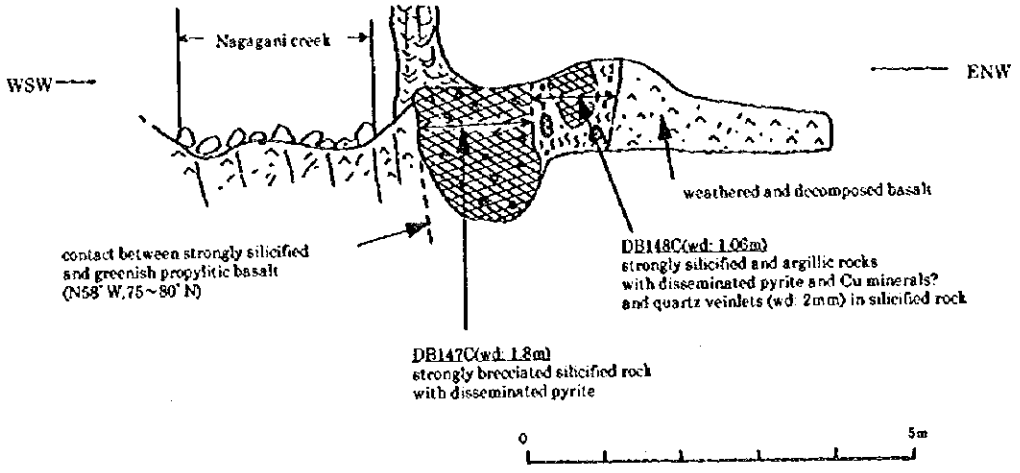

Dakuniba Prospect(Trench 30)

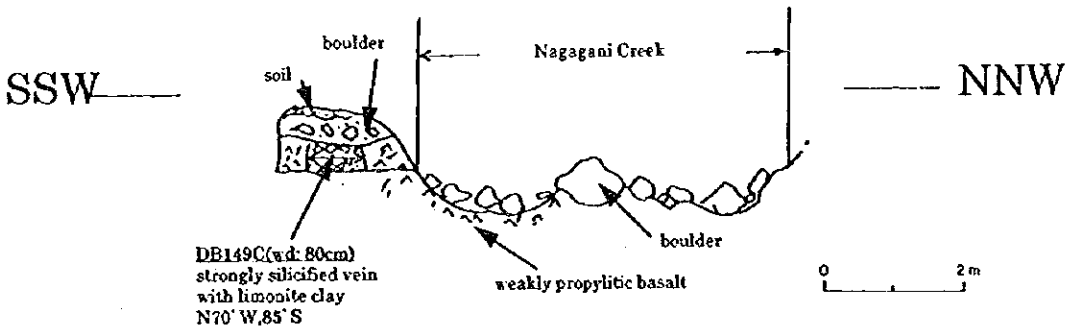

Dakuniba Prospect (Trench No.33)

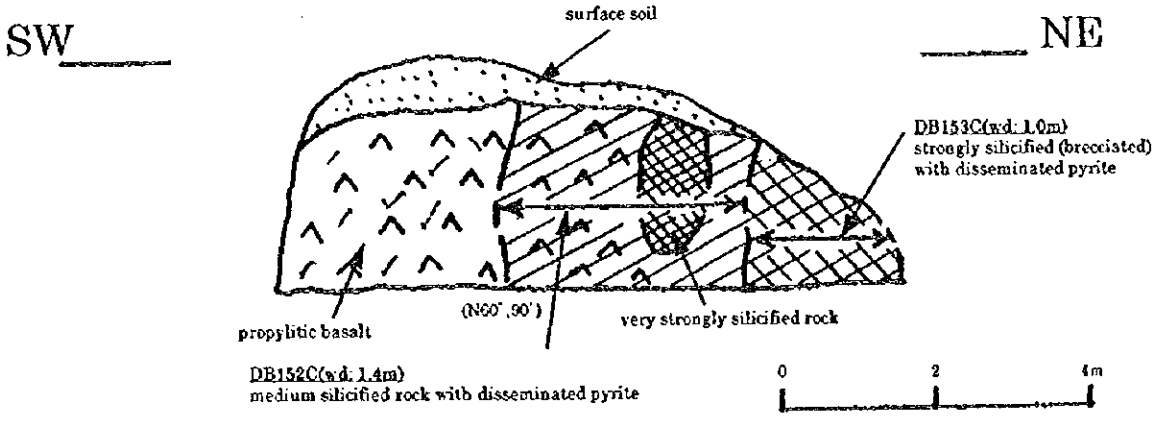

Fig. 2-A-18 Sketch of Trenches in the Dakuniba Area (7)

Dakuniba Prospect(Trench 39)

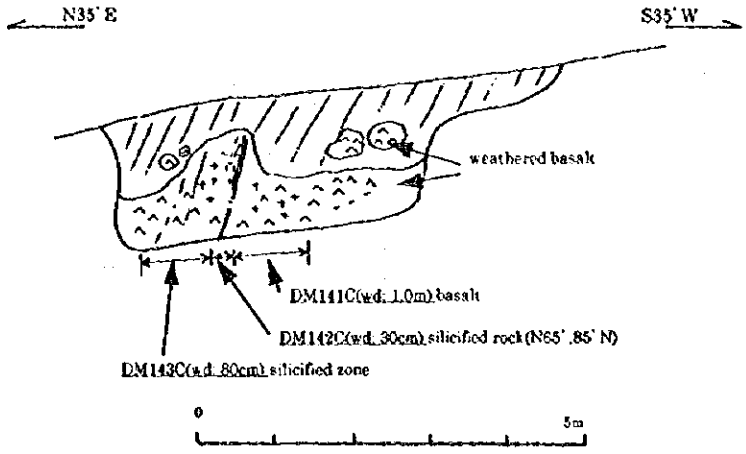

Dakuniba Prospect(Trench 43)

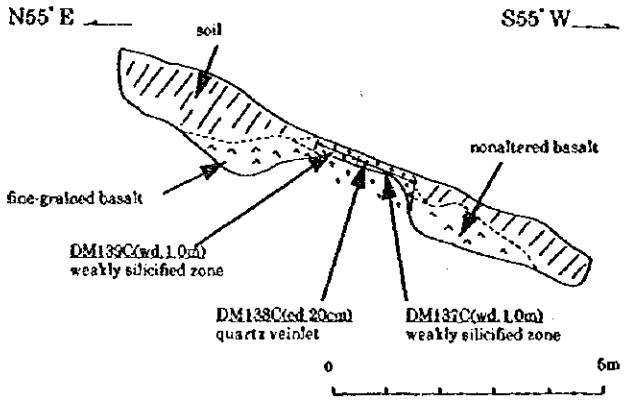

Dakuniba Prospect(Trench 45)

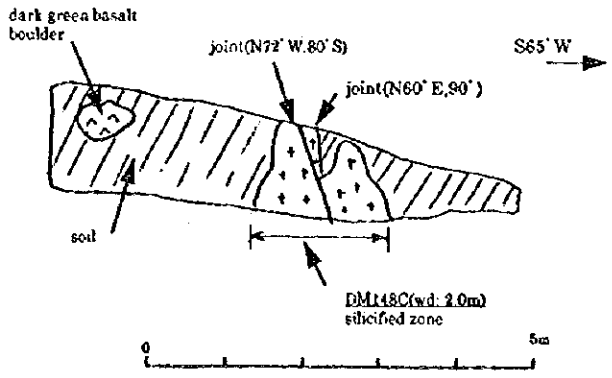

Fig. 2-A-19 Sketch of Trenches in the Dakuniba Area (8)

Dakuniba Prospect(Trench 47)

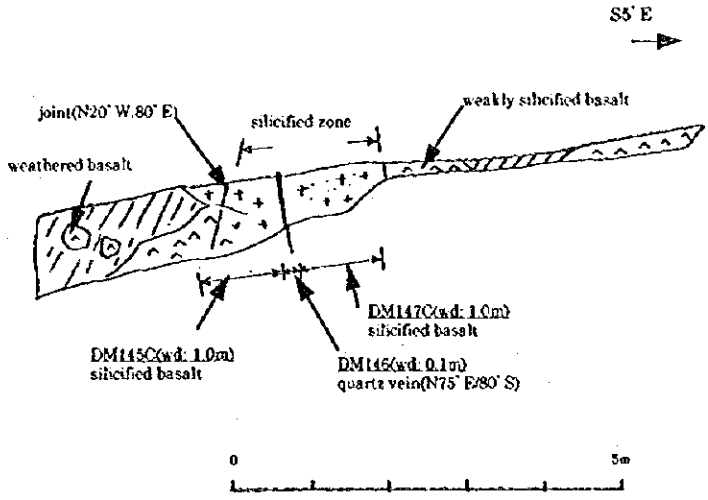

Dakuniba Prospect(Trench 48)

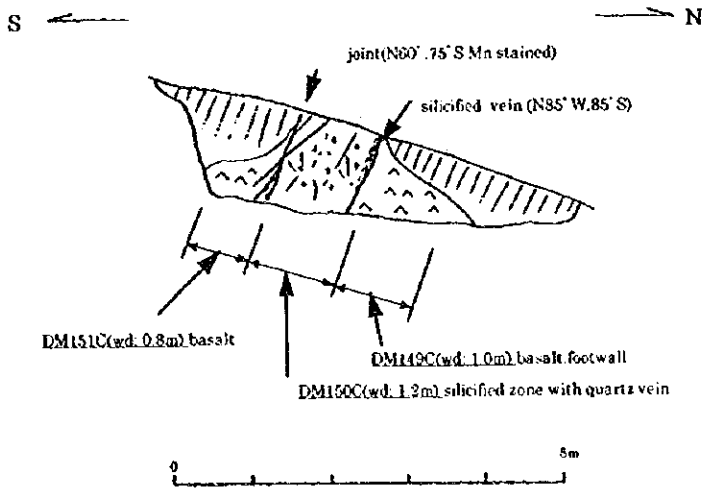

Dakuniba Prospect(Trench 49)

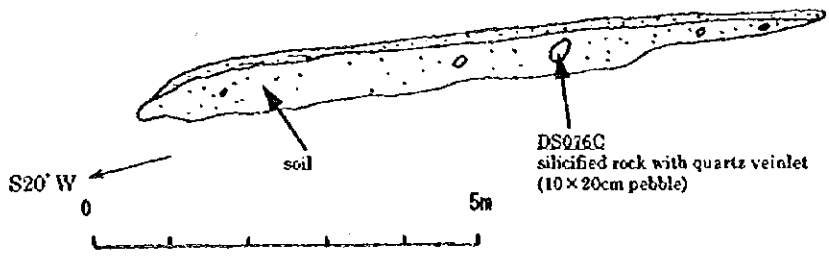

Fig. 2-A-20 Sketch of Trenches in the Dakuniba Area (9)

Dakuniba Prospect(Trench 52)

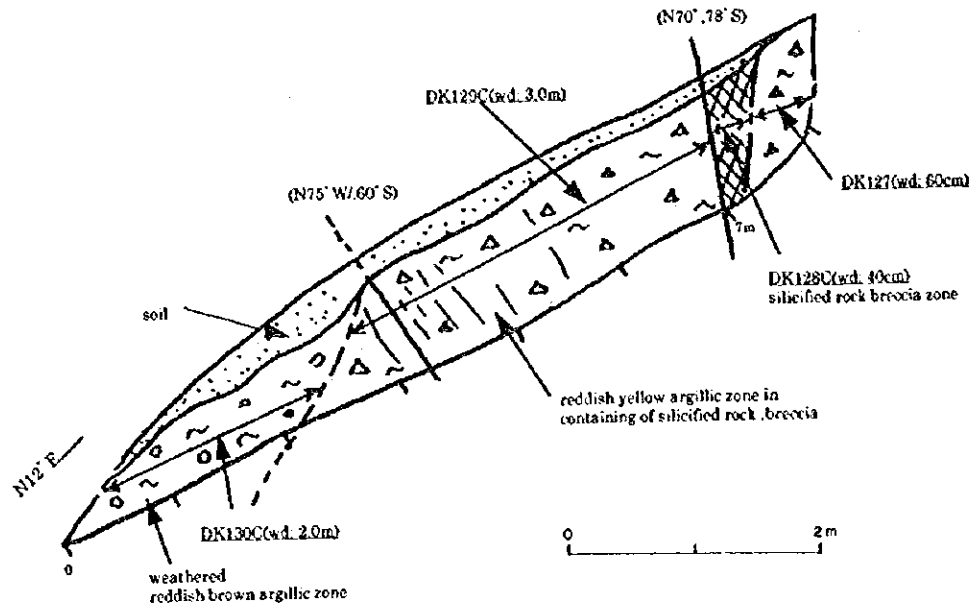

Dakuniba Prospect(Trench 53)

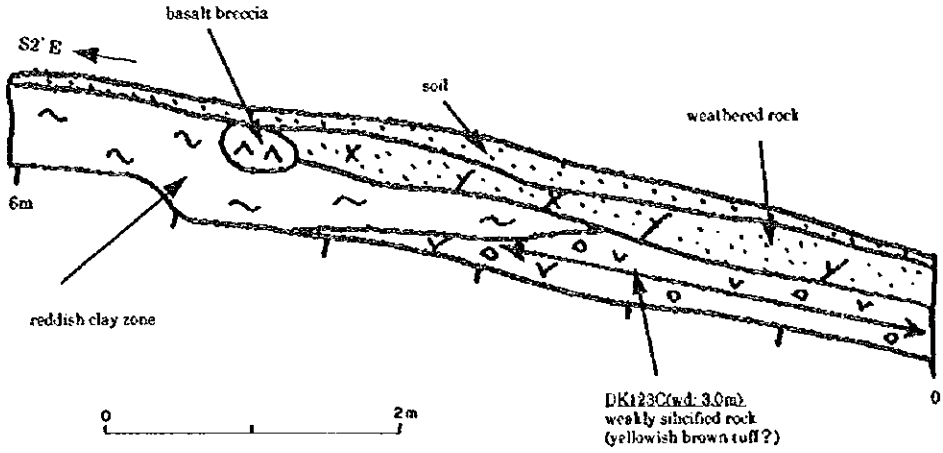

Fig. 2-A-21 Sketch of Trenches in the Dakuniba Area (10)

Dakuniba Prospect(Trench 54)

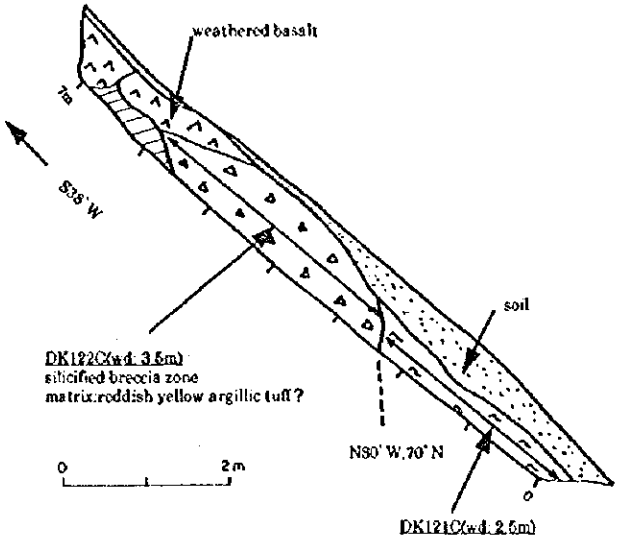

Dakuniba Prospect(Trench 57)

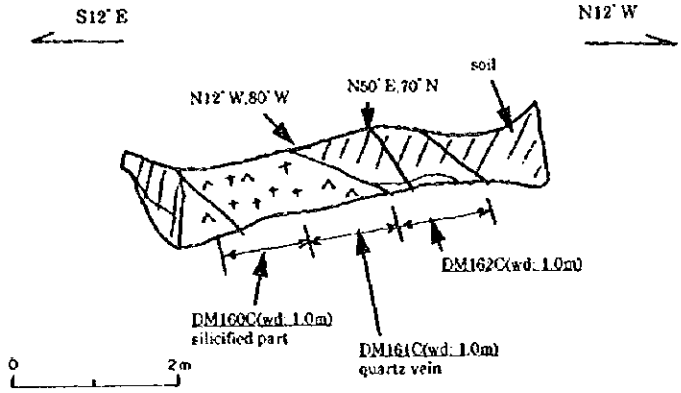

Dakuniba Prospect(Trench ?)

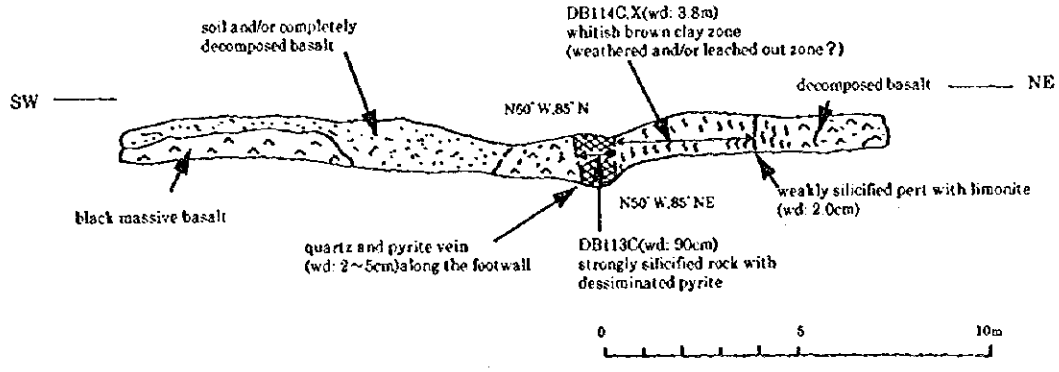

Fig. 2-A-22 Sketch of Trenches in the Dakuniba Area (11)

Dakuniba Prospect(Trench ?)

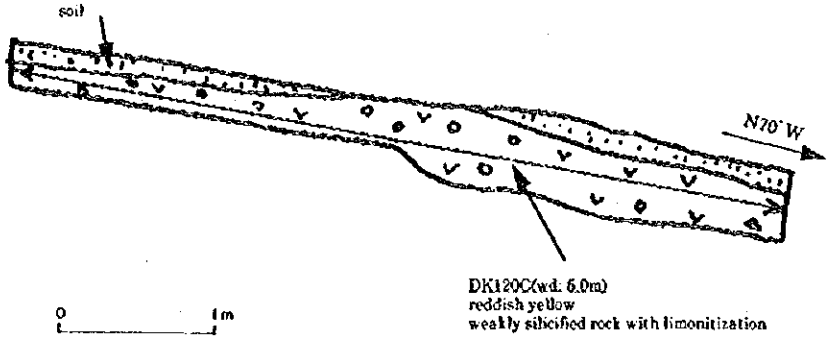

Dakuniba(Tarte's Costean)

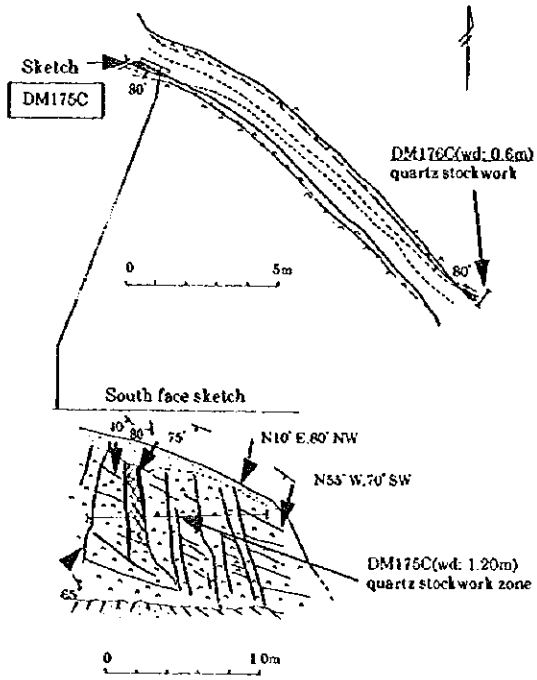

Fig. 2-A-23 Sketch of Trenches in the Dakuniba Area (12)

Dakuniba(8 gram Creek)

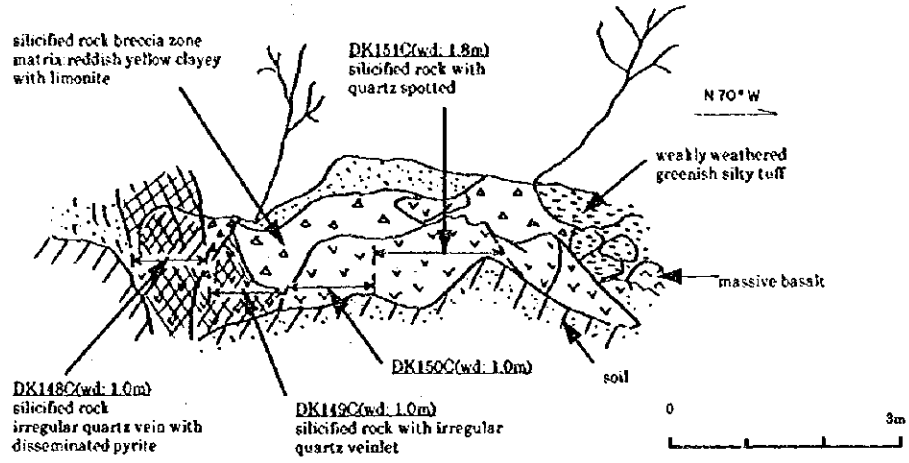

Dakuniba(Valenivuaka Creek)

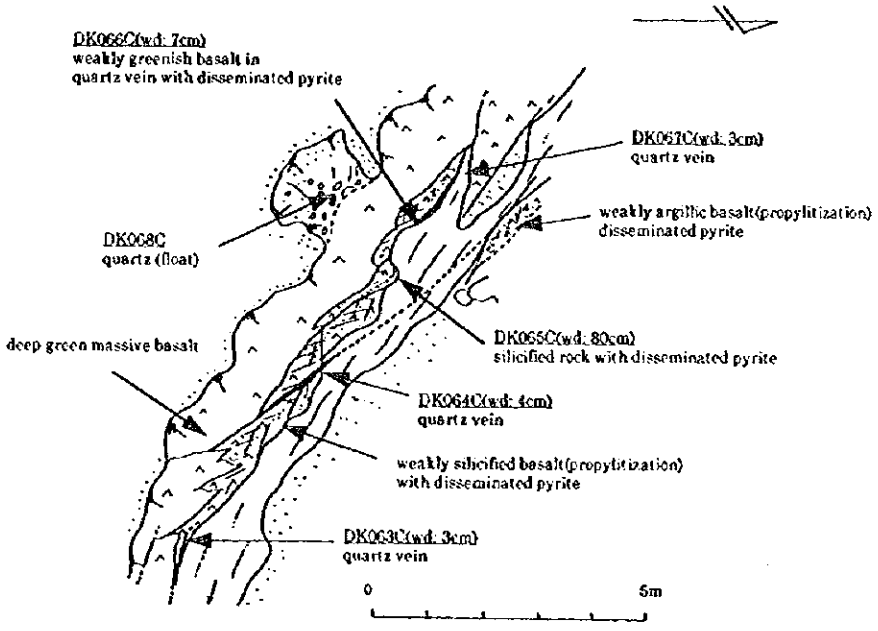

Fig. 2-A-24 Sketch of Trenches in the Dakuniba Area (13)

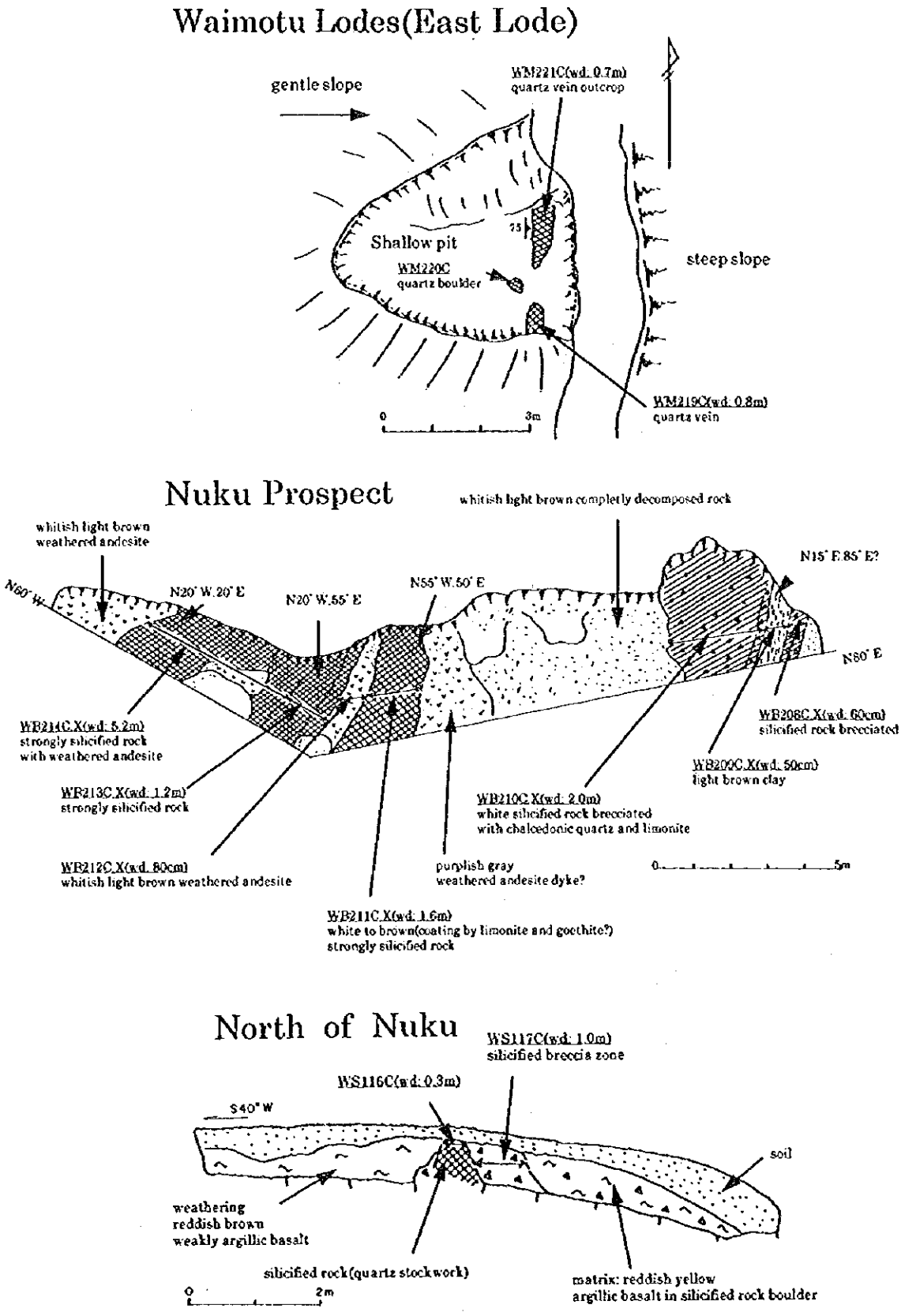

Fig. 2-A-25 Sketch of Trenches in the Waimotu Area

Chapter 5

Geophysical Survey

CHAPTER 5 GEOPHYSICAL SURVEY
(Array CSAMT and Time Domain IP Methods)

5-1 Outline of Geophysical Survey

5-1-1 Objectives

To clarify the relation between the subsurface structure and resistivity in the Nakoroutari Area, which was selected by previous surveys and the present geological survey, by Array CSAMT method and also to understand the relation between the CSAMT anomalies and mineralization by Time Domain IP method. Geophysical anomalies will be extracted at the same time in order to obtain guidance for drilling exploration.

5-1-2 Area of Survey

The geophysical survey was conducted in Nakoroutari Area located about 15 km south from Labasa of the Vanua Levu Island, it is shown in Fig.2-5-1.

5-1-3 Survey Methods

The method used is Array CSAMT (CSAMT) and Time Domain IP (TDIP). CSAMT is generally a method used for investigating a specific area. During the present survey, array method for studying a linear profile was used in order to clarify the resistivity structure of the Leli's prospect of Nakoroutari Area. Eight profiles totaling 12,000m and 120 stations were measured with the array method. With the IP method, for the resistivity anomalous area selected by CSAMT, five profiles totaling 7,500m were measured.

The lengths of traverse lines and the numbers of stations are as follows.

Array CSAMT Method				Time Domain IP Method			
Line	Length (m)	Number of stations	Station interval(m)	Line	Length (m)	Number of stations	Station interval (m)
A	1,500	15	100				
B	1,500	15	100	B	1,500	55	100
C	1,500	15	100	C	1,500	55	100
D	1,500	15	100	D	1,500	55	100
E	1,500	15	100	E	1,500	55	100
F	1,500	15	100	F	1,500	55	100
G	1,500	15	100				
H	1,500	15	100				
Total	12,000	120			7,500	275	Total

* Line interval : 200m

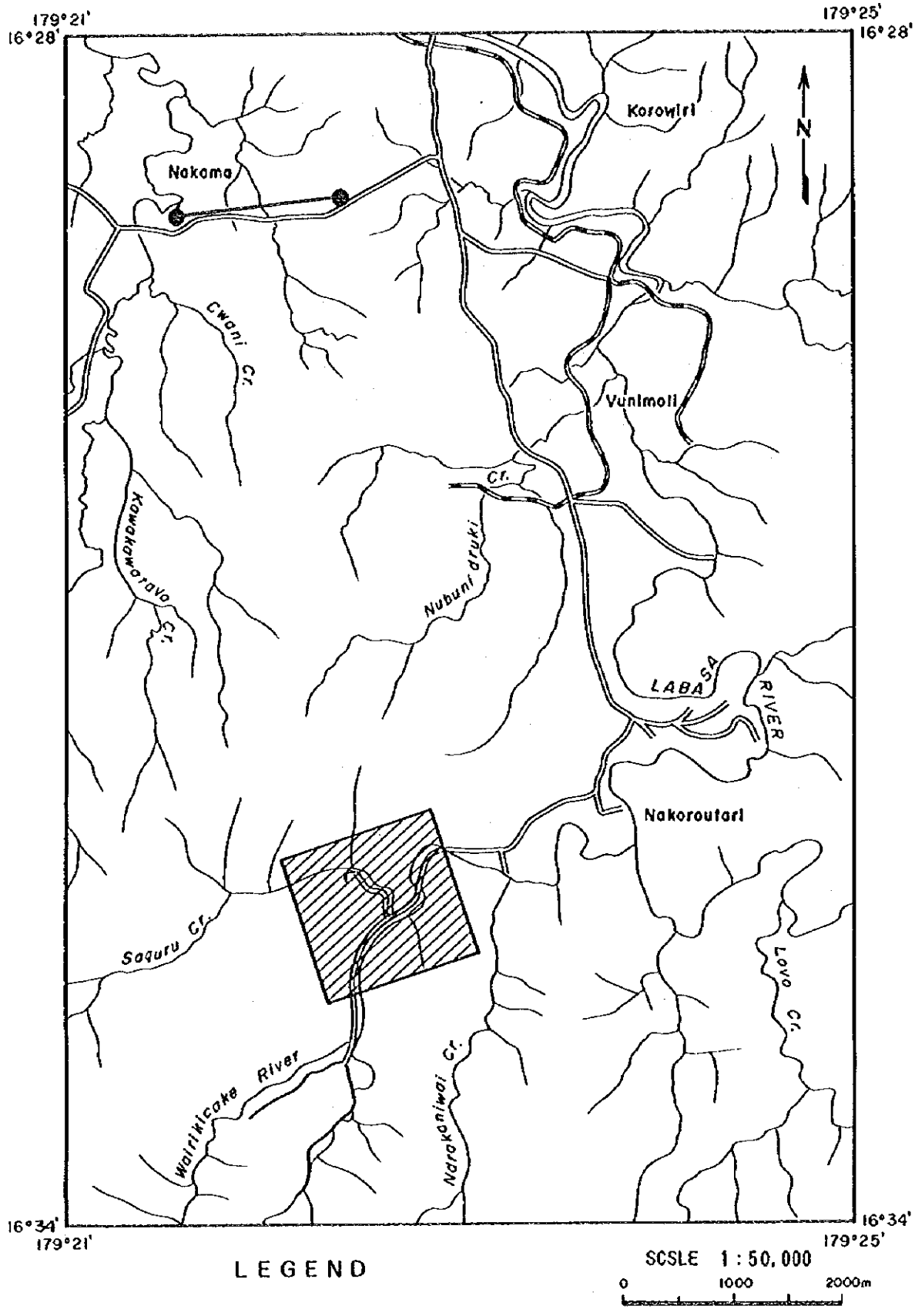

Fig. 2-5-1 Location Map of Survey Area and Transmitting Dipole

5-1-4 Selection of Traverse Lines

The analysis and interpretation of the reports of previous surveys indicated that the strike of the regional structure in the Nakoroutari Zone is N-S~NW-SE. In order to clarify the resistivity structure of the Ⅰeli's prospect of the survey area and to pursue the relation between geological structure and mineralization, eight CSAMT lines at 200m intervals transecting the silicified zone at N72°E were measured.

With IP method, five lines overlapping those of CSAMT were measured in order to determine whether the anomalies detected by the array CSAMT were caused by mineralization or not. Traverse lines are shown in Fig.2-5-2.

5-2 Methods Employed for Survey and Analysis

5-2-1 Array CSAMT Method

(1) Theoretical Background

One method of determining the resistivity distribution of the upper part of the earth's crust is the magnetotelluric method (MT method). This is a method of determining the subsurface resistivity structure by simultaneously measuring the telluric magnetism and telluric electric current. The CSAMT (controlled source audiofrequency magnetotelluric) method is one kind of MT method. It uses frequency in the audio range and artificial source for the signal. This method is now used quite often for resistivity structure determination related to metallic deposits and geothermal resources. The advantages of using this method can be summarized as follows; the S/N ratio is good because the signal source is controlled, the measuring time is shorter because the measuring frequency is high, and transportation of the equipment in the field, particularly in rugged terrain, is easier because of the smaller and lighter equipment. The theory and method of measurement of CSAMT is the same as conventional MT method with the exception of using artificial source for signals.

Fig. 2-5-3 illustrates the survey configuration. The apparent resistivity is calculated from the ratio of the electric field magnitude (Ex) and magnetic field magnitude (Hy) using the well known Cagniard equation (1) for MT.

$$Ra = \frac{1}{5f} \cdot \left| \frac{Ex}{Hy} \right|^2 \quad \text{(ohm-m)} \qquad (1)$$

Where Ra : apparent resistivity in ohm-m.

f : frequency in Hz.

Ex : the E-field magnitude in mV / km.

Hy : the Hy-field magnitude perpendicular to the Ex-dipole in nT (gammas).

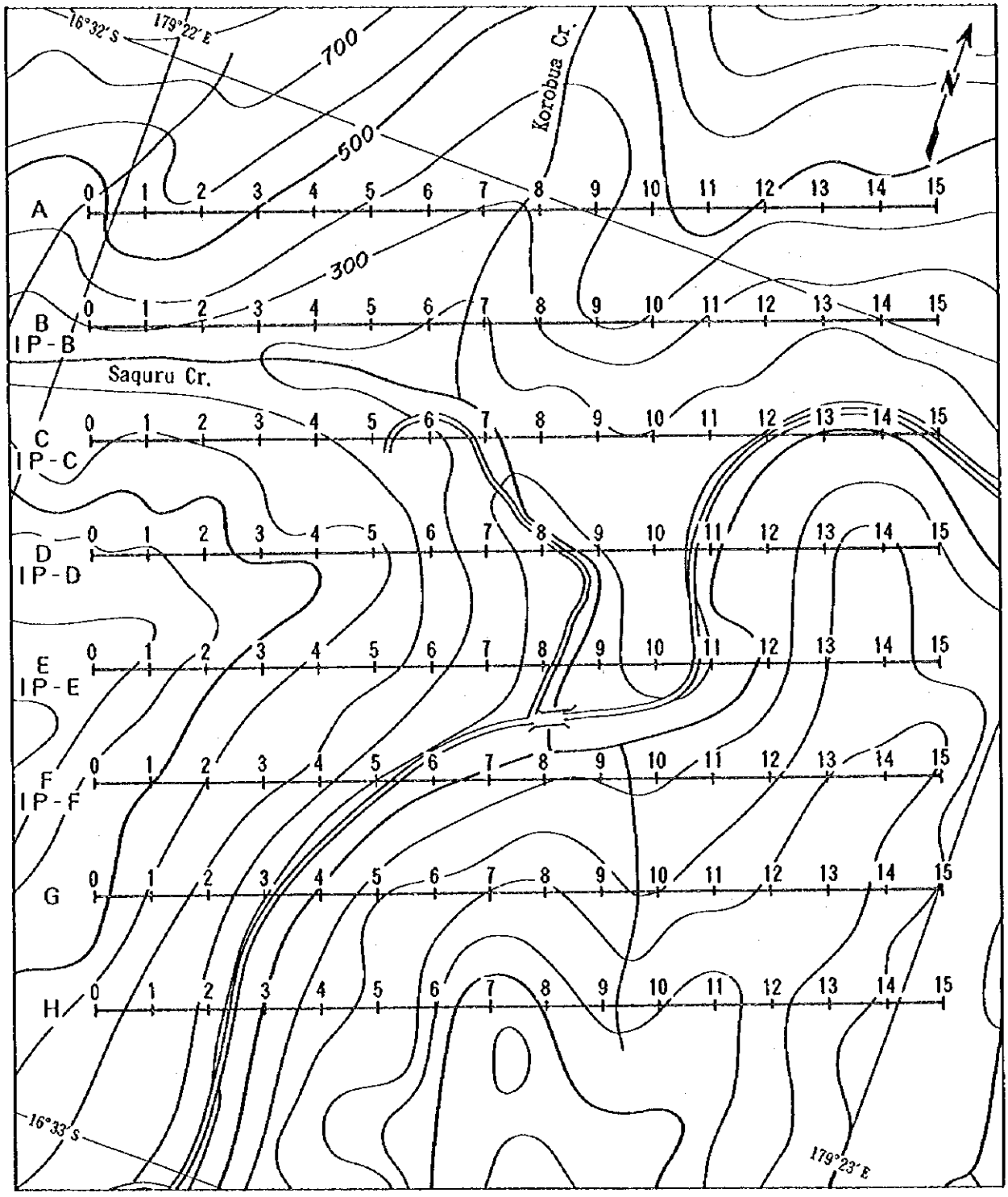

SCALE 1 : 10,000

0 100 200 300 400 500m

LEGEND

B 0 1 2 3 Survey Line for Array CSAMT

IP-B 0 1 2 3 Survey Line for IP Method

Fig. 2-5-2 Location Map of Survey Lines

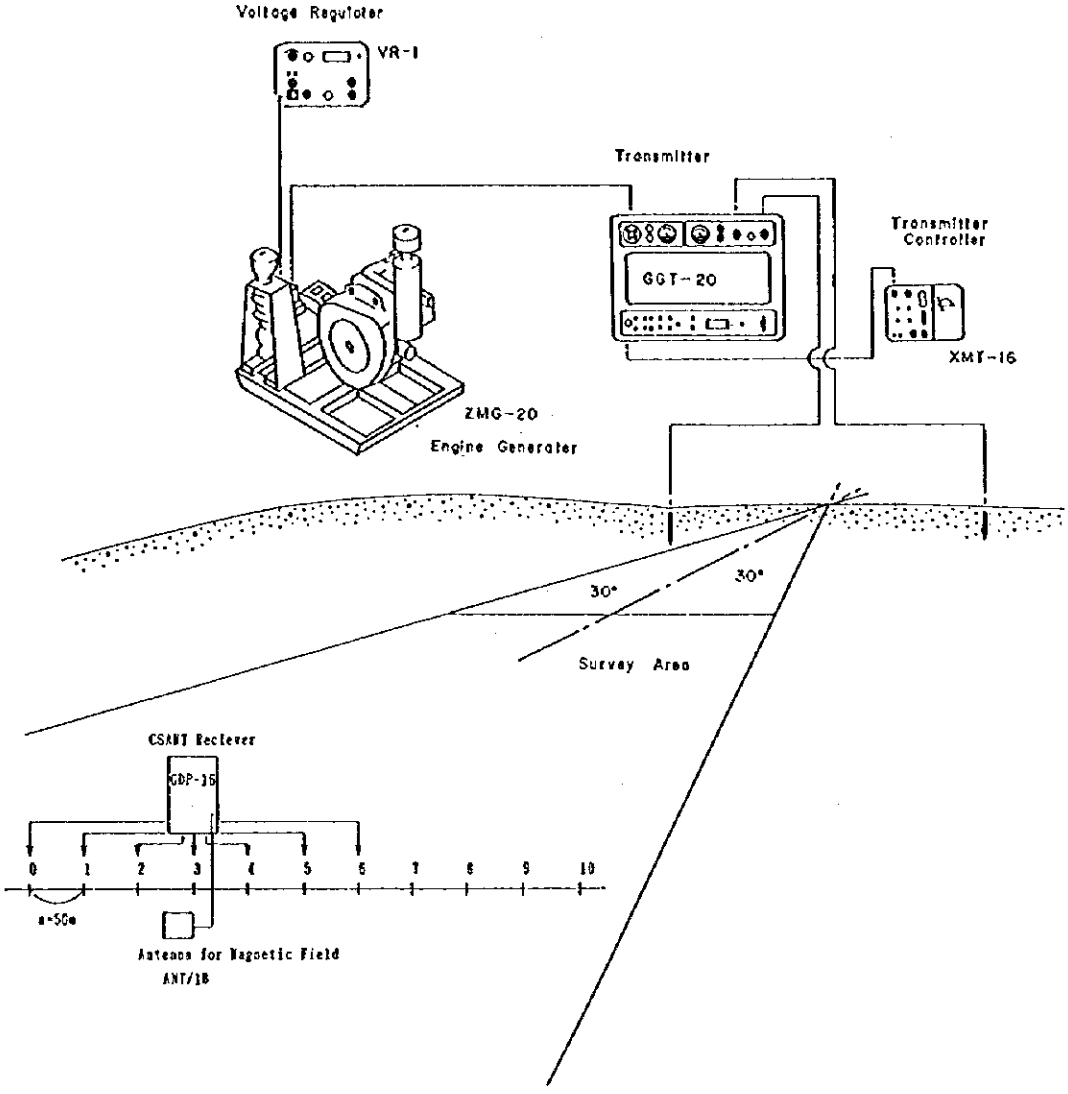

Fig. 2-5-3 Survey Configuration of CSAMT Method

In general, Frequencies are used in the broad range between 10 to 10,000Hz. The depth of apparent resistivity is shown by the skin depth, the skin depth is the effective depth of penetration of electromagnetic energy in a conductive medium when displacement currents can be neglected. The depth at which the amplitude of a plane wave has been attenuated to 1/e (or 37 percent):

$$\delta = 503\sqrt{\rho / f} \qquad \text{(meters)} \qquad (2)$$

Where

ρ : the resistivity of the ground in ohm-m.
f : the frequency of the transmitted signal in Hz.

For example, if the resistivity of the ground is assumed to be 100 ohm-m, the penetration is determined from the standard MT depth equation

$$D=\delta/\sqrt{2}=356\sqrt{\rho/f} \quad \text{(meters)} \quad (3)$$

Hence typical ground resistivity and effective penetration can vary as follows:

Ground resistivity (ohm-m)	Penetration range between 2048 Hz	and	4 Hz
1	8m	~	178m
10	25m	~	563m
100	179m	~	1,780m
1,000	249m	~	5,629m

At a distance from the transmitter dipole the transmitted electromagnetic field becomes a "plane wave" and this area is called "far-field". The Cagniard equation is valid in the "far-field" situation for the calculation of the apparent resistivity. The far-field distance, Δf, is given approximately by the following equation:

$$\Delta f > 3 \times (\text{skin depth}) = 1509\sqrt{\rho/f}$$

If the distance between the transmitter and the receiver is significantly less than Δf, the transmitted magnetic field is not "plane-wave" in character; it is referred to as the "near-field". On the other hand, if the measuring station is far from the transmitter dipole, receiving signal becomes weak and S/N ratio becomes small.

Hence field operation is carried out under the following conditions:

1) The station is far 3 δ rom the transmitting dipole (f:4Hz, ρ=30 ohm-m 3 δ=4100m)
2) The station is located less than 8 km from the transmitting dipole for the purpose of obtaining sufficient signal strength.
3) The survey area is less than 30 degrees from the perpendicular line to the transmitter dipole

(2) Field Operation and Equipment.

The standard configuration is four Ex dipoles and one Hy magnetic field measurements for each of the 12 frequencies, The Ex fields are measured with a dipole using non-polarizable porous pots. The survey traverse line, for the series of equally spaced Ex dipoles,

is parallel to the transmitter dipole. A horizontal magnetic sensor coil is placed on the ground, approximately at the center of the series of Ex field. It must be placed several meters away from the Ex dipole line and the receiver console, to avoid interference.

The measurements are performed at each of twelve frequencies with a binary step: 4,8,16, 32,64,128,256,512,1024,2048,4096 and 8192 Hz, and are three time operations to make sure the repeatability of data.

The equipment manufactured by Zonge in USA is shown Fig. 2-5-3 for field configuration. and in Table 2-5-1 .

The transmitter (powered by a suitable motor generator) sends current into the grounded dipole (distance of two electrodes is about 1500m), shown in Fig. 2-5-1, located 7 km NW from Nakoroutari Zone.

The transmitting dipole is at a distance of about 1.5 km in the N72°E direction.

The coordinates and conditions are as follows:

	Location	Elevation(m)	Orientation of dipole	Distance of dipole	Current (Amp)
A electrode	Lat. 16°28'55"S Long.179°21'55"E	24	N72°E	1,500m	12 Amp (Max.)
B electrode	Lat. 16°28'50"S Long.179°22'25"E	27			

The field conditions of random stations were the same as array system on the survey line with the exception of measurement of one Ex field.

(3) Data Processing and Interpretation

The magnitudes of Ex and Hy are measured at the stations, the resistivities and the parameters(the phase differences in Ex-Hy and the standard deviation) are calculated, stored in the RAM of the receiver unit and transferred into the field personal computer at the end of each day. The data were immediately processed at the camp. The field presentation of the results is in the form of a contoured apparent resistivity pseudosection plot and a plane map. The skin depth equation suggests that the data of lower frequencies inform us of deeper characteristics, the CSAMT data can be plotted with frequency as the sounding parameter (vertical axis) and receiver position as the lateral parameter(horizontal axis). This type of plot is called a sounding pseudosection, and the plane maps of each frequency are plotted with the apparent resistivity.

Table 2-5-1 Equipment of Array CSAMT Method

Item	Model	Specification		Quantity
Transmitting system	Chiba Electric Transmitter CH-120A	Output Voltage Output Current Wave Form Frequency Weight	:400,600,800,1000V :0.1 - 20A :Rectangular wave :DC - 8,192 :40 kg	1 pc.
	Zonge GGT-20 Transmitter	Output Voltage Output Current Wave Form Frequency Weight	:400,600,800,1000V :0.4 - 40A :Rectangular :DC - 8,192 :120 kg	1 pc.
	Zonge XMT-16 Transmitter Controller	Frequency Weight Power Requirement	:DC-8,192Hz :5.8kg :12 Volt Battery	1 pc.
	Zonge ZMG-20 Engine Generator	Maximum Power Frequency Output Voltage Power	:20 kw :400 Hz :115V :62Hp	1 pc.
Receiving System	Zonge GDP-16/8 Data Processor	Input Channel Sensitivity Weight Power Requirement	:0.03 μ V :8 ch :23kg :DC 12 Volt	1 pc.
	Zonge ANT/1B Antenna	1 Coil Weight	:6.2kg	1 pc.
	Electrode Current Potential	 Fe Plate Non-polarizable	 24cmx36cm $CuSO_4$ Porous Pot	 30 sheets 6 pcs.

One-Dimensional Inversion Analysis

The CSAMT curve, plotted with twelve frequencies as X-axis and apparent resistivity as Y-axis, is interpreted for one-dimensional multi-layer structure by computer as shown in the appendix.

1) The initial models are made by qualitative analysis of the observed CSAMT curve using the Bostick Inversion. Fig. 2-5-4 Flow Chart of 1-D. Automatic Interpretation for CSAMT Data

2) The parameters, namely resistivities and thickness of layers, are corrected by the non-liner minimum square method.

3) The theoretical CSAMT curve of the model is compared with the observed CSAMT curve.

4) The procedures 2) and 3) are repeated, the deviation between observed value and

the theoretical value of model are minimized.

These data which are analyzed, the resistivities and thickness of layers, are plotted on the cross section of resistivity and plane map on each levels of 0m,-100m, -200m, -500m below the sea level.

Two-Dimensional Inversion Analysis

There are two methods of two-dimensional analysis, one is called forward method, the suitable model made from the result of one-dimensional analysis is calculated. The other is called inversion method, the fitness model is obtained directly from observed values. In this report, two-dimension inversion analysis is applied for the CSAMT anomaly zones. The program was prepared by Ogawa and Uchida (1988, GSJ). This program calculates the coefficients of partial differential equation for the parameters of response function when the model is calculated by forward method. The second step is that new parameters are set by the inversion analysis applied numerical solution of singular value. The most fit model of minimum deviation with observed values is selected from these parameters.

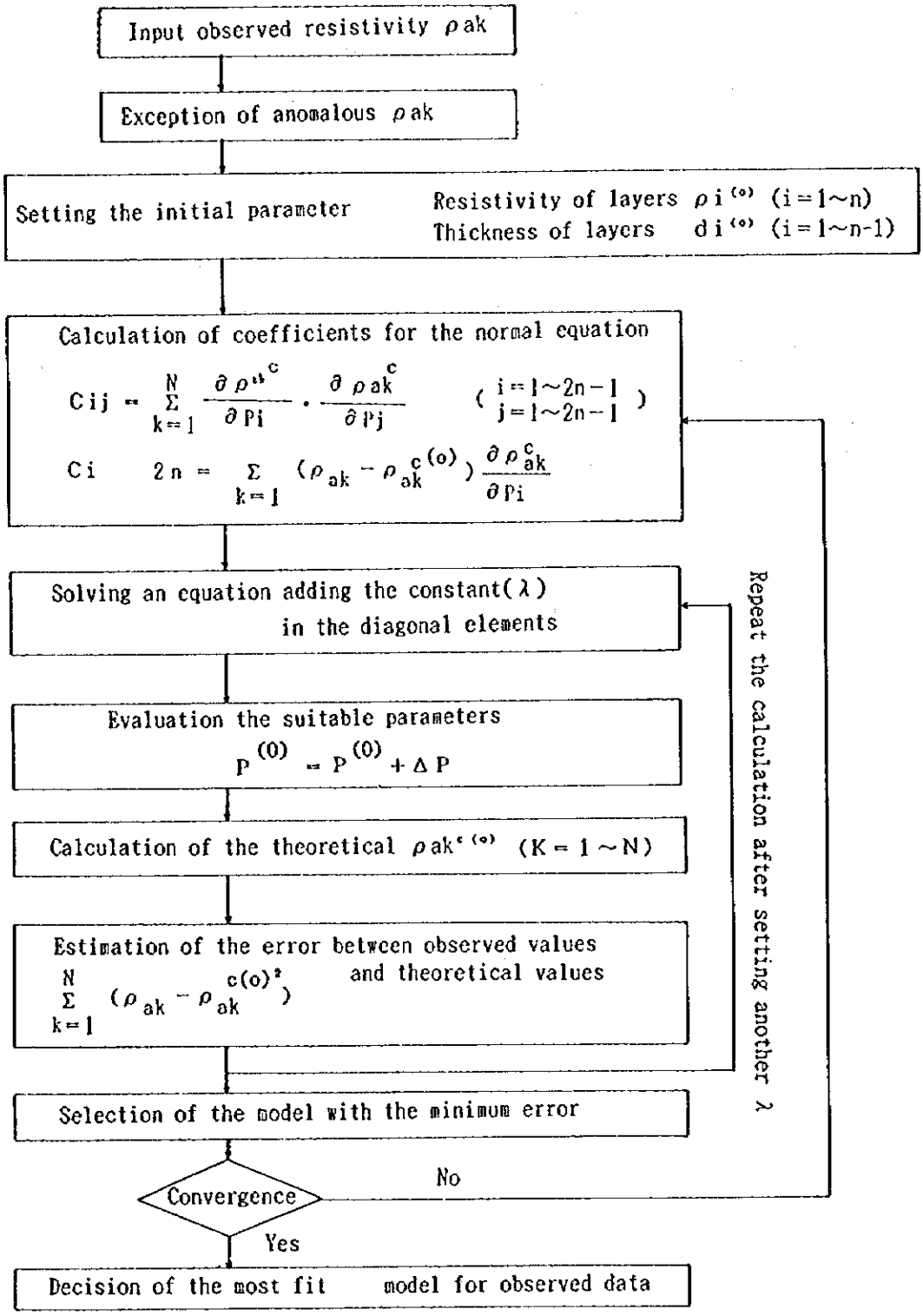

Fig. 2-5-4 Flow Chart of 1-d. Automatic Interpretation for CSAMT Data

5-2-2 Time Domain IP Method

(1) Theoretical Background

The electrical conduction in most rocks is essentially electrolytic, by transport of ions through interstitial water in pores. However, when a current is passed through a rock containing metallic minerals, the ionic conduction is hindered to a considerable extent by the mineral grains in which the current flow is electronic. The leads to an accumulation of ions at the interface between the minerals and solution, resulting in a growth of electrochemical voltage at the metallic grain surface. The process is similar to electrode polarization that occurs at the surface of metal electrodes dipped in an electrolyte. When the externally applied current is switched off, the electrochemical voltage is dissipated, but does not drop to zero instantaneously. The decay in voltage is observed to vary with time as shown in the below Figure, and can be measured as a fraction of the voltage V that existed when the current was flowing. The ratio Vt/Vp gives a measure of the concentration of metallic minerals in the rock formation. This is, in brief, the principle of the induced polarization or IP method.

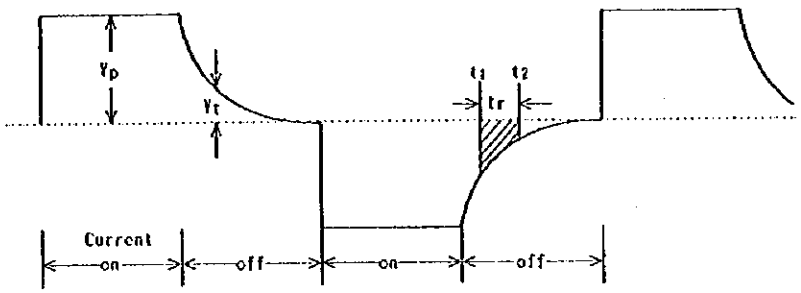

Induced polarization effects are observed even when metallic minerals are not present in a rock material. In particular clay bearing sediments show an appreciable IP. The surface of a clay particle has a net negative charge which attracts positive ions from the electrolyte present in pores. As a result of this polarized distribution of ions(called the membrane polarization), current flow is impeded. When the applied current is switched off the positive ions redistribute them to return to an equilibrium position. This process of redistribution of ions shows a decaying voltage as an IP effect. As yet only very limited application has been made of the IP effect associated with clay minerals.

Electrode polarization, as well as the membrane polarization, is essentially a surface phenomenon. The IP effects therefore greater if the metallic ore (or clay) is disseminated rather than compact.

Time-Domain IP : Induced polarization measurements can be made either using direct current or an alternating current.

When measurements are made by sending DC pulses(e.g., of 10s duration)into the ground, the magnitude of IP is expressed as Vt/Vp where Vt is the voltage remaining at a time t, say 2s, after the switch-off, and Vp is the voltage that existed when the current was flowing.

The ratio Vt/Vp is expressed as millivolts/volt, or as a percent

$$IP\ \% = 100\ (Vt/Vp) \qquad (mV/V \text{ or } \%)$$

Commercial IP outfits generally register the decaying V(t) over a definite time interval (t_1,t_2). The result is expressed by the time-integral measure of IP as " M ".

The quantity M, known as chargeability, is commonly used in time-domain measurements of IP.

The chargeability of Zonge GDP-16 is defined in the following calculations :

$$M = \frac{Vs \times 1{,}000}{Vp} \qquad (mV \cdot S/V)$$

Where

$$Vs = \frac{1}{t_r} \int_{t_1}^{t_2} Vt\ dt$$

t_1:time at beginning of the slice
t_2:time at end of slice
t_r:t_2-t_1 (integrating period)
Vp:voltage during the current On time
Vs:voltage measured by the receiver during the integrating period with the current off.

The apparent resistivity(AR) is defined as :

$$AR = \pi \cdot a \cdot (n+1)(n+2)\ Vp / I \qquad (ohm\text{-}m)$$

Where
a : interval of the respective dipole
n : coefficient of dipole - dipole
Vp : primary voltage of the respective dipole
I : transmitter current

(2)Field Operation and Equipment

(a) Method of measurement

The method of TDIP measurement in the field is as follows : the fine receiving dipoles and transmitting dipole are set on the survey line as shown in Fig.2-5-5.

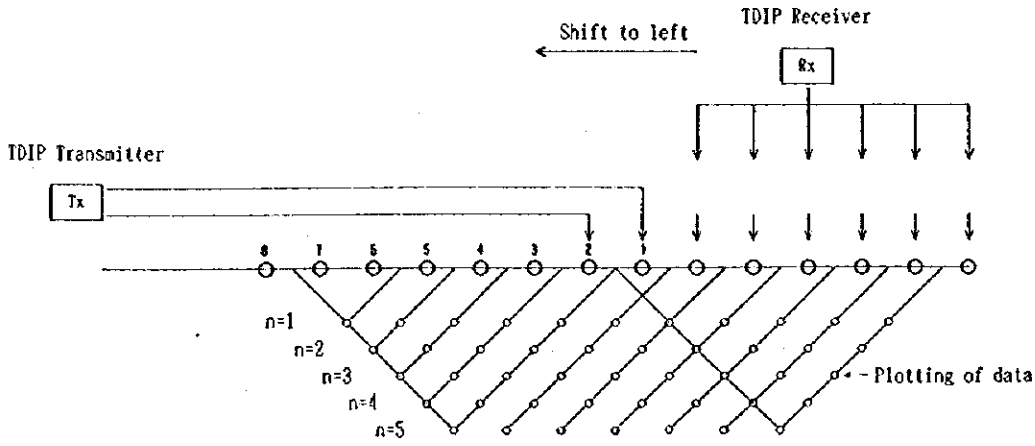

Fig. 2-5-5 Survey Configuration of IP Method

The specification of IP survey is as follows.

The configuration of electrode array	: dipole-dipole
The separation of electrode	: 100m
The coefficient of electrode separation	: n=1 — 5
The duty cycle of on / off time	: 2 sec.

(b) The equipment for TDIP survey

The equipments used in this survey are listed in Table 2-5-2.

(3) Data Processing and Interpretation

The measured resistivity and chargeability values are shown in tables for each line on the profiles. The subsurface depths are shown on plane maps by the electrode separation index. And the subsurface electric characteristics can be understood from these plane maps and profiles.

The resistivity values were affected by the topography and thus terrain correction was made by using carbon paper.

Two-dimensional model simulation was carried out for IP anomalies and chargeability and resistivity values were obtained quantitatively for the anomaly sources.

Table 2-5-2 Equipment of Time Domain IP Method

Item	Model	Specification		Quantity
Transmitting system	Zonge GGT-20 Transmitter	Output Voltage Output Current Wave Form Frequency Weight	:400,600,800,1000V :0.4 - 40A :Rectangular :DC - 8,192Hz :120 kg	1 pc.
	Zonge XMT-16 Transmitter Controller	Frequency Weight Power Requirement	:DC-8,192Hz :5.8kg :12 Volt Battery	1 pc.
	Zonge ZMG-20 Engine Generator	Maximum Power Frequency Output Voltage Power	:20 kw :400 Hz :115V :62Hp	1 pc.
Receiving System	Zonge GDP-16/8 Data Processor	Input Channel Sensitivity Weight Power Requirement	:0.03 μ V :8 ch :23kg :DC 12 Volt	1 pc.
	Electrode Current Potential	 Stainless steel rod Non-polarizable	 0.6 cm ϕ x60 cm(L) CuSO4 Porous Pot	10 pcs 6 pcs

5-3 Results of Geophysical Survey

5-3-1 Array CSAMT Method

A total 120 stations were measured with CSAMT method, and results were plotted on maps over three frequencies and on sections of apparent resistivity of each survey line. Results of one-dimensional analysis on CSAMT curves are shown on sections of resistivity structure of each line and four maps of different depths. Inversion analyses have been also conducted to find out a two-dimensional structure which corresponds to measurements of each line. The interval of contour lines is of a logarithmic of 1,3,10,30,100,300,etc.

Maps and sections are inserted to the end of this chapter.

The apparent resistivity ranges from 0.9 to 168 ohm-m. Areas of low resistivity prevail and background values are low at 15 to 25 ohm-m. The area over 50 ohm-m is deemed to be of high resistivity and less than 10 ohm-m is of low resistivity.

Sections of apparent resistivity

Fig.2-5-6 shows resistivities from surface to depths which correspond with high- to low-frequency.

Line A

High resistivity of intrusive rocks is delineated by discontinuance of stratiform contours which indicates sudden changes in resistivity between Nos.6 and 8 in the middle of the line. Resistivity highs in the field of high frequency between Nos.2 and 6, and Nos.9 and 12, correspond with the distribution of andesitic volcaniclastics. Except the middle of the line, a stratiform geological structure is indicated by low resistivity measured with frequencies less than 128 Hz.

Line B

Distribution of resistivity is similar to that of Line A. High resistivity on high frequency is detected in the area of andesitic volcaniclastics between Nos.8 and 10. Low resistivities of some 20 ohm-m are detected in the area of basalt in the west of the line.

Line C

Cuttings of stratiform contours are broadly found between No.5 and 8. The known fault is situated at No.8. Resistivity high is detected in the field of low frequency less than 256 Hz between Nos.5 and 6. Noticed is detection of low resistivity in the field of high frequency between Nos.8 and 12 in the east of the middle of the line, where volcaniclastic rocks are distributed. In the west of the line between Nos.0 and 4, where andesitic volcaniclastics of high resistivity occur, low resistivities of less than 30 ohm-m are detected, probably due to thinness of volcaniclastic rocks.

Line D

The pattern of resistivity is similar to that of Line A. Discontinuance of stratiform contours is found between Nos.7 and 9. Resistivity high corresponding to andesitic volcaniclastics is detected between Nos.0 and 5, with an indication of thickening of volcaniclastic rocks beneath Nos.2 and 3.

Line E

The pattern of resistivity is similar to that of Line D. Discontinuity of resistivity is seen at No.6 and No.8.

Line F

High resistivities in the field of high frequency are not a few in the middle of the line. Discontinuity of resistivity is recognized at Nos.4 and 7, but indistinct compared with those of Lines A to E.

Line G

Discontinuity of resistivity indicating an existence of fault is not found. In the field of high frequency, resistivity highs are detected in the west and in the eastern middle. The resistivity pattern of the line can be deemed to be similar to that of Line A.

Line H

A discontinuous contour pattern of resistivity is not recognized. In the middle of the line, high resistivity of a small scale is seen in the field of high frequency. A monotonous structure of resistivity is indicated.

In short, at the middle part of lines A to F, high resistivities of dike-shape are continuously detected which cut horizontal stratiform contours. This feature is apparent between Lines A and E, becomes smaller on Line F and disappears on Line G. Discontinuity of resistivity indicates fault(s). In the area of andesitic volcaniclastics in the north, a fault is detected as a resistivity high in the field of high frequency.

Maps of apparent resistivity

Fig.2-5-7 shows apparent resistivities on frequencies of 2,048 Hz, 256 Hz and 32 Hz, plotted on the scale of 1:10,000.

Map of 2,048 Hz. Fig.2-5-7(1)

The map shows a specific character of resistivity at a shallow depth. Zones of high resistivity were obtained at the northwest and the west of the area, probably due to an existence of andesitic volcaniclastic rocks. A small distribution of low resistivity is observed on the area of volcaniclastic rocks in the eastern middle of Line C, where alteration zone of mineral showing at Leli's prospect is known.

Map of 32 Hz. Fig.2-5-7(3)

The map shows a specific character of resistivity at depths. Zones of low resistivities were broadly detected in the eastern half and in the northwest. These are assumed to correspond with volcaniclastic rocks, andesite, and basaltic andesite lava. In the western middle of Lines B to C, and Lines D to F, zones of high resistivity of more than 50 ohm-m are shown, trending toward north-south.

Sections of resistivity structure

Fig.2-5-8 shows sections of apparent resistivity in ohm-m of layers and depths in meter of boundaries of layers, which were obtained from one-dimensional multi-layer structural analysis on each line.

Line A

Resistivity high is located below stations Nos.7 and 8, where discontinuity of resistivity is indicated, and moderate high values are observed in its vicinity between Nos.6 and 9. The analysis revealed sheets of highly resistive layers of 51 to 583 ohm-m at shallow depths, between stations Nos.2 and 7 and between stations Nos.8 and 12 where andesitic volcaniclastic rocks occur. Layers of low resistivity less than 10 ohm-m are widely observed below areas between stations Nos.0 and 4 and stations Nos.8 to 15, where volcaniclastic rocks, andesite and basaltic andesite lava are widely distributed.

Line B

Resistivity high is analytically found 50 to 264 m in depth between stations Nos.5 and 7. Resistivity high is also observed at shallow depths between Nos.8 and 10. Similar to Line A, wide distribution of low resistivity layers is seen in the eastern half of the line and west of No.4. Discontinuity of resistivity is inferred at Nos.6 and 7.

Line C

A zone of resistivity high lies widely beneath stations Nos.4 to 8. The top of resistivity high is 236 m deep from the surface. A layer of resistivity high is situated to the west of No.4 at the shallow depth. Discontinuity of resistivity is seen at Nos.4 and 8. The eastern half of the line and the west of No.4 are inferred to be underlain by one to two layers of resistivity low.

Line D

Resistivity high lies in the middle of the line between Nos.7 and 8. Discontinuity of resistivity is detected at the both sides of it. Thin layers of resistivity high are analytically inferred at the shallow depths of middle of the line and to the west of No.3. The distribution of resistivity low is similar to those of three lines mentioned above.

Line E

The analysis found high resistivity at the middle of the line between Nos.6 and 8, and Nos.3 and 4. The top of the former is 20 to 106 m deep, and the latter is 309 m deep. A layer of high resistivity exists to the west of the station No.4, being more than 100 m thick. The distribution of resistivity low is similar to those of four lines mentioned above.

Line F

Resistivity high underlies 56 m below the surface between stations Nos.5 and 6, and discontinuity of resistivity is seen at No.6. A layer of high resistivity lies widely in shallow depths between Nos.2 and 12. One to two layers of medium to low resistivity are distributed in the eastern half of the line.

Line G

The zone of high resistivity which extends in the middle of lines A to F, does not appear in this line. New resistivity high is obtained in the depth of 373 m between Nos.10 and 11. Layers of high resistivity are analytically noticed in shallow depths between Nos.1 and 3, and Nos.6 and 11. Areas of low resistivity less than 10 ohm-m are reduced.

Line H

To be noticed is wide distribution of high resistivity of 100 to 500 ohm-m at the depths more than 340 m from the surface between Nos.4 and 15, which can be assigned with fresh igneous rocks from its form and the value of resistivity.

Maps of resistivity structure

The results of one-dimensional multi-layer analysis of each station are plotted on maps at the heights of 0, -100, -200 and -400 m a.s.l. See Fig.2-5-9(1 to 4).

0 m level:

Widely distributed are zones of low resistivity less than 10 ohm-m in the eastern half of the area and western ends of survey lines. Hidden resistivity highs are inferred to extend in a north-south direction between Lines A and C, and between Lines D and E, which form a zone of high resistivity extending northwest to southeast overall. The zone between Lines C and D is correlative with the silicified zone of mineral occurrence at Leli's prospect. From this, the resistivity high is assumed to indicate the structure in the depths of silicified alteration zone.

-100 m a.s.l.:

The patterns of the map are very similar to those of map of 0 m level. No remarkable change in resistivity structure is noticed. Resistivity high in the middle of Lines D and E extends toward south, and reaches to Line E with reduction of the area.

-200 m a.s.l.:

The patterns of the map are similar to those of -100 m. A zone of high resistivity appears in the eastern half of Line H, and resistivity high of a small scale appears between Nos.3 and 4 on Line E. No change of distribution of resistivity low is noticed.

-400 m a.s.l.:

Resistivity high appears in the west of the middle of Line H and increases its extent. Others are of a resistivity structure similar to that of -200 m level.

One-dimensional structure analysis shows that the high resistivity of an intrusive rock-shape comprises resistivity highs extending north to south between Lines A and D, and between Lines D and F, which form the zone extending northwest to southeast. The origin of resistivity high is not certain whether due to silicification or fresh intrusive rock such as basalt, but, silicification origin is more acceptable because of accordance with the location of silicified zone in the surface.

Two-dimensional analysis

Fig.2-5-10 shows the results of two-dimensional analysis on all lines.

The central area is dominated by resistivity low, and zones of high resistivity are spread on Line A in the north and Lines G and H in the south, the north being of intrusive rocks and the south being of sheet-like spread such as basement rocks.

Compared with one-dimensional analysis, values of resistivity are lowered. The zone of high resistivity in the middle of lines in one-dimensional analysis is not seen on Lines B and C. Yet, the resistivity higher than that of surrounding area is noticed and a resistivity pattern similar to that of one-dimensional analysis has been obtained.

These results are summarized in Fig.2-5-11. Areas of zone of low resistivity less than 10 ohm-m and zone of high resistivity more than 50 ohm-m are shown, and discontinuity lines

and the geological structure inferred from sections of apparent resistivity and from resistivity structural map are also shown in this Figure.

5-3-2 Time Domain IP method

The time domain induced polarization method was conducted to clarify the relationships of geological structure and mineralization alteration with the zone of high resistivity delineated in the middle of Lines B to F of CSAMT method. Results are shown on sections of apparent resistivity in Fig.2-5-12 and on maps of Fig.2-5-13. Chargeability is also plotted on sections and maps as illustrated in Fig.2-5-14 and Fig.2-5-15.

Apparent resistivity

The values of 15 to 25 ohm-m of apparent resistivity are dominant as those of CSAMT method. Consequently, criteria of high and low resistivity are placed at more than 50 ohm-m and less than 10 ohm-m.

Sections of apparent resistivity; Fig.2-5-12

Zones of low resistivity continuously extend in the east of each line. Also, resistivity highs detected in shallow depths of middle of Lines C to E are continuous. Other resistivity highs are detected in the west end of Lines E and F. These distributions accord with those of CSAMT method.

Maps of apparent resistivity; Fig.2-5-13

Five maps were provided with each electrode separation.

Map of n=1; Fig.2-5-13(1)

Zones of high resistivity are detected in the middle of Lines B and C, and the western end of Lines E and F. The former is coincident at the trend of elongation and the scale of distribution with those of high resistivity zones detected by CSAMT method and assigned to be of alteration zone of silicification. The latter is in accord with distribution of andesitic volcaniclastic rocks. Moderate extent of resistivity low in the east of Lines A to E is correlative with distribution of volcaniclastic rocks, andesite and basaltic andesite lava.

Map of n=2; Fig.2-5-13(2)

Values of zones of high resistivity on Lines C and D at n=1 are decreased in this map. An area of more than 50 ohm-m is of small scale between Nos.7 and 8 on Line E. The high resistivity zone at the western end of Lines E and F disappears. From this, layers of andesitic volcaniclastic rocks are assumed to be thin. In contrast, the zone of low resistivity is widespread.

Map of n=3; Fig.2-5-14(3)

A zone of high resistivity is not seized at this separation. As for zones of low resistivity,

the zone in the east of the area found at n=1 and n=2, is detected and the resistivity low of a small scale is newly located on Line E.

Map of n=4; Fig.2-5-14(4)

The map has a distribution pattern of resistivity similar to that of map n=3. Only difference is seen with an existence of low resistivity of a small scale on Line A.

Map of n=5; Fig.2-5-14(5)

A zone of low resistivity less than 10 ohm-m extends with a trend of northwest to southeast in the central part of the area. The zone appears to be increasing its extent toward southeast. The zone of low resistivity in the east of the area is divided into two directions of northwest and southeast.

Chargeability

Dominant values of chargeability are less than 2 mV·S/V, and values from 5 mV·S/V to 10 mV·S/V can be counted for weak anomalies, and values of more than 10 mV·S/V are counted for anomalies on chargeability.

Sections of chargeability; Fig.2-5-14

Weak anomalies more than 5 mV·S/V are successively detected in a northwest to southeast direction, at the western middle of each lines. These anomalies coincide with those seized by Geoterrex in 1988, of which details are not known. Patterns of anomalies of each line are of pants-legs, which indicate a shallow origin of anomalies. Couples of negative and positive anomalies have been detected in depths between Nos.2 and 4 of Line C, between Nos.10 to 12 of Line D, and between Nos.6 to 10 of Line D. Anomalies are reproducible with data on n=4 to n=5 in depths, but their origins are unknown.

Maps of chargeability

Five maps were provided on each electrode separation.

Map of n=1; Fig.2-5-15(1)

Weak anomalies of a northwest to southeast direction are distributed in the central part of the area. The location and the scale of anomalies coincides with the zone of high resistivity on the map of n=1 on apparent resistivity. Anomalous values are of the order of 5 mV·S/V and assumed to be of alteration zone of weak pyritization. Other weak anomalies of a small scale are also found at the eastern end of Line D and the western end of Line E. Negative anomalies are found at No.3 on Line B, No.3 on Line D and No.1 on Line F.

Map of n=2; Fig.2-5-15(2)

The distribution of weak anomalies in the central part of the area has been transfigured. The anomalies spread on Lines C and D, and tend to reduce their extent on Lines B and E. Except the anomaly at the eastern end of Line D, weak anomalies and negative anomalies on the map of n=1 are not observed and a couple of negative and positive anomalies more

than 10 mV·S/V is detected at the west end of Line C.

Map of n=3; Fig.2-5-15(3)

The anomalies at the central part of the area are of reduced extent, and weak anomaly of a small scale and negative anomaly are detected in the middle of Lines E and F.

Map of n=4; Fig.2-5-15(4)

Anomalies more than 10 mV·S/V are detected at Nos.2 and 3 of Line C, and zonal weak anomalies surround them in a north northwest to south southeast or north-south direction over an area from Line B to Line F. Weak or negative anomalies of a small scale are scattered in the east to the south of the area.

Map of n=5; Fig.2-5-15(5)

High chargeability of 28.6 mV·S/V is detected at Nos.10 and 11 on Line D. Surrounding weak anomalies extend toward east of the middle of Lines D and E. Another weak anomaly spreads in the west of Lines B to D. Weak and negative anomalies appear alternatively in the middle of Lines E and F.

Simulation of two-dimensional model

Values of resistivity and chargeability of each grid are set for the initial model with reference to the results of CSAMT analysis. Discrepancies occurred between measurements and the model on patterns and values of apparent resistivity, and setting of model is repeated with the method of trial and error to obtain a model of approximate values and contour patterns similar to the results of time domain induced polarization method.

Line B Fig.2-5-16(1)

Modeling: Resistivity zone (code :2) over 30 ohm-m is detected at the shallow part below the surface of stations between 5 and 7. The low resistivity zone (code :3 and 6) is detected below of stations between 10 and 13. The weak chargeability anomaly over 5 mV·S/V(code :6) is detected at the deep part of stations between 3 and 6.

Results of simulation : The model brings the results most similar to apparent resistivity of the measurement. Chargeability also accords with the field data on the whole, but does not relate in detail, the negative anomaly at the shallow part below stations between 3 and 4, the part less than 3 mV·S/V between stations 6 and 7, and weak anomaly over 5 mV·S/V are not detected in the model.

Line C Fig.2-5-16(2)

Modeling: The high resistivity zone(code:4) at the shallow part below stations between 5 and 7 and the low resistivity zone (code:1) are detected, and the "pants leg" pattern of chargeability anomaly (code : 4) below stations between 3 and 8 is measured. The pair of negative anomaly and zone over 10 mV·S/V is neglected because of limiting over the simulation.

Results of simulation The sections of resistivity and chargeability show the results almost

similar to the those of measurements, but are not simulated in detail. The distribution of origin of resistivity and chargeability on the whole are known.

Line E Fig.2-5-16(3)

Modeling: The resistivity zone over 100 ohm-m at the west part of the survey line is coded by "6". The high resistivity part shallow part below stations between 7 and 9 and chargeability anomaly of the "pants leg" pattern below stations between 4 and 9 are coded by "4" and "5".

Results of simulation The model shown in figure is brought the results most similar to resistivity and chargeability of the measurement.

The analytical results of TDIP method is summarized in Fig.2-5-17. The zone of low resistivity less than 10 ohm-m and of high resistivity more than 50 ohm-m are illustrated on the map of apparent resistivity. The location of the origin of anomalous chargeability and the geological structure obtained analytically by the simulation of two-dimensional model are also shown.

5-3-3 Laboratory investigation

To know the resistivity and chargeability of rocks, samples were measured with the same instruments used in the field. Localities of thirty samples including drill-cores are shown in Fig.2-5-18. Rock samples comprise fifteen pieces of andesite, five of basalt, six of volcaniclastic rocks, and four of silicified rocks. Physical properties are listed in Table 2-5-3. The distributions of resistivity and chargeability are illustrated in Fig.2-5-19.

The average resistivity and chargeability of andesite stand at 857 and 4.8 respectively, at 1203 and 2.4 of basalt, at 211 and 11.7 of volcaniclastic rocks, and at 2884 and 8.0 of silicified rocks.

The resistivity is highest in silicified rocks, and followed by basalt, andesite and volcaniclastic rocks in descending order. The values of silicified rocks are of about twice of resistivity in basalt, and basalt has some 50% higher values than those of andesite. The values of resistivity in volcaniclastic rocks are of a quarter of those of andesite.

The chargeability is highest in volcaniclastic rocks and followed by silicified rocks, andesite and basalt in descending order.

Distribution of resistivity in rocks is of scattered, and rocks have common ranges of resistivity values, as illustrated in Fig.2-5-19. Rocks cannot be specified from values of resistivity.

Chargeability has a distribution with small dispersion, and many samples show low values.

Table 2-5-3 Results of Physical Property of Rock Samples

No.	R o c k	Resistivity ohm-m	Chargeability mV·S/V	Remarks
1	Andesite	507	2.2	dark green,basaltic
2	Andesite	976	2.6	dark green,basaltic
3	Andesite	119	1.3	
4	Andesite	833	1.0	
5	Andesite	1098	2.4	
6	Andesite	1113	6.6	
7	Andesite	* 92	* 3.5	dark gray, weathered
8	Andesite	411	2.0	basaltic, porous
9	Andesite	2501	1.6	
10	Andesite	1272	2.3	
11	Andesite	1543	7.9	glassy
12	Andesite	514	4.6	porphyritic
13	Andesite	325	4.5	porphyritic
14	Andesite	471	8.4	porphyritic
15	Andesite	312	25.1	DDH-2 -166m core
	Average value	857	4.8	
16	Basalt	* 69	* 1.7	green altered,porous
17	Basalt	1290	2.9	black
18	Basalt	489	2.5	black,with copper film
19	Basalt	2808	3.3	
20	Basalt	226	0.8	light gray, massive
	Average value	1203	2.4	
21	Silicified rock	3911	2.3	dark gray,intensively
22	Silicified rock	1330	7.9	float, intensively
23	Silicified rock	2959	9.2	milky color, intensively
24	Silicified rock	3334	12.7	float
	Average value	2884	8.0	
25	Volcaniclastic rock	28	6.8	andesitic braccia
26	Volcaniclastic rock	492	6.8	lapilli tuff
27	Volcaniclastic rock	281	12.3	white, altered
28	Volcaniclastic rock	116	2.9	pearly green, basaltic
29	Volcaniclastic rock	37	12.2	
30	Volcaniclastic rock	313	29.0	light gray,lapilli tuff
	Average value	211	11.7	

* : omitted value for average calculation

5-4 Summary of Geophysical Survey and Discussions

5-4-1 Array CSAMT Survey

Results of CSAMT method are summarized as follows.

1. The background value of apparent resistivity ranges from 15 to 25 ohm-m and low values are dominant on the whole.

2. Zones of high resistivity more than 50 ohm-m are detected in shallow depths at the northwest and the west of the area, and inferred to be related with andesitic volcaniclastic rocks. Distribution of the zone of low resistivity is limited, with a small scale, only in the eastern middle of Line C where volcaniclastic rocks are dominated.

3. Zones of low resistivity are widespread at the almost eastern half and the northwest of the area in depths, and inferred to be originated in volcaniclastic rocks, andesite and basaltic andesite lava. Zones of high resistivity more than 50 ohm-m are detected in the middle of Lines B to C, and Lines D to F.

4. Zones of high resistivity of dike-shape, disturbing the horizontal contours of stratiform structure, are detected in sections of apparent resistivity at the middle of each line on Lines A to F. The phenomena are obvious on Lines A to E, diminish the scale at Line F and terminate on Line G.

5. By the one-dimensional analysis of resistivity structure, the dyke-like zones of high resistivity are inferred to be of two bodies of high resistivity between Lines A to C and Lines D to F, extending in a north-south direction. However, two bodies are deemed to form a zone which extends in a direction of northwest to southeast. The high resistivity originates in whether silicification or intrusive rock such as fresh basalt, but from its coincidence of distribution with that of silicified zone, silicification origin is probable.

Discussion

An outline of silicified alteration zone of Leli's mineral showing was revealed by CSAMT method which covered an area of the silicified zone and its vicinity. However, when more detailed survey is necessitated, delineation of each silicified dyke becomes necessary. In case of this, it is considered that an electrode interval and spacing of survey line should be reduced to be of 25 to 50 m and 50 to 100 m respectively. With such specifications of investigation, more detailed mapping of resistivity becomes possible and it enables to analyze geological distribution and its structure in detail.

Fig.2-5-20 shows results of one-dimensional analysis on the field test with an electrode interval of 25 m between Nos.4 and 12 on Line C. The zone of high resistivity of more than 50 ohm-m detected between Nos.4 and 8 is of the zone seized with the interval of 100 m. In addition, resistivity high more than 100 ohm-m is detected between Nos.6 and 7 by means of the interval of 25 m. The zone of high resistivity extending to depths is located at 25 m east of No.6, giving more accurate result compared with the case of 100 m interval.

Similarly, to select a target area of detailed investigation or to select a drilling site, specifications of survey with a small electrode interval should be added where necessary.

5-4-2 Time domain IP Survey

Results of TDIP method are summarized as follows.

Resistivity

1. Values of apparent resistivity are generally low and the background value ranges from 15 to 25 ohm-m.
2. A zone of low resistivity less than 10 ohm-m has been detected successively between Nos.10 and 13 of each line, in a trend of north to south. Also, a zone of low resistivity has been found between Nos.6 and 8 in depth. Zones of low resistivity on small scales are known in shallow depths at the west of Lines A and C.
3. Apparent resistivity of IP method is generally in accordance with distribution of apparent resistivity of CSAMT method, but values of apparent resistivity of the former tend to be lower than those of the latter.

Chargeability

1. Values of chargeability in the background are of 2 to 3 mV·S/V, of which lower values predominate.
2. Values of chargeability more than 10 mV·S/V have been obtained at three stations, No.3 on Line C, No.10 on Line 10 and No.7 on Line F. These are of isolated anomalies and of low reliability.
3. A zone of higher values of chargeability more than 5 mV·S/V is detected in the depths between Nos.5 and 7 successively in a direction of northwest to southeast, and correlated to the IP anomalies found by Geoterrex in 1988.
4. The zone of high apparent resistivity delineated in the west of the middle of the area is situated at the almost same place where the concealed zone of high resistivity is found between Lines B to F by CSAMT method in a north-south trend. The concealed zone is assumed to be of silicified alteration zone. It is inferred that two methods revealed the same zone of high resistivity, and the area of weak anomaly on chargeability also coincides with the zone. From this, it is indicated that the silicified alteration is pyritized to some extent.
5. Judging from the point of view on chargeability, intensive mineralization of sulfide minerals over a wide range is not expected in this area.

Discussion

By TDIP method, the weak anomaly of chargeability more than 5 mV·S/V is detected at the west of the central area. The anomaly is the same with the IP anomaly revealed by Geoterrex in 1988. Due to unavailability of previous data, absolute values of IP anomaly cannot be compared with those of present investigation. Yet, previous records revealed